Chemically reduced graphene oxide in electrochemical sensing for bioapplications

Janessa Wahlström

School of Electrical Engineering

Thesis submitted for examination for the degree of Master of Science in Technology.

Espoo 18.08.2016

Thesis supervisor:

Prof. Tomi Laurila

Thesis advisor:

D.Sc. (Tech.) Emilia Peltola

Aalto University
School of Electrical
Engineering

AALTO UNIVERSITY
SCHOOL OF ELECTRICAL ENGINEERING

ABSTRACT OF THE
MASTER'S THESIS

Author: Janessa Wahlström

Title: Chemically reduced graphene oxide in electrochemical sensing for bioapplications

Date: 18.08.2016 Language: English Number of pages: 10+101

Department of Electrical Engineering and Automation

Professorship: Microsystem technology

Supervisor: Prof. Tomi Laurila

Advisor: D.Sc. (Tech.) Emilia Peltola

Electrochemical sensing with voltammetric methods are based on measuring the current induced by an applied potential with an electrode. The current originates from oxidizing or reducing analytes and is related to the concentration of the analyte, which can be almost any ion or molecule found from human body. Neurotransmitters such as dopamine and serotonin, the main interfering compounds, ascorbic acid and uric acid as well as glucose and β-nicotinamide adenine dinucleotide are important analytes for medical purposes.

Graphene has high electrical conductivity, mechanical strength and surface area, which makes it a suitable electrode material. A simple mass production method is to chemically reduce oxidized graphene. Chemically reduced graphene oxide contains structural defects and oxygen bearing functional groups, which enhances the electrochemical properties. Large surface area provides a platform for surface functionalization, which results in large amount of electroactive sites.

The surface of chemically reduced graphene oxide can be covered with metallic nanoparticles, nanostructures or recognition elements, which increases selectivity and sensitivity. Especially bimetallic nanostructures are widely used and are concidered more stabile than *e.g.* enzymes. Nanoparticles or nanostructures can be immobilized on the surface of chemically reduced graphene oxide with stabilizing layers, which also prevent them from aggregating, since aggregation of nanoparticles results in lower surface area and thus lower electrochemical responce.

Comparison of different chemically reduced graphene oxide sensors based on published research is problematic due to the wide variety of oxidizing methods, reductants, scan rates, solution pH, reference electrodes, substrate electrodes and stabilizers, which all affect the electrochemical responce. This is why a comparative study should be conducted in order to evaluate the effectiveness of different surface functionalization methods.

Keywords: graphene, electrochemical sensing, graphene oxide, chemical reduction, dopamine, serotonin, ascorbic acid, uric acid, glucose, β-nicotinamide adenine dinucleotide

AALTO-YLIOPISTO
SÄHKÖTEKNIIKAN KORKEAKOULU

DIPLOMITYÖN
TIIVISTELMÄ

Tekijä: Janessa Wahlström

Työn nimi: Kemiallisesti pelkistetyn grafeenioksidin käyttö sähkökemiallisessa detektoinnissa biosovelluksissa

Päivämäärä: 18.08.2016 Kieli: Englanti Sivumäärä: 10+101

Sähkötekniikan ja automaation laitos

Professuuri: Mikrosysteemitekniikka

Työn valvoja: Prof. Tomi Laurila

Työn ohjaaja: TkT Emilia Peltola

Sähkökemiallinen detektointi voltammetrisesti perustuu mitattavaan virtaan, joka syntyy elektrodille syötetyn jännitteen avulla. Virta syntyy tutkittavan aineen hapettuessa tai pelkistyessä ja on verrannollinen mitattavan aineen pitoisuuteen. Hermovälittäjäaineet, kuten dopamiini ja serotoniini, häiriötä aiheuttavat aineet, kuten askorbiinihappo ja virtsahappo, sekä glukoosi ja β-nikotiiniamidi adeniini dinukleotidi ovat tärkeitä sähkökemiallisesti mitattavia aineita kehossa.

Korkea sähkönjohtavuus, mekaaninen vahvuus ja suuri pinta-ala mahdollistavat grafeenin käytön elektrodimateriaalina. Hapetetun grafeenin kemiallinen pelkistys on yksinkertainen, massatuotantoon soveltuva valmistusmenetelmä, sillä kemiallisesti pelkistetty grafeenioksidi sisältää rakenteellisia virheitä ja funktionaalisia happiryhmiä, jotka parantavat materiaalin sähkökemiallisia ominaisuuksia. Suuri pinta-ala mahdollistaa myös pinnan funktionalisoinnin, joka lisää sähkökemiallisesti aktiivisia kohtia entisestään.

Kemiallisesti pelkistetyn grafeenioksidin pintaan voidaan lisätä metallisia nanopartikkeleja, nanorakenteita tai tunnistuselementtejä, jotka lisäävät selektiivisyyttä ja herkkyyttä. Varsinkin kaksoismetallisia nanopartikkeleja käytetään laajalti, sillä niiden on todettu olevat stabiilimpia kuin entsyymien. Nanopartikkelit voidaan kiinnittää erilaisten stabiloivien materiaalien avulla, jotka lisäksi ehkäisevät nanopartikkelien kasautumista, joka aiheuttaa pinta-ala pienenemistä ja sähkökemiallisen vasteen heikentymistä.

Kemiallisesti pelkistetystä grafeenioksidista valmistettuja antureita on vaikea verrata ainoastaan julkaistujen tutkimusten perusteella, sillä käytetyt hapetusmenetelmät, pelkistysaineet, pyyhkäisynopeudet, pH, referenssielektrodit, tukielektrodit ja stabilointiaineet vaihtelevat suuresti. Tämän takia vertaileva tutkimus olisi tarpeen, jotta voidaan arvioida erilaisten pinnanmuokkausmenetelmien tehokkuutta.

Avainsanat: grafeeni, sähkökemiallinen mittaus, grafeenioksidi, kemiallinen pelkistys, dopamiini, serotoniini, askorbiinihappo, virtsahappo, glukoosi, β-nikotiiniamidi adeniini dinukleotidi

Preface

I would like to thank Professor Tomi Laurila for providing me the topic for this thesis and my instructor D.Sc. (Tech.) Emilia Peltola for her guidance throughout this project. Huge gratitude goes to my mom for her endless support and urge. I would also like to thank Kari for his help at the end and my dearest friend Jonna for her help, peer support and alternatively taking my mind off from work. And last, but not least, Kjell, who every day puts a smile on my face.

This spring has been one of the happiest in my life.

Paippinen, 24.06.2016

Janessa Wahlström

Symbols and abbreviations

Symbols

A	electrode area
A_S	surface area
C	concentration
c_0	analyte concentration
C_d	double-layer capacitance
C_O	concentration of oxidized species
C_R	concentration of reduced species
D	diffusion coefficient
d_1	thickness of a single layer
δ	diffusion layer thickness
E	electrode potential
E_f^0	formal potential
E_w	potential difference between a working and a reference electrode
η	overpotential
F	Faraday constant
i	current
I_D	intencity of the D-band in Raman spectra
I_G	intencity of the G-band in Raman spectra
J	total flux
J_{diff}	diffusional flux
k^0	heterogenous electron transfer rate constant
k_b^0	heterogenous electron transfer rate constant for basal plane
k_e^0	heterogenous electron transfer rate constant for edge plane
L_a	basal plane width
L_c	edge plane width
n	number of electrons transferred
N	number of oxidized molecules
N_{layer}	number of layers
Q	integrated charge
R	universal gas constant
R_d	double-layer leakage resistance
R_s	solution resistance
R_{sh}	sheet resistance
ρ	density
σ	bulk conductivity
τ	sample thickness
v	electron transfer reaction rate
v_d	diffusional velocity
x	distance from electrode

Chemical abbreviations and formulas

Ag	silver
AgCl	silver chloride
Au	gold
$C_6H_6O_2$	hydroquinone
$C_6H_6O_3$	pyrogallol
CH_4N_2O	urea
CH_4N_2S	thiourea
CO	carbon monoxide
CO_2	carbon dioxide
Cu	copper
CuO	copper oxide
H_2O	water
H_2O_2	hydrogen peroxide
H_2SO_4	sulfuric acid
H_3NO	hydroxylamine
Hg/Hg_2Cl_2	saturated calomel
HNO_3	nitric acid
$K_4[Fe(CN)_6]\cdot 3H_2O$	potassium ferrocyanide
KCl	potassium chloride
$KClO_3$	potassium chlorate
$KMnO_4$	potassium permanganate
KOH	potassium hydroxid
MnO_2	manganese dioxide
$N_2H_4 \cdot H_2O$	hydrazine monohydrate
$NaBH_4$	sodium borohydride
$NaNO_3$	sodium nitrate
NaOH	sodium hydroxide
$NH_2OH \cdot H_2O$	hydroxylamine hydrochloride
NH_4OH	ammonium hydroxide
PbS	lead(II) sulfide
Pt	platinum
SiO_2	silicon dioxide
SiC	silicon carbide
TiO_2	titanium dioxide
ZrO_2	zirconium dioxide

Abbreviations

5-HT	serotonin
A	adenine
AA	ascorbic acid
AFM	atomic force microscopy
AFP	alpha-fetoprotein
APAP	acetaminophen
BET	Brunauer–Emmett–Teller surface area
BPPG	basal plane pyrolytic graphite
C	cytosine
CdS	cadmium sulfide
CDV	chemical vapor deposition
CEA	carcinoembryonic antigen
CND	carbon nitrite dots
CNT	carbon nanotube
C/O ratio	carbon to oxygen atomic ratio
CPE	carbon paste electrode
CRGO	chemically reduced graphene oxide
CSHM	chitosan/silica hybrid membrane
CV	cyclic voltammetry
DA	dopamine
DPV	differential pulse voltammetry
DOS	density of electronic states
DMF	N,N-dimethylformamide
DNA	deoxyribonucleic acid
dsDNA	double stranded deoxyribonucleic acid
EPPG	edge-plane pyrolytic graphite
ERGO	electrochemically reduced graphene oxide
FSCV	fast scan cyclic voltammetry
G	guanine
GABA	gamma-aminobutyric acid
GC	glassy carbon
GluOx	glucose oxidase
GO	graphene oxide
HET	heterogenous electron transfer
HI	hydriodic acid
HOPG	highly ordered pyrolytic graphite
HRP	horseradish peroxidase
Ig	immunoglobulin
LOD	level of detection
LSV	linear sweep voltammetry
MB	methylene blue
MIP	molecular imprinted polymers
MWCNT	multiwalled carbon nanotube
NAD	nicotinamide adenine dinucleotide
NADH	β-nicotinamide adenine dinucleotide

NMP	N-methyl-2-pyrrolidone
NP	nanoparticle
OX	oxidized species
PAMAM	poly(amido-amine)
PANI	polyaniline
PBS	phosphate buffered saline
PD	polydopamine
PEI	polyethyleneimine
PFIL	polyethylenimine-functionalized ionic liquid
PDDA	Poly(diallyldimethylammonium chloride)
PPy	polypyrrole
PSS	polysodium 4-styrenesulfonate
RED	reduced species
SC8	p-sulfonatocalix[8]arenes sodium
SCE	saturated calomel electrode
SEM	scanning electron microscopy
SHE	standard hydrogen electrode
SPE	screen printed electrode
ssDNA	single stranded deoxyribonucleic acid
STM	scanning tunneling microscopy
T	thymine
TEM	transmission electron microscopy
TNF-α	tumor necrosis factor-alpha
TPP	tetraphenylporphyrin
TRGO	thermally reduced graphene oxide
UA	uric acid
XPS	X-ray photoelectron spectroscopy

Contents

1 Introduction

Selective, sensitive, fast and inexpensive method to detect biomolecules is an important objective in clinical diagnostics. Measuring the concentration of different analytes such as neurotransmitters, hormones, proteins and vitamins is essential in understanding the functions of human body and provides insight about *e.g.* exocytosis and drug delivery, human behavior and disorders [1]. Electrochemical measuring provides a simple and inexpencive alternative to monitor even small concentration changes with a fast responce time and even in the presence of other interfering substances in human body. Electrochemical measuring is based on a biological event converted to an electrical signal with an electrode. Electrodes convert a current in the body carried by ions to a current in the electrode and its lead wire carried by electrons. The electrode provides a platform for oxidation or reduction process which in turn results in potentials or currents that can be measured. The measured potential or current is proportional to the concentration of a compound in a surrounding medium. Electrochemical measuring techniques are simple, inexpensive and can provide high spatial and temporal resolution [2].

Different carbon nanostructures such as carbon nanotubes and carbon nanofibers are widely used as an electrode material because of their low cost, chemical stability, large surface area and low levels of detection. The surface of carbon materials are also easily modified [3]. The recently discovered member of carbon based material is graphene which consists of carbon atoms bonded by sp^2 bonds in a hexagonal form. Graphene is a two-dimensional sheet with a large surface area, high thermal and electrical conductivity, mechanical strength and elasticity [3]. Multiple layers of stacked graphene forms graphite and the interesting properties of graphene was first discovered year 2004, after 60 years of research and since then, research about graphene has increased remarkably [3].

Graphene has raised interest among electrochemical researchers because of the low material cost of graphite as a source material, biocompatibility and lack of metallic impurities compared to widely used carbon nanotubes. Metallic impurities are electrochemically active and lead to distorted conclusions in many cases even at low levels [3]. Graphene has interesting properties for electrochemical sensing, which furthermore can be altered many ways such as exposing electric and magnetic fields, as well as varying dimension, number of layers and surface chemistry. Mass production of high quality graphene is a rather complex task but fabricating graphene like material with similar electronic and mechanical properties via oxidation and reduction has proven to be a simple and inexpensive method, due to low material cost of graphite and the reagents. The most common oxidation method is the Hummers method, which uses sodium nitrate, sulfuric acid and potassium permanganate solution. Oxidation inflicts oxygen bearing functional groups to the surface of graphite. Graphite oxide is then exfoliated usually by sonicating and stirring in water to obtain few or single layer graphene oxide. Oxidation results in diminished electrical conductivity. Electrical conductivity is an essential characteristic for a material used in electrochemistry, which is why the weaker electrical conductivity of graphene oxide is restored by reduction. Reduction ideally removes the oxygen

functional groups and repairs the structural defects caused by the oxidation prosess. However different oxygen bearing functional groups and defects increase the electron transfer rate between the electrode and the solution, which is why a satisfactory compromise should be found. Reduction is most commonly done chemically with reductants such as hydrazine hydrate or sodium borohydride for electrochemical sensing purposes because of its simplicity and low cost. Chemical reduction does not result in the highest electron transfer rate compared to other common reduction methods. However the electrochemical properties of chemically reduced graphene oxide can be easily enhanced with different surface modification methods.

The aim of this work is to review electrochemical detecting with chemically reduced graphene oxide in bioapplications, to find similarities and differences between the electrochemical properties of often structurally complex sensors and to compare various techniques for improving selectivity based on rather controversal research from this field. This Master's thesis first briefly describes the basics of electrochemical measuring. The most common electrochemical measuring technique is voltammetry, where the current is measured as a function of the applied potential. The establishment of the electrode potential and mass transport phenomenon are presented as well as the difference between electrochemical sensors and biosensors with their basic principals and requirements for bioapplications. Thesis then introduces the main electrochemical analytes such as neurotransmitters, glucose, β-nicotinamide adenine dinucleotide (NADH) as well as the main interfering compounds in electrochemical measuring such as ascorbic acid and uric acid. The main neurotransmitters in this work are dopamine and serotonin since they are related to several common neurological diseases such as Parkinson's disease, Alzheimer's disease and depression. Glucose on the other hand is related to diabetes, which is one of the leading causes of death and NADH is a common dehydrogenaze related molecule in human body. The structure and the characteristics of graphene are then presented and the fabrication methods of graphene are compared with electrochemical measuring borne in mind. Hence oxidation followed by reduction is a simple method to produce pristine graphene like material with superior electrochemical properties, different reduction methods are described. Chemically reduced graphene oxide contain enough oxygen functional groups and defects for electrochemical detection, which is why it is a potential candidate for an electrochemical sensor or biosensor material. Different surface modification methods are then evaluated and electrochemical properties and selectivity compared during the detection of various analytes.

2 Electrochemical measuring

Electrochemical measuring is based on applying a potential or current to an electrode immersed in a solution and monitoring the resulting current or potential. The measured current or potential results from oxidation or reduction of an electrochemically active compound at the surface of the electrode. During oxidation electrons transfer from the solution to the electrode material. During reduction electrons flow from the electrode material to the solution. In order for the oxidation or reduction to take place the molecules of interest have to be in physical contact with the electrode. The electrode is either oxidizing or reducing depending on the applied potential or current and the level of the applied potential or current can be controlled. The measured current or potential is proportional to the concentration of a compound in a surrounding solution and to the rate of diffusion of the compound from the solution to the electrode/solution interface [4]. Each compound has its unique potential window for oxidation and reduction, which also depends on the electrode material [2]. The most common electrochemical measuring methods are voltammetric techniques, where the current is measured at a constant potential as a function of time or varying potential and measuring the current as a function of potential. Voltammetric methods are simple, sensitive and inexpensive for electrochemical detection.

2.1 System of measurement

Electrochemical measuring is usually conducted with three electrodes but can also be done with only two. The three electrode measuring system consists of:

- a reference electrode
- a counter electrode (also referred as auxillary electrode) and
- a working electrode (also referred as sensing or redox electrode).

The reference electrode and the working electrode separated by an electrolyte forms an electrochemical cell. The electrolyte used in bioapplications is commonly either a physiological solution such as an extracellular fluid or a phosphate buffered saline (PBS). An absolute potential value of a single electrode cannot be measured but a potential difference between the electrochemical cell can be measured with a voltmeter or controlled with an external power supply [2]. The working electrode is located at the reaction site and the reference electrode further from the reaction site. As electrochemical measuring is most commonly conducted voltammetricly by varying the applied potential rather than the current, varying potential causes electrons to transfer between the solution and the electrode and produces a flow of current. Since the reference electrode is at a stable potential, all changes in the potential of the electrochemical cell corresponds to changes in the working electrode potential so the working electrode is basically a transducer in the reaction and no current flows through the reference electrode [2]. A schematic illustration of an electrochemical experiment (voltammetricly) with a potential step pulse and the corresponding current *vs*. time curve is presented in Figure 1.

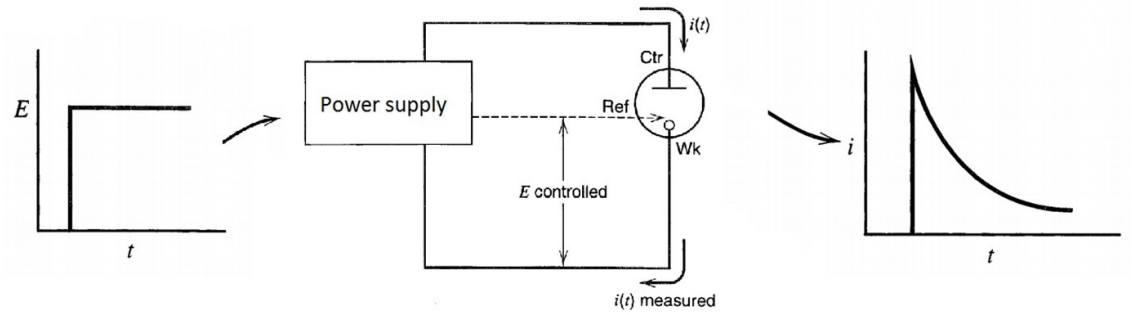

Figure 1: A schematic illustration of an electrochemical experiment (voltammetricly) with a potential step pulse and a corresponding current *vs.* time curve. Ctr is the counter electrode, Wk is the working electrode and Ref is the reference electrode. Modified from [2] and [4].

The counter electrode forms an electric circuit with the working and the reference electrode. The counter electrode passes the same current as the working electrode and provides a possibility for a controlled potential to be applied to the working electrode [5]. The counter electrode also prevents large currents from flowing through the reference electrode which is why the size of the counter electrode is usually significantly larger than the working electrode [2]. The counter electrode is separated from the working electrode and it can be any convenient electrode which does not interfere the behavioural of the working electrode by producing substances that could reach the detection site [2].

The reference electrode is usually a silver-silver chloride (Ag/AgCl) electrode [6]. The Ag/AgCl electrode is easy to fabricate and it consists of a Ag metal coated with a layer of AgCl. Ag/AgCl electrodes are rather stable in biological applications. Addition of the AgCl layer also decreases the electric noise [7]. Another commonly used reference electrode is a saturated calomel electrode (Hg/Hg_2Cl_2, SCE). SCE consists of a glass tube filled with a calomel paste and a saturated potassium chloride (KCl) solution [7]. Standard hydrogen electrode (SHE) can be used as the primary reference electrode for other reference electrodes. Working electrodes are described in more detail in the following chapter.

2.2 Voltammetric methods

As mentioned earlier voltammetric methods are based on measuring the current while applying a potential pulse, potential sweep or constant potential. The measured current is proportional to the concentration of the analyte. The obtained current as a function of potential curve is referred as a voltammogram. The speed of the redox (*i.e.* oxidation and reduction) reaction and redox potentials and corresponding currents can be evaluated from the shape of the curve.

Cronoamperometry is a simple potential pulse method. The working electrode is first held at a resting potential at which no oxidation or reduction takes place. Then the potential is stepped to a larger value to oxidize or reduce. Afterwards the

potential is stepped back to the initial value and the species that were oxidized reduces back or the species that were reduced oxidizes [2]. Cronoamperometry is usually used in measuring the stability of the analytes [8]. Constant-potential amperometry on the other hand is based on a constant potential. The level of the potential is large enough to oxidize or reduce the measured compound or molecule at the surface of the working electrode [8]. The method cannot be used in identifying the analytes, although the method is fast when measuring a known analyte [2]. Diagram of the potential pulse used in constant potential amperometry, chronoamperometry and the corresponding current *vs.* time diagrams are presented in Figure 2A and B. The time resolution of both amperometric methods is high with a sampling rate in kHz range, which results in signal detection in a submillisecond timescale [8]. Amperometric methods are especially suitable for measuring secretion from cells [2] but less practical in measuring concentrations at a resting state [8] because of a nonzero background signal from a charging current [2]. The charging current originates from changing the electrode surface potential [2]. However the charging current decays exponentially after the potential step [2].

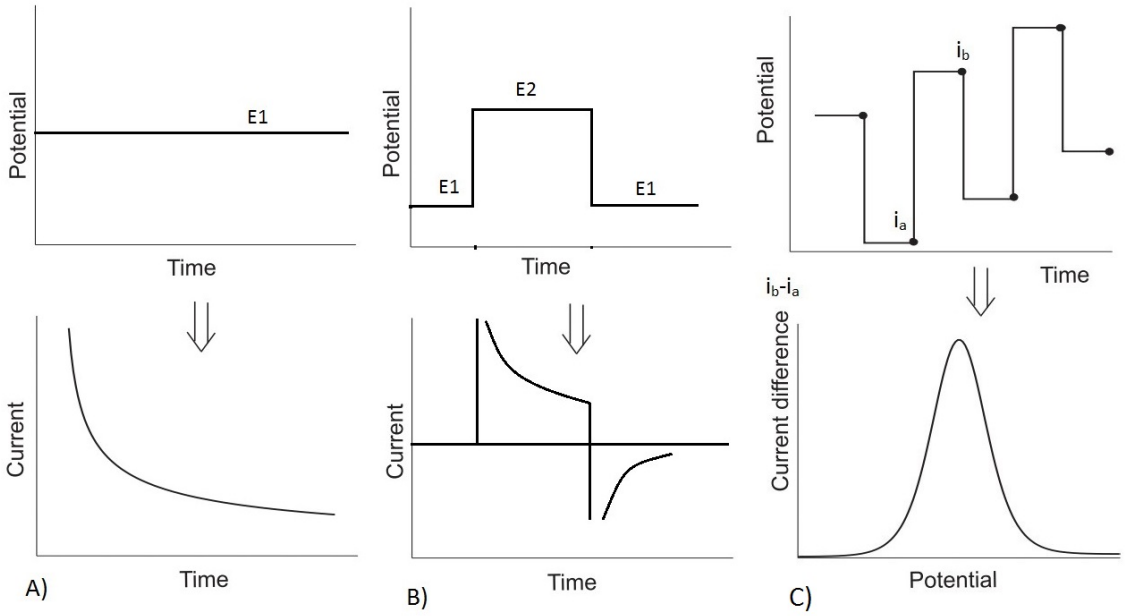

Figure 2: A) Diagram of a constant potential in constant potential amperometry and B) potential pulse in chronoamperometry and the corresponding current *vs.* time diagrams. C) Diagram of a potential pulse used in differential pulse voltammetry and differential pulse voltammogram. Modified from [2, 4, 5].

Normal pulse voltammetry (NPV) is also a potential pulse method. NPV is based on a series of potential pulses with varying potential values and after each pulse the potential is stepped back to the initial value. The current is measured before and after each pulse and is proportional to the concentration of the analyte. The difference between these two measured currents forms a plot of current as a function of potential. In differential pulse voltammetry (DPV) the potential is not

fully stepped back to the initial value which makes the method more sensitive and rapid compared to NPV and decreases the charging current between the pulses [2]. The signal is a small amplitude (typically 25 mV) square wave [8]. Diagram of the step potential pulse used in DPV and the corresponding voltammogram is presented in Figure 2C. DPV can be used in detecting multiple compounds provided that their oxidation potentials varies more than 100 mV [8]. However the method is relatively slow compared to other voltammetric methods, because the duration of one scan is typically more than 30 seconds [8].

Linear sweep voltammetry (LSV) and cyclic voltammetry (CV) are potential sweep methods and common in electrochemical measuring of biological analytes. In LSV the potential is linearly swept and in CV the potential is first swept to a specific potential and then swept back to the initial potential. During the first sweep the potential exceeds the oxidation or reduction potential and during the second sweep the oxidized compounds reduces or the reduced compounds oxidizes [2]. The oxidation and reduction currents are constantly measured during the sweeps. CV is faster than DPV, which results in more easily distinguished voltammogram of different analytes. Diagram of the sweep potential pulse in LSV and CV as well as the corresponding voltammograms is presented in Figure 3A and B, where diagram a is a reversible reaction, b quasi-reversible reaction and c irreversible reaction. In reversible reaction the electron transfer rate between the electrode and the solution is faster than the rate of mass transport from the solution closer to the surface of the electrode [9]. In quasi-reversible reaction the rate of electron transfer is comparable to the mass transport rate and in irreversible reaction the electron transfer rate is smaller than the mass transport rate [9].

Fast scan cyclic voltammetry (FSCV) uses a multiple sweep potential pulses usually during a minute long measurement. Scan rate is fast, typically 400 V/s [1], in order to improve temporal resolution and selectivity. The duration of the pulse can be *e.g.* 10 ms and the pulse is repeated at intervals of 100 ms [8]. Between each sweep the potential is typically held at a negative value. FCSV signal has a background current that needs to be eliminated by substraction, which removes the unwanted components from the signal [1]. FSCV can be used in detecting multiple compounds simultaneously such as *e.g.* measure dopamine concentration and monitor changes in O_2 and pH [1]. Diagram of the sweep potential pulses in FSCV and the corresponding voltammogram is presented in Figure 3C.

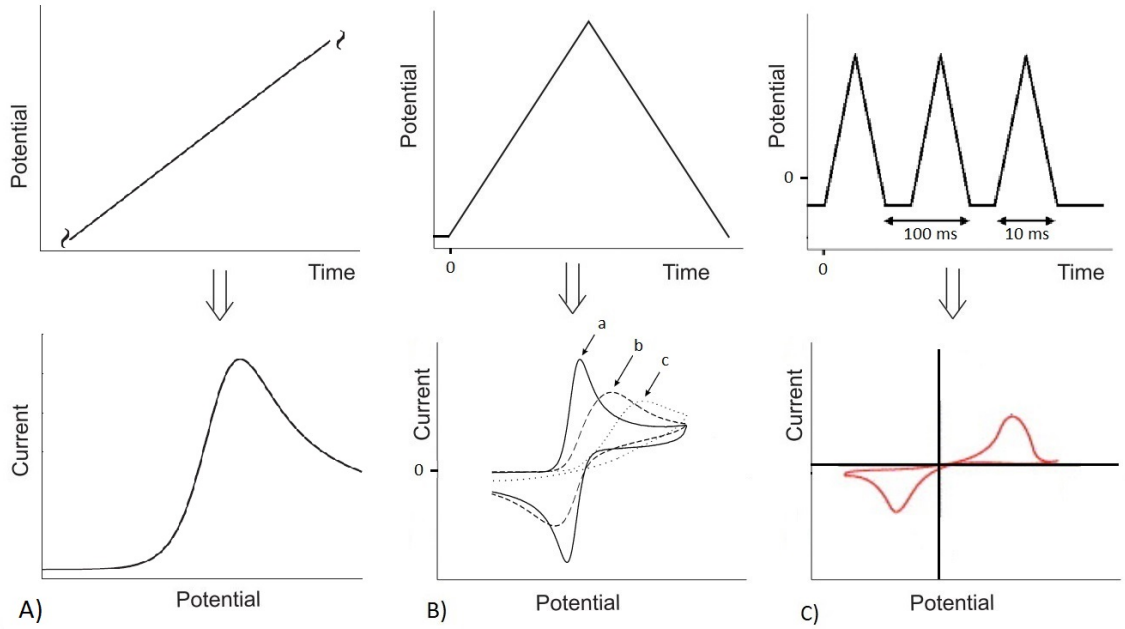

Figure 3: Diagram of a potential sweep pulse used in A) LSV and B) CV and the corresponding voltammograms, where a) is reversible, b) quasi-reversible and c) irreversible reaction. C) Multiple potential sweep pulses used in FSCV and the corresponding voltammogram. Modified from [5, 2, 10, 9].

3 Electrodes

Electrochemical sensing is based on establishing the electrode potential and the kinetics between the electrode (*i.e.* working electrode) and the aqueous solution containing ions. The solution can be *e.g.* blood, urine, extracellular fluid or PBS. Electrochemical reaction of interest occurs at the surface of the working electrode immersed in the solution. The electrode potential is established and changing the potential during voltammetric measurement with an external power supply causes a current to flow. The current induced by the applied potential is mainly proportional to the rate of mass transfer from the solution to the surface of the working electrode and the rate of electron transfer between the surface of the working electrode and the solution. [4]. The rate of mass transfer is related to the concentration of ions in the solution and ultimately determines the magnitude of the measured current. The following subchapters describe the establishment of the electrode potential and how the current is related to the concentration of ions in theory.

3.1 Electrode potential

At the electrode/solution interface chemical reactions *i.e.* oxidation and reduction of atoms at the surface of the electrode, and anions and cations in the solution takes place [7]. An atom at the electrode interface oxidizes and forms a cation into the solution and releases electrons which remain at the electrode [7]. Alternatively the anions at the solution oxidizes at the interface to a neutral atom and releases electrons to the electrode [7]. Both of these reactions can be reversible and occur the opposite way referred as reduction [7]. Reduction and oxidation at the electrode/solution interface can be presented with the following equation:

$$OX + ne^- \longleftrightarrow RED, \tag{1}$$

where OX and RED are oxidized and reduced species and n is the number of electrons (e) transferred. [4, 5]

Electrode surface is at electrochemical equilibrium when the rates of oxidation and reduction are equal (*i.e.* 50 % of the species are reduced and 50 % oxidiced) [4]. Electrons are charged particles so if the reaction in equation (1) before equilibrium occurs to the left, the electrode will have a negative charge at equilibrium and the solution will have an equal magnitude of positive charge and vice versa [4]. Therefore in equilibrium the net charge transfer is zero across the interface [7]. Charged species form an electrical double layer on the electrode/solution interface. In other words a charge separation exists between the electrode and the solution and therefore also a potential difference called the half cell potential E is established. Half cell potential depends on the electrode material, the concentration of ions in a solution and the temperature [7]. Half cell potential for a single electrode/solution interface is given by the Nernst equation:

$$E = \phi_M - \phi_S = E_f^0 + \frac{RT}{nF} ln \frac{C_O}{C_R}, \tag{2}$$

where ϕ_M is the electrical potential of the metal electrode and ϕ_S is the electrical potential of the solution, E_f^0 is the formal potential, R is the universal gas constant, T is the absolute temperature, n is the number of electrons transferred and F is the Faraday constant. C_O is the concentration of the oxidized species and C_R is the concentration of the reduced species. E_f^0 is constant at a given temperature and pressure and can be derived from standard electrode potential and activity coefficients of the reduced and oxidized species. [4, 5] Standard electrode potential is the electrode potential difference compared to SHE because the half cell potential of SHE is zero at all temperatures. For example standard electrode potential for Ag/AgCl electrode is +0.197 V vs. SHE and for Hg/Hg_2Cl_2 electrode +0.242 V vs. SHE. [4] At equilibrium $E = E_f^0$ since $C_O = C_R$.

As mentioned earlier electrode potential of a single electrode cannot be measured experimentally so an additional reference electrode is introduced. The potential difference E_w between the working and the reference electrode is presented with the following equation:

$$E_w = (\phi_M - \phi_S)_{working} - (\phi_M - \phi_S)_{reference}. \tag{3}$$

Since $(\phi_M - \phi_S)_{reference}$ is constant, changes in E_w result directly from changes in the working electrode potential [5]. The rates of oxidation and reduction are equal when the potential applied to the working electrode corresponds to the equilibrium half cell potential (when $E = E_f^0$) and so the reaction is in dynamic equilibrium and no current flows [5]. When the applied potential changes, a current starts to flow and the electrode is said to polarize [7]. Applying more negative potentials than the equilibrium potential induces coulombic repulsion and electrons transfer from the electrode surface to the surrounding solution. A reduction reaction dominates and a catodic current is measured. Applying more positive potentials than the equilibrium potential attracts electrons from the solution to the electrode surface. Oxidation dominates and an anodic current is measured. [2] During reduction C_O decreases and C_R increases at the electrode surface and vice versa for the oxidation [4].

The degree of polarization is called an overpotential η. The overpotential is the difference between the half cell potentials at equilibrium and when the current flows. The overpotential is divided into ohmic, concentration and activation overpotentials. The ohmic overpotential results from the resistance of the electrolyte which causes a voltage drop (also referred as an iR drop). The concentration overpotential results from the concentration differences in ions at the electrode/solution interface when the current flows. The activation overpotential is related to the difference in the activation energy needed for the oxidation and reduction reactions. The total applied potential to pass the current is presented with the following equation:

$$E_{tot} = E_w + \eta \tag{4}$$

Equation (4) shows that more energy is needed for the reduction and oxidation because overpotential tends to resist the reactions. [7, 11]

3.2 Mass transport

In order for the electrons to flow, the electroactive species must transfer close enough to the surface of the electrode [5]. A schematic illustration of the mass transport is presented in Figure 4. Mass transport can be divided into diffusion, migration and convection [11]. Diffusion is a mass transport phenomenon where molecules transfer from high concentration regions to low concentration regions *i.e.* down the concentration gradient. The speed of molecules diffusing to and from the electrode determines the rate of the oxidation and reduction [2]. The aim of migration of electrically charged species is to disperse the charge formed during the establishment of the electrode potential. Migration can be directed towards the surface of the electrode or towards the solution and in the opposite or the same direction as the diffusional flux [5]. Direction of the migration depends on the sign of the charge at the electrode surface and the charge of the electroactive species [5]. Migration phenomenon is significant especially in solutions of low concentration whereas it can be neglected in high concentration solutions [5]. On the other hand transport by convection can also affect the distribution of electroactive species in the solution. Convection occurs due to internal or external forces and it can be exploited because sensitivity enhances due to increased rate of the reaction [5]. Electrochemical measuring is usually conducted in less than 5 minutes because of the effect of natural convection [11].

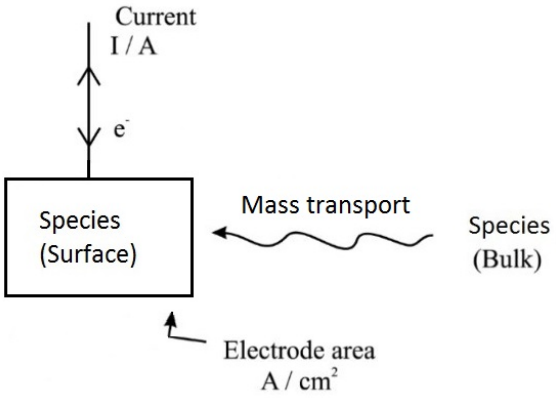

Figure 4: Mass transport of electroactive species. Modified from [5].

The current i is related to mass transport *i.e.* the rate of the concentration change at the electode surface by the following equation:

$$i = nF\frac{dC}{dt}, \tag{5}$$

where n is the number of electrons transferred, F is the Faraday constant, C is the concentration and t is the time. Concentration flux J is the rate of concentration change per electrode area A according to the following equation:

$$AJ = \frac{dC}{dt}, \tag{6}$$

where the total flux J is a sum of the diffisional, migrational and convectional fluxes. Combining equations (5) and (6) results in the following equation for the current:

$$i = nFAJ, \tag{7}$$

where current is proportional to the total flux and the surface area of the electrode. [11]

When the potential is applied during voltammetric measurement, the concentration of the analyte quickly decreases at the surface of the electrode. Diffusion of analytes to the surface of the electrode is described by Fick's first law, which corresponds to a change in concentration with location and is described with equation (8).

$$J_{diff} = -D\frac{dC}{dx}, \tag{8}$$

where J_{diff} is the diffusion flux ($mol\ m^{-2}\ s^{-1}$), D (m^2/s) is the diffusion coefficient, C is the concentration, and x is the distance from the electrode surface [2, 4]. Mass transport by convection and migration are usually ingnored with high concentration solutions so only diffusion is concidered (*i.e.* J = J_{diff}) [11]. Combining equations (7) and (8) gives the following equation for the current:

$$i = nFAD\frac{dC}{dx}. \tag{9}$$

Concentration gradient changes over time t and becomes less steep as the amount of analyte decreases during the measurement according to Fick's second law of diffusion for planar electrodes:

$$\frac{\partial C}{\partial t} = -\frac{\partial J_{diff}}{\partial x} = D\frac{\partial^2 C}{\partial x^2}. \tag{10}$$

Equation (10) yields the following Cottrell equation for planar electrode when a potential step pulse is applied:

$$i(t) = nFAc_0\sqrt{\frac{D}{\pi t}}, \tag{11}$$

where c_0 is the analyte concentration at a Nernst diffusion layer thickness apart from the electrode surface [2, 5]. The Nernst diffusion layer is a layer where the concentration of the analyte differs from the concentration of the bulk solution. According to the Cottrell equation the current decays to zero over time. [11]

Another important parameter in addition to the current is the number of consumed molecules during the oxidation or reduction prosess. The number of consumed molecules at a certain time for the planar electrode using the potential step pulse can be calculated with the help of charge Q, which is obtained by integrating Cottrell equation (11) with respect to time [2]. The following equation yields the number of moles of reactant N:

$$N = \frac{Q}{nF} = 2A\sqrt{\frac{Dt}{\pi}}c_0, \tag{12}$$

Thickness of the diffusion layer (δ) and velocity of the diffusion (v_d) are also interesting parameters concerning electrochemical measuring. An approximation of a diffusion layer thickness at time t can be estimated with the following equation:

$$\delta(t) = \sqrt{2Dt} \tag{13}$$

and diffusion velocity with the following equation:

$$v_d(t) = \frac{\delta}{t} = \sqrt{\frac{2D}{t}} \tag{14}$$

[4]. Equations (13) and (14) indicates that over time the diffusion layer thickness increases and the rate of diffusion decreases.

The current induced by the applied potential is also proportional to the rates of other chemical reactions on the surface of the electrode before or after the electron transfer [4]. Also other nonfaradaic (*i.e.* no charge crosses the interface) surface reactions such as adsorption, desorption or crystallization affect the mass transport phenomenon because the current can flow due to changes in electrode area or solution composition [4].

3.3 Electrode structure

The electrode material, surface chemistry, and dimension influence the performance of the electrodes used in electrochemical measuring [6]. Electrodes should be small in size, selective enough and sensitive to detect even small concentrations from a biological environment. Also the resistance of the solution must be low enough in order for the electrochemical reaction to be detected [4]. Electrochemical sensors can detect electrochemically active compounds whereas electrochemical biosensors contain an additional biological recognition element immobilized on the surface of the electrode for the detection of electrochemically inactive compounds.

3.3.1 Electrode circuit model

Electrical characteristics of a metal electrode immersed in a solution can be described with a double-layer capacitance C_d and a parallel leakage resistance R_d accross the double layer. R_d is the sum of charge transfer resistance and mass transport resistance [12]. Solution can be described with a series resistance R_s, which causes a drop in the applied potential. Equivalent circuit for a metal electrode is precented in Figure 5. The values of these components are determined by the material and geometry of the electrode and the characteristics and concentration of the solution [4, 7]. Impedance of the electrode depends also on the frequency and the surface area of the electrode [7]. Impedance of the reference electrode is usually neglected, because larger surface area results in larger capacitance and smaller resistance [12].

3.3.2 Electrochemical sensors

Electrochemical sensors are developed in demand of an inexpensive and simple method to detect biomolecules. They usually are sensitive and have a fast response

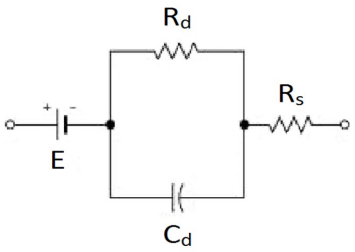

Figure 5: Equivalent circuit for a metal electrode where E is the half cell potential, R_d is the resistance accross the double layer, R_s is the resistance caused by the solution and C_d is the double-layer capacitance [7].

time. A basic electrode for electrochemical measuring is a fine metal wire or a fiber which is fully insulated except for the exposed tip of the electrode [7]. An insulator is basically a film of a polymeric material [7]. The metal used as an electrode material should be electrically conductive [7]. Common electrochemical sensor materials are solid metals such as gold, platinum, tungsten and aluminium and various forms of carbon-based materials and semiconductors such as silicon [4, 13]. An example of a basic insulated metal needle electrode is precented in Figure 6.

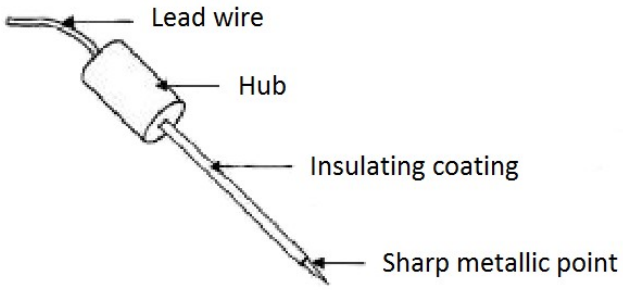

Figure 6: A basic insulated metal needle electrode [7].

Carbon-based materials are widely used as an electrode material because of low cost, chemical stability, good electron transfer kinetics, biocompatibility, wide potential window, low background current and the ability of surface structure modification [7, 13, 14]. Common carbon-based electrodes are *e.g.* glassy carbon (GC), doped diamond, carbon fibers and carbon nanotubes (CNTs) [7]. Carbon can also be made nanometer scale in size and has a high mechanical strength [2, 15]. Nanometer size carbon electrodes have a large surface-to-volume ratio and carbon has been proved to reduce electrode fouling [7].

Electrochemical sensor can be coated with different protective layers or deposited with nanoparticles (NP). Protective layers decrease electrode fouling and can increase selectivity. For excample Nafion, phenylacetate, conducting polymers such as polypyrrole and its derivatives are used as protective layer [13]. NPs can be made of *e.g.* metals (Au, Ag, Pt), oxides (SiO_2, TiO_2, ZrO_2, MnO_2), or semiconductors (CdS, PbS) [16]. NPs are used in increasing the surface area of the electrode which increases the measured current [13]. NPs are also used in enhancing the electrochemical

reaction by decreasing the potential required for the redox reaction of the molecule of interest [16, 14]. NPs increase the electron transfer rate between the electrode and the solution [16, 14]. NPs are usually charged particles so they can absorb other charged biomolecules from the solution [16]. NPs are usually 1-100 nm in diameter and biocompatible [16]. Dendrimers (*i.e.* symmetric and branched macromolecules) such as poly(amido-amine) (PAMAM) can also be used. The branched structure increases the interaction between the molecule of interest and the electrode. PAMAM dendrimer is biocompatible [17] and can also be used with NPs *e.g.* in order to gain more even distribution [18].

3.3.3 Electrochemical biosensors

Electrochemical biosensors are electrochemical sensors with an additional biological recognition element attached. Electrochemical biosensors can be divided into three main categories: enzyme biosensors, immunosensors and DNA biosensors [19, 20]. A schematic illustration of the electrochemical biosensors are presented in Figure 7. Enzyme biosensors are based on enzymes (Figure 7A) and DNA biosensors are based on DNA probes (Figure 7B) immobilized on the surface of the electrode whereas immunosensors are based on the antigen–antibody interaction (Figure 7C). Biological recognition element can be attached to the surface of an electrode *e.g.* covalently, by absorption or with NPs [16].

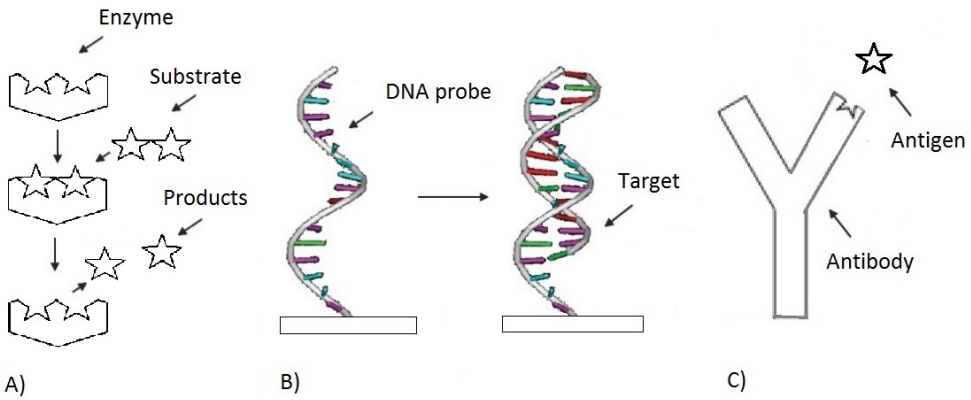

Figure 7: Electrochemical biosensors based on: A) enzyme/substrate interaction, B) DNA hybridization and C) antigen/antibody interaction.

The most commonly used enzymes in electrochemical **enzyme biosensors** (Figure 7A) are glucose oxidase (GluOx) and horseradish peroxidase (HRP) [6]. Enzymes can be *e.g.* encapsulated or covalently immobilized on the surface of the electrode [6]. Enzymes undergo the following reactions when immobilized on the surface of the electrode:

$$substrate_{RED} + enzyme_{OX} \longrightarrow product_{OX} + enzyme_{RED}, \tag{15}$$

$$enzyme_{RED} + co{-}substrate_{OX} \longrightarrow enzyme_{OX} + co{-}product_{RED}, \tag{16}$$

where RED refers to the reduced and OX the oxidized form [2]. Enzymes form an electrochemically active compound ($co{-}product_{RED}$) which can be oxidized and detected at the electrode surface [2]. Electrochemical enzyme biosensors are sensitive and versatile but are usually unstable [21]. Enzymes are expensive and the immobilization is complex because the enzyme has to remain stable and active after the immobilization [21]. Also the activity of the enzymes can be influenced by temperature, humidity and pH [15, 21] which results in deterioration of the activity of the enzyme over time and thus limiting the lifetime of the electrode commonly to 2-8 weeks [6].

Electrochemical **immunosensors** (Figure 7C) can be designed to function two ways: either the antigen or the antibody can be immobilized on the surface of the electrode [22]. Usually the antigen is the target analyte and the antibody is located firmly on the surface of the electrode. The antibody is Y-shaped and can be divided into nonbinding and binding parts. Immunosensors are highly accurate, specific and selective because the antibodies are analyte specific hence recognises only one antigen [23]. Glycoproteins such as immunoglobulins (Ig) can be used as antibodies and the specificity depends on the amino acid sequence of the antibody [23].

Immunosensors are simple, inexpencive and fast. Although the immobilization of antibody on the surface of the electrode is critical because the functionality of the antibody is preferred to remain undisturbed which ultimately affect the sensitivity and dynamic range of the electrode [23]. The activity of the antibody depends on their orientation and they are sensitive to the environment [6]. Immobilization can be done by covalent binding, physical adsorption or by trapping antibody electrically or physically with a polymer matrix such as polypyrrole or polyaniline [6, 23]. NPs can also be used in immobilization [16]. However antibodies and antigens are not usually electrochemically active so an addition of an electroactive compound such as an enzyme is still required [23]. The enzyme is coupled to a secondary antibody and an enzymatic reaction generates an electrical signal [6].

DNA biosensors (Figure 7B) are simple, selective, sensitive, fast and inexpensive. DNA biosensors can be used in detecting specific target DNA sequences such as four free DNA bases, guanine G, adenine A, thymine T and cytosine C or mutated genes in single stranded DNA (ssDNA) and double stranded DNA (dsDNA). [24, 22] DNA biosensors senses DNA hybridization with an immobilized DNA probe. ssDNA or dsDNA can be used as a DNA probe [22] but also a sequence of a DNA or RNA oligonucleotide, called an aptamer, can bind to various molecules [6]. Aptamers are easily immobilized, reproducible, have longer life span than antibodies and higher attraction and specificity to target molecules [6]. DNA probe can be immobilized with NPs or NPs can be used as labels in the DNA probes to enhance hybridization or enable simultaneous detection of different DNA sequences [16].

Molecular imprinted polymers (MIP) are artificial recognition elements. Since biomolecules such as enzymes and antibodies are relatively unstable as a recognition element both chemically and physically, MIPs offer a stable, durable, man-made recognition element for electrochemical biosensors [25]. MIPs are moulded to match the shape of the molecule of interest, since molecules tend to drift towards surfaces with similar fitting shapes, which makes MIPs selective to a specific target

molecule [25].

3.4 Requirements for bioapplications

The most essential characteristics of an electrochemical sensor for bioapplications are selectivity and sensitivity [13]. Extracellular fluid contains high concentrations of other electroactive species that interfere with the measurement. Selectivity and sensitivity are usually improved with different surface modifications such as layers or NPs. Successful detection in a submillisecond time scale also requires a **fast response time**. The responce time can be improved with an electrode material with fast electron transfer properites.

Electrodes used in electrochemical sensing should be **conductive** and **chemically stable** which is why platinum, gold, carbon and silicon are commonly used [6]. Wide potential window on the other hand allows several analytes to be detected simultaneously. Chemically inert materials are not easy to oxidize so the current induced originates primarily from the oxidation or reduction of ions in the solution. When using metal electrodes the electrode material and the part of the lead wire which is in connection with the electrolyte should be made of same metal [7]. Different metals have different half cell potentials with the electrolyte which increases electric artifact and may result in corrosion of one of the metals [7]. This can be avoided by insulating the electrode and the lead wire with a layer of *e.g.* a polymeric material.

High surface area and **small size** decrease the effect of surroundings to the electrical properties of the electrode [6]. Higher surface area on the other hand provides more area for the desired species to diffuse [26]. High surface area also decreases the electrode impedance [7], which leads to increased signal-to-noice ratio [26]. The electrode must be able to fabricate small enough for the detection of endocytosis, exocytosis and blood-brain barrier transfer [27]. The small nanometer scale size of the electrodes increase the sensitivity because the difference between the size of the biologically important compound and the electrode is smaller [6]. Implantation of smaller diameter electrodes also induce less tissue or cellular damage which might cause inflammation and foreign body responce [7, 14]. The small electrodes can be placed much closer to the measurand in order to gain high temporal resolution, fast responce time and better selectivity because biochemical events of interest usually occur on a ms time scale [7, 13].

In addition to small size the electrodes should be **mechanically strong** enough to be implanted and still remain mechanically stable [7]. Lateral dimension also influence the deformability of the electrode which is important because the electrode must be capable to undergo torque cellular forces [27]. The electrodes should also have capacity for long term implantation for continuous monitoring of biologically important metabolites which would highly benefit the monitoring of *e.g.* glucose in diabetic patients [14].

The most important characteristics limiting the measurement accuracy is **noise and distortion**. Particularly using nanoelectrodes signal smoothing usually loses information so traditional voltammetric methods are useless [14]. When implanting an electrode an electrical double layer is formed at the electrode/solution interface.

The movement of the electrode with respect to the solution disturbs the layer of charge which results in a change in the half cell potential of the electrode. The disturbance is called motion artifact and causes severe interference and thus should be minimized by a careful and stable implantation [7]. The motion artifact can also be decreased with the use of electrodes with greater plasticity and flexibility [7] .

Electrochemical reaction is influenced by **chemical reactions** in the solution because chemical reactions alter the concentration of the solution [5]. If the chemical reactions include water near the electrode/solution interface local activity of hydrogen and hydroxyl ions changes which leads to changes in acidity or alkalinity [7]. These changes may result in tissue damage. An electrolysis of water due to electric current may lead to small bubbles of hydrogen or oxygen gas which should also be avoided [7].

Adsorption of impurities or electrochemically active species also affect the surface properties of a solid electrode [4]. Biological solution in the body include high molecular weight proteins, lipids and peptides. Adsorption of these electrochemically inactive species is common. The absorption forms a blocking or a partially blocking layer on the surface of the electrode which leads to electrode fouling and distortion of the detected signal [13, 4]. Adsorption may even enhance the reactivity of some species [13, 4]. Due to adsorption the electrochemical response of the electrode changes over time and the time is proportional to the rate of the diffusion of the species from the solution to the electrode surface [13, 4]. Electrode fouling also decreases the sensitivity of the electrode.

Adsorption of electrochemically active species can alter the energy needed for the oxidation or reduction so that adsorbed species may be problematic to *e.g.* reduce compared to the same species in a solution near the electrode [4]. Adsorbed oxygen or hydrogen layers are usually formed on metal surfaces which can be desorbed by applying a potential step pulse [4]. The applied potential step pulse renews the surface *e.g.* by reducing the formed oxygen layer [4]. The observed background current due to the oxygen or hydrogen formation is also related to pH and composition of the solution which is why the properties of different electrodes are not easily comparable [28]. In conclusion small background current lead to a wider potential window, meaning larger potentials can be applied before electrode fouling [28]. Electrode fouling can be decreased with a fast measurement such as FSCV and different selective surface layers that repel the adsorption of impurities [13]. However selective layers might decrease the sensitivity and responce time. The stability of the electrode in the presence of possible absorbants should be tested both in use and during storage. A summary of the most important requirements for electrochemical sensors and biosensors are presented in Figure 8.

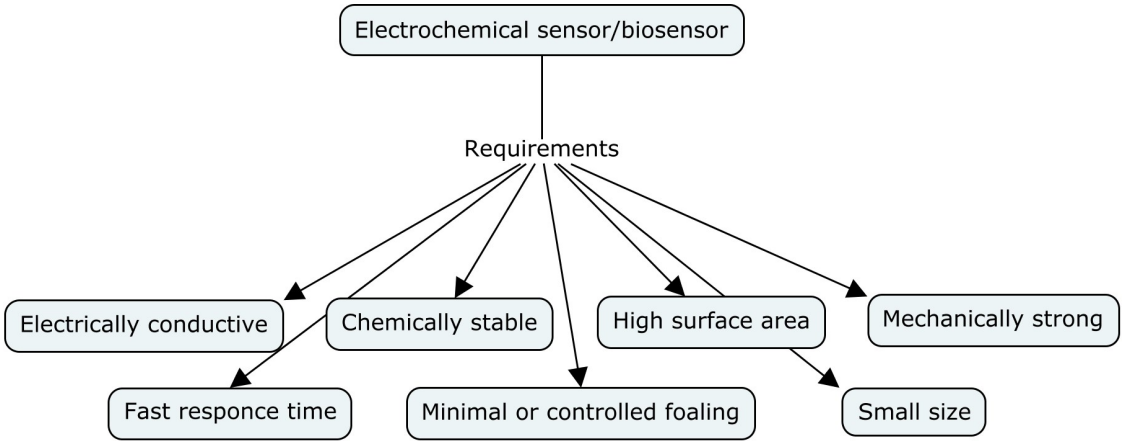

Figure 8: Requirements for electrochemical sensors and biosensors.

4 Significant biological compounds in electrochemical measuring

Electrochemical measuring of biological compounds provides information about chemical prosesses in cells and tissues. Measurement can be done both through the skin and directly at the surface of a single cell. Biological compounds can be oxidized or reduced either directly or indirectly. Biological compounds are divided into two categories according to their electrochemical properties: electrochemically active and electrochemically inactive. Electrochemically active molecule can be either oxidised or reduced and directly detected at the electrode surface. Electrochemically inactive molecules can be indirectly oxidized or reduced with the aid of *e.g.* an enzymatic reaction. The potential sufficient for oxidation or reduction depends on the electrode used and the molecule of interest. Also the chosen electrochemical method limits the potential window for the measurement.

The following paragraphs introduces the main analytes and some other interesting compounds usually detected with electrochemical sensors and biosensors. Neurotransmitters such as dopamine and serotonin are among the main neurotransmitters in the brain and central nervous system. Glucose is concidered one of the leading causes of death and NADH is related to several diseases. Ascorbic acid (*i.e.* vitamin C) and uric acid on the other hand are common molecules interfering electrochemical measurement signals, because *e.g.* dopamine, ascorbic acid and uric acid all exist in serum and the extra cellular fluid of central nervous system.

4.1 Neurotransmitters

Monitoring neurotransmitter concentrations from living brain tissue provides information about brain function, disorders and injuries. Traditionally neurotransmitters are monitored with microdialysis but the large probe (diameter about 300 μm) may cause tissue damage and in addition the probe is significantly larger than the cells, blood capillaries and vessels. [29] Neurotransmitters such as dopamine (DA), norepinephrine, epinephrine, serotonin (5-hydroxytryptamine, 5-HT), melatonin, histamine and adenosine are electrochemically active, are easily oxidized and thus can be electrochemically detected. All of these neurotransmitters oxidize at a specific potential depending on the electrode used. [8] Detection of neurotransmitters require an electrode small enough to be implanted in the synaptic cleft between two neurons and a submillisecond time scale because of the fast binding of the neurotransmitter to a receptor [1].

DA affects various cognitive and motoric functions and low levels of DA causes *e.g.* schizophrenia and Parkinson's disease [30]. Normal concentration of DA in the extracellular fluid is 0.01-0.03 μM in the resting state whereas during activation, concentration can be 0.1-1 μM [31]. DA first oxidizes to dopamine-*o*-quinone [2] as shown in Figure 9. After the oxidation, dopamine-*o*-quinone leads to leucodopaminechrome by intramolecular cyclization [32]. Leucodopaminechrome further oxidizes to dopaminechrome [32]. Detection of DA can be problematic because during this prosess the polymerization reaction of dopaminechrome leads to electrode

fouling via deposition of melanin-like polymer [32]. Cyclization and polymerization can be prevented with *e.g.* decreasing the solution pH [33]. Also the oxidation peaks of DA, ascorbic acid (AA) and uric acid (UA) are very close with conventional electrodes, which is why the detection method has to be accurate enough [21]. Interfering signal from AA can be decreased by *e.g.* increasing the scan rate because charge transfer rate of AA is usually slow at the electrode surface [2]. Selectivity towards DA in the presence of AA and UA can also be increased with surface coatings or NPs, which decrease the potential for AA and UA oxidation and thus separates the potential from the DA oxidation potential [16, 34]. Acetaminophen (APAP) is also a common interfering molecule during the detection of DA, AA, and UA.

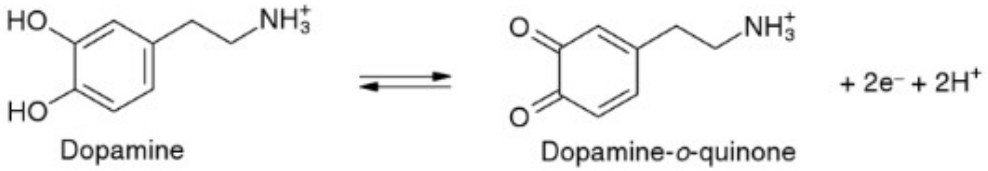

Figure 9: Oxidation of dopamine [2].

5-HT regulates mood, sleep and emotional behaviour [30] and is assosiated with several mental and neurological diseases such as depression [35]. High levels of 5-HT is toxic and potentially fatal [36]. 5-HT forms a ketone when oxidized [2] as shown in Figure 10. During the oxidation of 5-HT the oxidative product absorbes strongly to the surface of the electrode, forms an insulating layer and decreases the electrode stability over time [37, 38]. This can be prevented with a proper choise of electrode material and surface layer but also with a fast scan rate [37, 38].

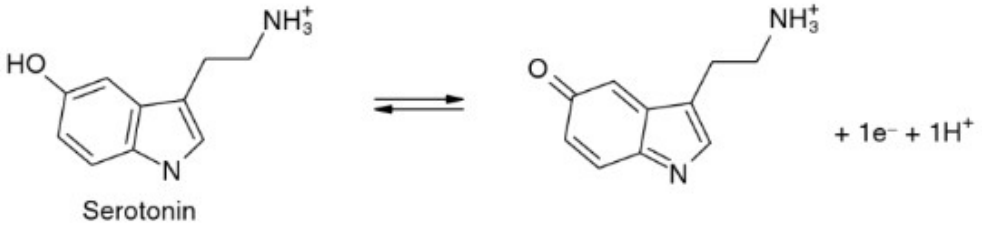

Figure 10: Oxidation of serotonin [2].

Simultaneous detection of DA and 5-HT is important because some diseases such as schizophrenia affect both DA and 5-HT secretion and uptake. Simultaneous detection is difficult because DA and 5-HT have similar oxidation potentials but the reduction potentials varies [37]. On the other hand the potential used in detecting DA reduction causes electrode fouling by 5-HT and the potential usually used to detect 5-HT reduction without electrode fouling does not reduce DA [37]. The problem is traditionally overcome by *e.g.* a carbon nanotube electrode which are known to reduce electrode fouling and increase electron transfer [37].

Electrochemically inactive neurotransmitters are *e.g.* acetylcholine and amino acids such as glutamate and gamma-aminobutyric acid (GABA). These can be detected with an enzyme biosensor [8]. Neuropeptides are also electrochemically inactive [8]. Neuropeptides consists of amino acid building blocks and are large and complex molecules [39]. Neuropeptides are difficult to detect because of extremely low concentrations (1-100 pM) so the chosen method to detect these needs to be sensitive enough. Neuropeptides can be electrochemically detected if an electrochemically active group such as *e.g.* tyrosine or tryptophan is attached [8] or with the help of *e.g.* an antibody labelled with a marker [39].

4.2 Ascorbic acid and uric acid

AA and UA are important molecules in the extra cellular fluid and are both electrochemically active [8]. Levels of AA in the brain fluctuates between 200 and 400 μM which makes AA one of the most dominant neurochemical in the brain. AA is also the main interfering molecule when detecting DA because they coexist in *e.g.* blood serum and the concentration of AA is 100-1000 times higher that of DA. In addition AA increases the reduction of dopamine-*o*-quinone back to DA so that the signal from DA increases at the electrode [2]. Selectivity towards AA in the presence of DA can be increased with electrode coating techniques such as polymers and polyelectrolyte films (*e.g.* polypyrrole and Nafion) and surface modification techniques such as addition of enzymes [2]. The oxidation of AA is presented in Figure 11.

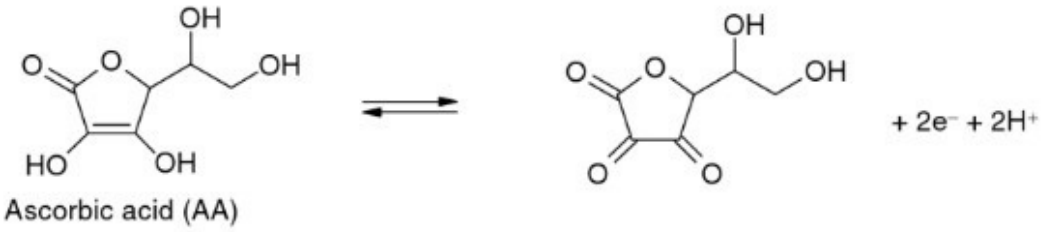

Figure 11: Oxidation of ascorbic acid [2].

UA is an important metabolite from the liver and is the end product of purine metabolism. UA circulates in plasma and urine and is excreted in the kidneys and intestines. [40] Normal concentration of UA in serum is about 140-430 μM [41]. UA concentration is increased in deseases such as leukemia and high concentration of UA can lead to *e.g.* gout, metabolic syndrome and even cardiovascular diseases especially in diabetic patiens [40]. High UA concentration in serum is also related to low insulin sensitivity which indicates a risk of Type II diabetes [42]. The oxidation of UA is presented in Figure 12. Oxidatation overpotential of UA is high and the electrochemical detection of UA is interfered by AA which is usually oxidized at a similar potential [43]. Selectivity towards UA can be increased *e.g.* by different enzymes or polymer layers on the surface of the electrode [43].

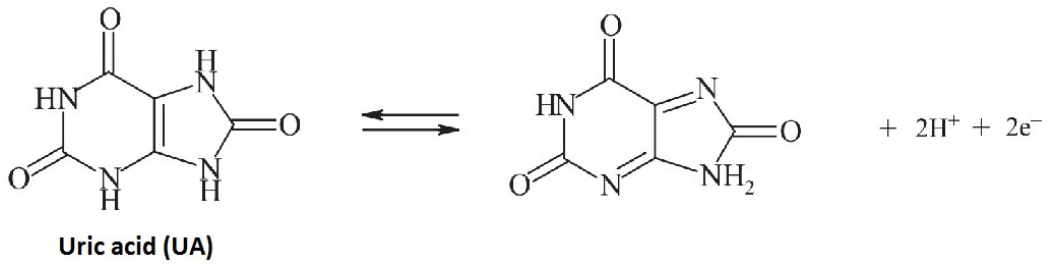

Figure 12: Oxidation of uric acid [44].

4.3 Glucose and NADH

Diabetes is a metabolic disease which causes diminished insulin uptake from pancreas. Diabetes causes concentration of blood glucose to increase higher than the normal range of 4-6 mM [45]. Diabetes is estimated to be the 7th leading cause of death in 2030 by WHO [46]. The diagnosis and management of the disease involves intense monitoring of the blood glucose concentration.

Glucose is electrochemically inactive and is traditionally indirectly measured with an enzyme [8]. Glucose oxidises to gluconic acid by glucose oxidase enzyme (GluOx) by equation (17). Reduced GluOx enzyme reacts with oxygen, oxidizes and forms hydrogen peroxide (H_2O_2) according to equation (18). [23] H_2O_2 is electrochemically active and can be electrochemically detected because H_2O_2 oxidizes at the electrode surface according to equation (19) [45, 23].

$$glucose + GluOx_{OX} \longrightarrow gluconic\ acid + GluOx_{RED}, \tag{17}$$

$$GluOx_{RED} + O_2 \longrightarrow GluOx_{OX} + H_2O_2, \tag{18}$$

$$H_2O_2 \longrightarrow 2H^+ + 2e^-. \tag{19}$$

The production rate of H_2O_2 is directly related to the concentration of glucose [2]. High levels of H_2O_2 is also related to cancer and neurodegenerative diseases *e.g.* Parkinson's disease [22]. Tumour cells release more H_2O_2 compared to healthy cells [22], which is why a selective detection of H_2O_2 is important. H_2O_2 can also be detected with HRP and catalase enzymes, Prussian blue or directly without an enzyme, although direct detection usually requires a high overpotential with conventional electrodes [47].

Glucose can also be measured nonenzymatically with *e.g.* metal NPs such as gold, nickel, copper and silver *e.g.* from serum after dilution in NaOH. Nonenzymatic techniques have been developed because of the instability and high cost of the enzymes and in order to improve sensitivity and reliability. [48] NPs are chemically more active than the bulk material in electrodes because of high surface area. NPs can also be used with an enzyme to improve selectivity [16] because the electrochemical measuring of glucose may be interferred by ascorbic acid and uric acid [49].

β-nicotinamide adenine dinucleotide (NADH) is related to several hundred dehydrogenase enzymatic reactions. Nicotinamide adenine dinucleotide (NAD) is a

coenzyme existing in living cells and related to cellular metabolism, growth and energy production [50]. Oxidized form of NAD is NAD^+ and reduced form NADH. [51] Changes in NAD/NADH ratio leads to changes in cell metabolism [52]. NAD^+ is an important electron carrier, which transfers electrons and hydrogen atoms and contributes to glycolysis which converts glucose into pyruvate and protects against neuronal degeneration which may lead to Alzheimer's disease, Parkinson's disease and multiple sclerosis [50]. The oxidation of NADH is presented in Figure 13.

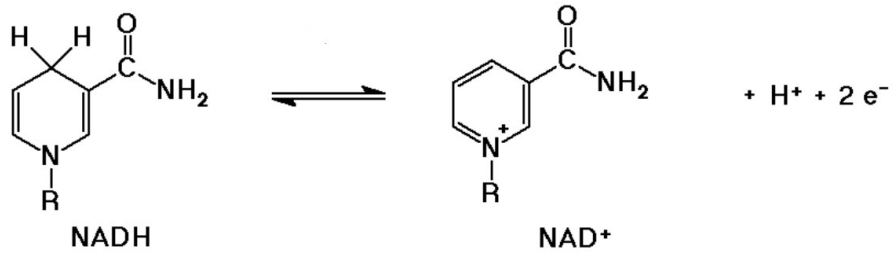

Figure 13: Oxidation of NADH where R is the adenine dinucleotide. Modified from [50].

Electrochemical oxidation of NADH usually involves high overpotential (*e.g.* 1.1 V for carbon and 0.5 V with glass carbon electrode [21, 53]) because of electrode fouling [51]. High overpotential decrease the selectivity because other electroactive molecules oxidize simultaneously [53]. The electrode fouling is due to polymerization of some of the oxidation products such as NAD^+ at the surface of the electrode which decrease electrode stability [51]. The electrode fouling can be decreased by increasing the electron transfer kinetics with an appropriate electrode material and electrode surface modification [53].

4.4 Other interesting biomolecules for electrochemical sensing

There are numerous interesting biomolecules to be electrochemically detected in addition to the before mentioned. For excample fast, selective and sensitive electrochemical detection of nucleic acids would be important in clinical diagnostics. Detection of free DNA bases: G, A, T and C can be done directly or with a DNA probe, although direct oxidation usually reqires high potentials [54]. Detection of single nucleotide polymorphisms is important because variations in nucleotides in the human genome leads to increased susceptibility to different *e.g.* psychiatric or neurophysiological disorders [24].

Hemoglobin (Hb) is a protein in the red blood cells transporting oxygen from the lungs to the tissues and organs and carbon dioxide from the tissues to the lungs. Hemoglobin concentration measurement is one of the most common blood test performed as a part of a complete blood count. Low hemoglobin concentration is related to anaemia and high concentration to reduced oxygen transportation [55]. Hb can be either immobilized on the surface of an electrochemical sensor, directly

measured with an electrochemical sensor or indirectly measured with a recognition element. Hb can also be used as a recognition element to detect *e.g.* H_2O_2 [56].

Cholesterol is another important measurand obtained from serum. Cholesterol is a sterol existing in all human cell membranes. High levels of cholesterol lead to coronary heart disease and atherosclerosis. In electrochemical measuring cholesterol is usually detected with a cholesterol oxidase enzyme [22]. Different hormones can also be electrochemically detected. For example detection of hormones related to obeisity and anorexia (*i.e.* hunger and saciety regulation) might provide help for obese patiens, without the need of highly expensive gastric bypass surgery. These hunger and saciety related hormones can also be measured noninvasively from saliva [57].

Early detection of biomarkers related to different disease is the most effective way to inhibit the progress of cancer and different tumors. Cancer biomarkers and virus can be detected with *e.g.* immunosensors [58]. Proteins can be detected either indirectly with an enzyme or with an aptamer, antibody/antigen reaction or with a MIP. [47]. Cells, bacteria and pathogens can also be detected with an aptamer immobilized on the surface of the electrode [58].

5 Graphene

Graphene consists of a layer of carbon atoms, which are one of the most common elements in the universe [59]. Stacked layers of graphene forms graphite which is also a common material in nature [60]. Graphene has high electron mobility, thermal conductivity, surface area and breaking strength [9]. Graphene is the most recently discovered nanometre scale material although graphite has been widely used since pencils discovery in 1564. It took over 60 years of research to produce a single graphene sheet, because for long graphene was considered to be thermodynamically unstable and to exist only theoretically as well as other 2D crystal structures [60]. A monolayer of a nanometre scale material was also difficult to fabricate because materials tend to coagulate to form islands. This results from the systems attempt to minimize its surface energy. [61] Graphene was intially isolated from graphite and the unique properties were first discovered year 2004 [9] and since the 2010 Nobel Prize in Physics was awarded to Andre Geim and Konstantin Novoselov, graphene has been an interesting topic of research [62]. Graphene can be made by several methods such as mechanical exfoliation, chemical vapor deposition and epitaxial growth. Electrochemical properties of graphene can also be easily altered with different fabrication and surface modification methods which increases the selectivity towards different target analytes.

5.1 Structure

Graphene consists of a single plane of carbon atoms in a hexagonal form. Each carbon atom is connected to three parallel carbon atoms by sp^2-bonds (also referred as σ-bond). [3, 63] The distance between the carbon atoms in the sp^2-bond is 1.42 Å [60]. One electron is located above and below the plane and forms a π-bond [3, 63]. The π-bond can make a covalent binding to the neighboring carbon atoms which forms a connection between another graphene layer [60]. The distance between the layers *i.e.* between the carbon atoms in the π-bond is 3.35 Å [63]. The layers are weakly bonded with van der Waals forces [3, 60]. Different forms of sp^2-bonded carbon is presented in Figure 14. Two dimensional carbon structured graphene (Figure 14C) can be formed into a 0D fullerene (Figure 14A), rolled and reconnected from the carbon bonds into a 1D carbon nanotube (Figure 14B) or piled to a 3D graphite (Figure 14D). Graphene can be produced as a single layer, bi-layer, few-layer (3-10 layers) or multi-layer (10-100 layers, referred as graphene platelet) [3, 64]. The electronic properties of graphene platelet resemble highly ordered pyrolytic graphite (HOPG, *i.e.* highly pure synthetic graphite). However more than 100 layers of graphene is considered as a 3D graphite because of the considerable changes in the electronic structure of the material [59, 64].

The easiest method to visually estimate the number of layers is optical microscopy but the method requires a trained eye. Another convenient technique is Raman spectroscopy which can be used in measuring structural characteristics, density of defects and the number of layers. Raman spectroscopy is based on scattering of monochromatic light [65]. The number of layers can also be measured with

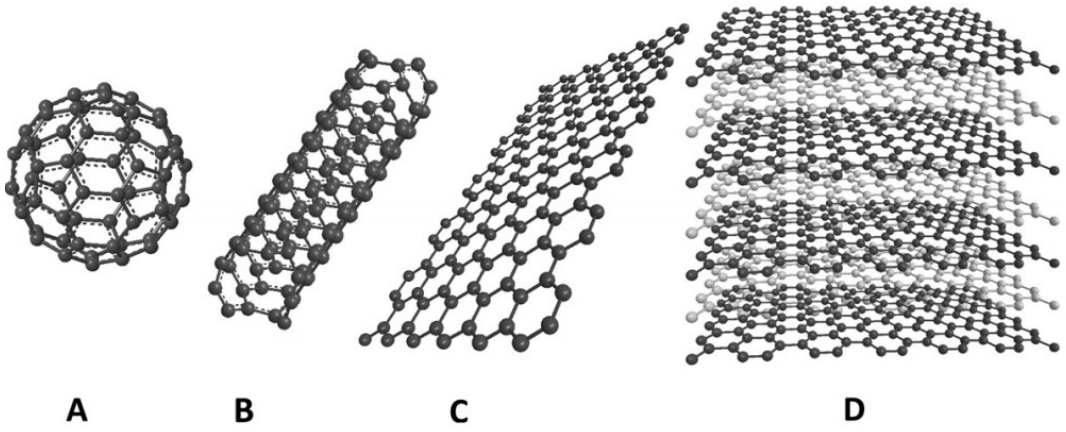

Figure 14: Different forms of sp^2-bonded carbon: A) fullerene, B) single-walled carbon nanotube, C) graphene, D) graphite [3].

scanning probe methods such as scanning tunneling microscopy (STM) and atomic force microscopy (AFM) [66, 64, 65]. Scanning probe methods are also useful in measuring the structure and size of the layers, although AFM and STM are expensive instruments and the analysis is slow [64, 65]. The size of the layers can also be measured with X-ray diffraction [28].

The top plane of a graphene layer is referred as basal plane and the edges of the layer edge planes. The edges can have either zig-zag or armchair structure as presented in Figure 15. The difference in the structure of the edges has influence on *e.g.* the electronic, chemical and electrochemical properties of graphene [64, 28]. However the edges are rarely exclusively zig-zag or armchair, instead often some kind of combination [67]. Graphene usually contains some defects, also referred as sp^3-sites, in the carbon atom structure and oxygen functional groups attached to the surface. Oxygen functional groups results from the spontaneous oxidation in air and occur mainly at the edges of graphene sheet because the basal plane does not usually react with air at room temperature [65]. The type and coverage of the oxygen functional groups varies greatly. Raman spectroscopy can be used in determining the amount of edge planes and defects in the graphene layer [64]. Defects in the basal plane can be determined with scanning electron microscopy (SEM), transmission electron microscopy (TEM) and STM [9]. Also the transparency, wrinkles and size of the graphene sheet can be evaluated with SEM and TEM. Oxygen functional groups can be studied with *e.g.* x-ray photoelectron spectroscopy (XPS), thermal desorption spectrometry and optical spectroscopy [65]. SEM, TEM and STM can be used even in nanometer-scale samples to visualize carbon atom structure although the electron beam used in SEM and TEM might cause structural damage to the graphene layer [65].

Surface area (A_s) of graphene per unit mass (m^2/g) is determined with the following equation:

$$\frac{A_s}{m} = \frac{2}{\rho N_{layer} d_1}, \tag{20}$$

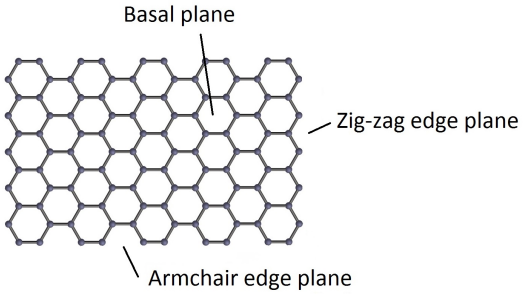

Figure 15: Different planes of a monolayer graphene. Modified from [64].

where ρ is the material density, N_{layer} is the number of layers and d_1 is the thickness of a single layer [27]. d_1 for a monolayer graphene is 0.35 nm [9]. A single layer graphene has a large surface area because all of the atoms are exposed to the surroundings from both sides of the layer [59]. The surface area of a single layer graphene can be up to 2630 m^2/g which is the maximum theoretical value of an sp^2-bonded carbon layer. Surface area of a single layer graphene is twice as large as the single-walled CNTs and the surface area diminishes as the number of layers increases. [3] High surface area increases the possibilities of physical adsorption and catalytic chemical reactions on the surface [27]. As stated earlier high surface area combined with small size is an important feature concerning implantable electrodes, because high surface area decreases the electrode impedance and small size increases the electrode sensitivity and induces less tissue damage. High surface area and hydrofobicity also increases restacking of graphene via van der Waals forces which is why graphene tends to form graphite-like materials [65, 63]. This can be prevented with solvents such as N-methyl-2-pyrrolidone (NMP), dimethylformamide (DMF), dimethyl sulfoxide (DMSO) and γ-butyrolactone (GBL) [65, 63]. BET (Brunauer–Emmett–Teller) surface area on the other hand is measured by the amount of gas, *e.g.* nitrogen absorbed to the surface [66, 64].

5.2 Characteristics

The most significant properties of graphene are surface area, number of layers, lateral geometry and chemistry of the surface [27]. All of these ultimately define the characteristics of graphene. Graphene's mechanical, electrical, thermal and optical properties are interesting since the properties can be easily altered by exposing electric and magnetic fields, changing its geometry, the number of layers or by chemical doping [59, 60]. This kind of altering of properties is not usual concerning thin nanometre scale metal films [59, 60]. Although some of the superior properties of graphene are not yet easily achievable via mass production.

5.2.1 Mechanical and thermal properties

Mechanical characteristics are important in electrochemical sensing applications because electrodes needs to be strong enough for implantation and remain mechanically

stable. Graphene is one of the thinnest and strongest known material [68]. Graphene is light (0.77 mg/m [63]) and at the same time fragile, ductile and flexible [68]. Graphene has a high thermal conductivity which has been measured for over 5000 W/mK for a single layer graphene at room temperature whereas thermal conductivity for graphite is about 1000W/mK and for CNTs about 3000-3500 W/mK. [69, 63]

Graphene's mechanical strength is high, almost 200 times greater than steel [3]. An intrinsic tensile strength is the maximum stress that a material can support before failure. The intrinsic tensile strength of graphene should approach the teoretical maximum of molecular intrinsic strength because of the monolayer stucture and strong σ-bonds, but the value of the intrinsic strength depends on the structural defects and grain boundaries in the layer. The intrinsic tensile strength of a monolayer graphene has been measured for 130 GPa [70] which is 100 times stronger than *e.g.* steel [63]. The breaking strength of graphene is 42 N/m and Young's modulus (*i.e.* elastic stiffness) about 1 TPa [70]. The bending stiffness of graphene increases as the number of layers increase [27]. This is an important aspect concerning implantable devices because electrodes must sustain torque cellular forces. Therefore the number of layers ultimately determines both the surface area and the bending stiffness of graphene.

5.2.2 Electrical properties

The electronic properties of graphene depends strongly on the number of layers which is why the properties can be easilly altered [60]. Graphene's characteristics are a combination of a semiconductor and a metal [60]. Band gap determines the electrical conductivity of a material and is the gap between a conduction band and a valence band. Single layer and bi-layer graphene are zero band gap semiconductors and their electronic spectrum is simple. Whereas the spectrum of a multi-layer graphene becomes complicated because of overlapping conduction and valence bands and appearance of charge carriers thus the electronic properties resemble metals. [59] Lateral dimensions and the type of edge plane exposed also affect the electronic properties. Zig-zag edge plane behaves like a metallic conductor while armchair edge plane can be metallic or semiconducting [64]. Lateral dimension on the other hand has influence on the ratio between edge plane and basal plane.

Soon after graphene was first successfully fabricated it was realized that graphene has a superior crystal quality. [68] Because of the strong bindings of carbon atoms it is very difficult for other atoms to replace carbon atoms in the honeycomb structure. This leads to the ability of charge carriers to travel (*i.e.* ballistic transport) high (almost micrometer [60, 68]) distances without scattering even in a rough environment and covered with impurities. [59] Although impurities, environment, number of layers, defects and structure of the edges do affect the charge carrier mobility of graphene [71]. The electron mobility of graphene is over 15,000 $cm^2V^{-1}s^{-1}$ whereas the teoretical limit is 200,000 $cm^2V^{-1}s^{-1}$ [63]. This leads to graphene's high electrical conductivity [60]. Graphene is also chemically one of the most inert material and impermeable to gases, which results in graphene's ability to remain stable and only weekly reacting with air at room temperature thus the reactions do not demolish graphene's crystal

structure or high electrical conductivity. [61, 68]

Density of electronic states (DOS) is an important aspect for an electrode material [9, 28]. DOS varies greatly even between different carbon-based materials. If a material has large number of atomic orbitals to form bands and high DOS, the material has high electronic conductivity [28]. According to the conservation of energy, electron transfer between the metal electrode and the solution is fastest when the energy of the electron is equal in the metal and in the solution [28]. Higher DOS of the electrode material results in more electrons of correct energy available for the transfer prosess [28]. Semiconductor electrodes on the other hand have no electron transfer between the electrode and the solution with potential values in the gap region where there are no electronic states [28]. DOS of gold is typically 0.28 states $atom^{-1}\ eV^{-1}$ resulting in high conductivity, whereas minimum DOS of HOPG is about 0.0022 states $atom^{-1}\ eV^{-1}$ and basal plane of pristine monolayer graphene has even lower DOS [9]. DOS of graphitic materials can be increased by inducing structural defects and increasing the number of layers, because edge plane sites increase the DOS [9]. This is why *e.g.* edge plane pyrolytic graphite (EPPG) has higher DOS than HOPG.

The capacitance (*i.e.* material's ability to store energy) of graphene is typically some tens of farads per gram [65]. Higher capacitance lowers the electrode impedance and as mentioned earlier, lower impedance results in higher signal to noice ratio. However capacitance strongly depends on the production method and the number of layers. The capacitance increases as the number of layers and thus the amount of edge plane sites increases [65]. On the other hand the capacitance of graphene decreases as the amount of oxygen functional groups on the surface increases [65]. Capacitance can be increased with different surface modification methods such as addition of NPs, pores, wrinkles or doping [65]. Also different stabilizing surfactants affect the capacitance of graphene [65].

Electronic properties such as sheet resistance and bulk conductivity are determined with the help of equation (21). Sheet resistance R_{sh} $(\Omega/square)$ measures the electrical resistance of the sheet, independent of the thickness of the sheet [66, 72].

$$R_{sh} = \frac{1}{\sigma\tau}, \tag{21}$$

where σ is the bulk conductivity (S/m) and τ is the sample thickness (m). Sheet resistance of a few layered graphene has been measured about 400 Ω/square at room temperature [72], which results in bulk conductivity in the order of about 10^6 S/m.

5.2.3 Electrochemical properties

Important electrochemical characteristics are electron transfer rate, electrochemical potential window, redox potentials and surface coverage [73, 65]. All of these are affected by the choice of the electrode material and surface modification methods [65]. Potential window and redox potentials are commonly measured with voltammetric methods such as CV and DPV. Heterogenous electron transfer (HET) rate is the rate at which electrons transfer from the solution to the electrode or the opposite way [64].

The electron transfer between the target molecule and the electrode is related to the analyte of interest, solution, applied potential, electrode material, number of layers and amount of functional groups, defects and impurities in the material [63, 65, 28]. The HET rate also depends on the DOS of the electrode material, since higher DOS (*i.e.* more electrons available for transfer) increases the HET rate. [9]. Electron transfer resistance on the other hand indicates electron transfer rate since higher resistance results in lower electron transfer rate. Electron transfer resistance can be measured *e.g.* with electrochemical impedance spectroscopy (EIS). EIS is a common procedure during electrochemical research and measures the current responce with an AC voltage probe [74]. Current responce determines the resistive and capacitive components from the electrode impedance (equivalent circuit presented earlier in Figure 5) [74]. EIS provides a Nyquist diagram and smaller curve indicates lower electron transfer resistance.

Sites where the HET rate is high are referred as electroactive sites. HET rate is the highest at the edge planes of a graphene sheet whereas the basal plane is electrochemically less active. [3, 64, 9] Increasing the defect density of the basal plane by 1 % results in a 10^3 increase in the HET rate [9]. However the type of edge plane exposed plays a role in the value of the HET rate [67] because zig-zag edge plane has higher DOS than armchair edge plane [9]. Also increasing the amount of layers increases the amount of edge plane sites which in turn increases the HET rate. A sheet of graphene which consists of more than 7 layers is considered electrochemically reversible, since the amount of edge plane sites is enough for a proper electrochemical responce [9]. The exact optimal amount of layers for electrochemical detecting on the other hand depends on the production method. The difference in the amount of electroactive edge planes can be seen from Figure 16 when comparing stacked graphene nanofibers and multiwalled carbon nanotubes (MWCNT). Figure 16 shows how stacking graphene layers significantly increases the amount of electroactive edge sites.

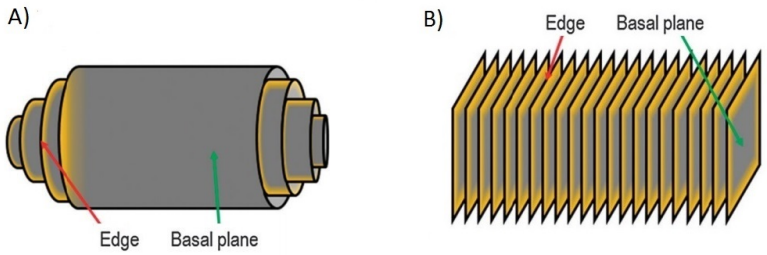

Figure 16: The amount of electroactive edge planes in A) MWCNT and B) stacked graphene nanofiber [75]. Electroactive sites are presented in yellow.

HET rate for metal electrodes is usually 0.6-1.0 cm/s and for GC 0.003 cm/s [65, 76, 77]. However values above 1.0 cm/s are difficult to measure [65]. The HET rate of edge plane pyrolytic graphite (EPPG) is rather high (0.005-0.022 cm/s), because of high amount of electroactive sites [76, 77]. Basal plane pyrolytic graphite (BPPG) on the other hand has a slow HET rate ($< 10^{-9}$-2.26 x 10^{-5} cm/s) due to the lack of electroactive sites [76, 77]. The HET rates were measured with ferrocyanide

as a redox probe. Figure 17 presents the cyclic voltammogram of 1 mM potassium ferrocyanide ($K_4[Fe(CN)_6] \cdot 3H_2O$) in 1 M KCl solution using BPPG and EPPG. Figure 17 shows how increasing the amount of edge plane sites increases the HET rate and results in a more distinguished peak and smaller peak-to-peak separation. Figure 18 shows how blocking the EPPG and BPPG with a layer of 20 ng pristine graphene platelets decreases the electrochemical properties because the basal plane of the graphene layer blocks most of the electroactive edge sites of EPPG and BPPG. Figure 19 on the other hand shows how the addition of the edge plane sites by increasing the number of graphene layers enhances the electrochemical responce.

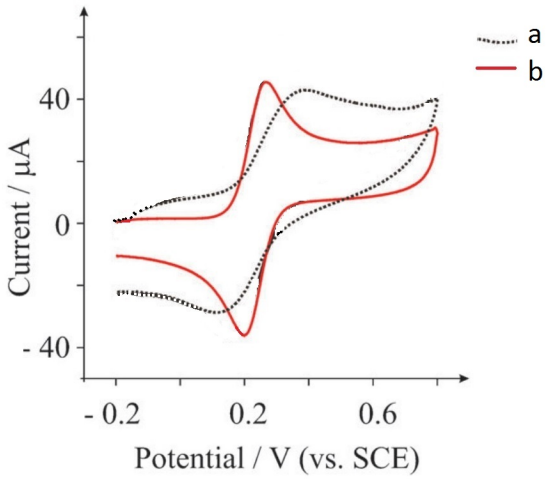

Figure 17: CV of a) BPPG and b) EPPG. Scan rate 100 mV/s, 1 mM $K_4[Fe(CN)_6] \cdot 3H_2O$/1 M KCl solution. Modified from [78].

If the basal plane contains defects or impurities they are considered edge planes because of the high electron transfer rate [3, 64]. A structural defect on the basal plane of graphene increases the HET rate of an order of magnitude [65]. Also the high surface area of graphene increases the possibility of defects and thus increases the amount of electroactive sites [67]. Impurities can be originated either from the original starting material or from the fabrication prosess but in these cases the amount and distribution of impurities are usually challenging to control. Alternatively surface defects can be added deliberately into the graphene structure after the fabrication prosess by mechanical damaging or ion or electron irridation [9].

Electrocatalysis is a redox reaction assisted by chemical interaction between the surface of the electrode and the solution. Chemical reactions between the electrode and the solution depends on the electrode material and surface modification which also affect the available catalytic sites [28]. Electrocatalytic reactions are common with graphene based electrodes because of the high surface area. Electrocatalysis can be exploited in increasing the electrode selectivity because variations in the surface chemistry lead to differences in the electrochemical responce. Addition of catalytic sites can also decrease the overpotential in many reactions [71]. Electrocatalysis can also be enhanced with reagents that react with a certain catalytic site and the product of the reaction either increases or inhibits a particular redox reaction [28].

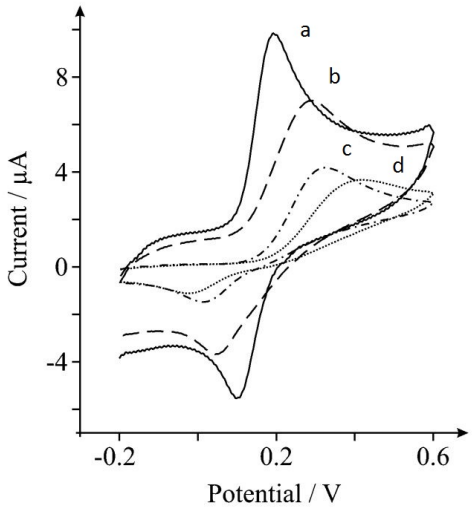

Figure 18: CV of a) unmodified EPPG, b) graphene modified EPPG, c) unmodified BPPG and d) graphene modified BPPG. Scan rate 100 mV/s (*vs.* SCE), 50 μM DA in pH 7 phosphate buffered saline (PBS) solution. [79]

Catalytic sites on the surface of the electrode can be *e.g.* oxygen containing groups such as carbonyl or carboxylate or hydrogen bonding sites [28]. Catalytic sites affect the electrochemical responce either by increasing or decreasing the redox reaction depending on the analyte of interest [65, 28, 9]. As stated earlier oxygen containing groups forms at the graphene surface due to spontaneous oxidation in air and the amount of oxygen functional groups is significantly higher at the edge sites. Oxidation can also be introduced deliberately as will be discussed in the next chapter. Carboxylates results in a negative surface charge which affects the adsorption and electron transfer rate of some ionic analytes [65]. Especially the oxidation of DA is strongly affected by electrocatalysis as the hydrogen bonding sites on the electrode surface increases the HET rate [28]. AA is also strongly affected by the oxygen functional groups [65]. The presence of oxygen functional groups, especially carboxylic groups, increase the adsorption of NAD^+ on the edge plane and edge-like defects of the electrode surface [81]. A $-COO^-$ group on the surface of graphene attracts positively charged nitrogen in the NAD^+ molecule which results in electrode fouling [81]. Nevertheless spontaneous surface oxidation and hydrogen formation is decreased with carbon-based electrodes compared to other metal electrodes which results in a wider potential window [28].

Noble metal NPs or nonmetallic doping elements (*e.g.* nitrogen, sulfur or boron) are also electrocatalytically active and can be added to the surface and used as catalytic sites [71, 65]. Metallic impurities such as cobalt, copper, iron, molybdenum and nickel oxide particles are included in graphene fabricated from graphite and influences the electrochemical responce [9]. Also the stabilizing surfactants which are used in preventing graphene from restacking affect the electrochemical properties of graphene. Surfactants are not usually electrochemically active but still can influence the voltammetric signal from *e.g.* NADH [65]. Surfactant such as sodium cholate on

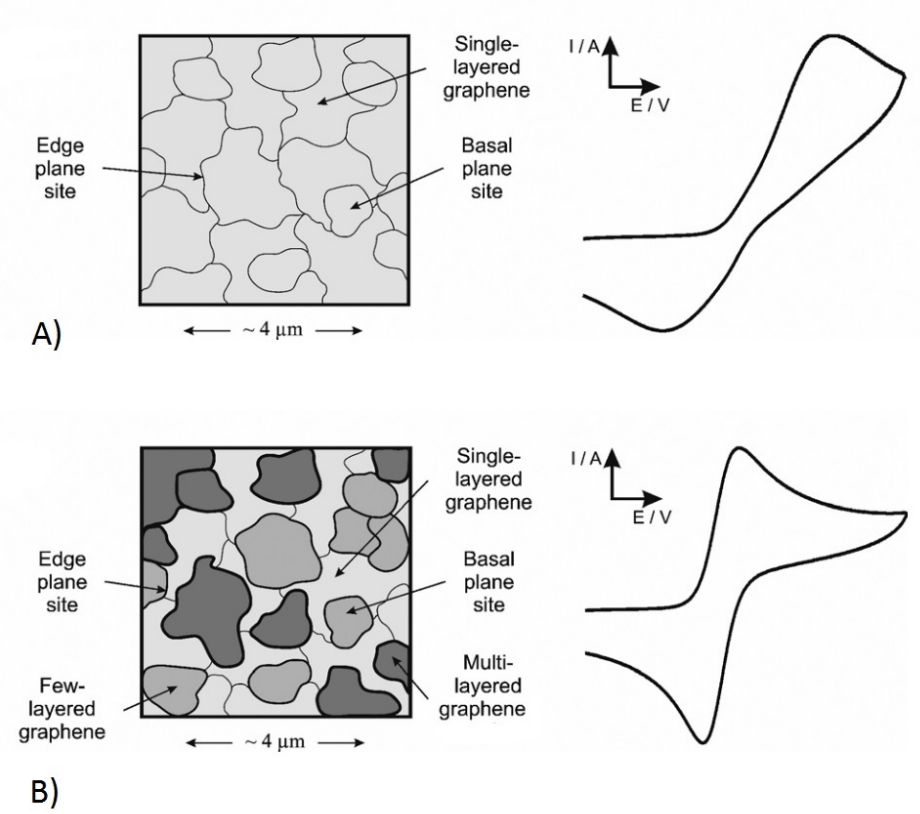

Figure 19: A schematic representation of the effect of increasing the amount of graphene layers on electrochemical responce. A) single layer graphene and B) multilayer graphene. Modified from [80].

the other hand is electrochemically active and can dominate the electrochemical signal, which is why the effect of surfactants should always be considered in electrochemical measuring [9]. Different surface films can also decrease the electron transfer rate because the electrons needs to tunnel through the film in order to migrate to the surface of the electrode [28]. Carbon easily forms strong covalent bonds with different materials especially to the edge planes and defected sites [65]. 1-2 nm thick monolayers such as adsorbed organic molecules, are common on the electrode surface and usually do not significantly slow down or prevent the transfer prosess. Although the tunneling rate depends on the layer thickness but is still usually faster than typical measuring time of *e.g.* CV [28]. Adsorbates can be removed from the surface of the electrode by *e.g.* polishing, heat treatment, solvent treatment, laser activation and ultrasonication [65].

In order to evaluate the electrochemical properties of graphene, quality, coverage and orientation of the graphene sheet needs to be properly analysed. The effect of the underlying electrode, surfactant or other subjects has to be eliminated from the results in order to distinguish the electrochemical properties originating from graphene. Electrochemical properties of graphene is a complex and diverse matter which is affected by the smallest variations in the structure and surface composition.

Single layer pristine graphine has slow HET kinetics compared to *e.g.* graphite, but the electrochemical properties can be easily altered by changing the number of layers, structure and surface chemistry. The electrochemical sensor or biosensor on the other hand is usually a complex structure consisting of several materials which is why the electrochemical properties are rarely determined by a single material.

5.2.4 Toxicity and biocompatibility

Biocompatibility and toxicity of graphene as an electrochemical sensing material depends on the size, shape and surface chemistry of the electrode, duration of the implantation and the biological surroundings [82]. Graphene induces cytotoxicity as well as SWCNTs but at higher concentrations (100 μg/ml) than SWCNTs (0.1 μg/ml), because the needle shaped SWCNT penetrates the cell membranes (*i.e.* induce cell damage) easier than flat graphene plane [82]. Smaller lateral dimension (nm scale) on the other hand induce more cellular damage than larger (μm scale) graphene sheet, but larger graphene material induce more inflammatory response than the smaller ones, because of the stress towards the cells [82]. The induced cellular damage of graphene can also be exploited, since graphene has been proven to be antibacterial in contact with *e.g.* E. coli, because graphene inhibits the growth of the bacteria via membrane damage [83]. Gram positive bacteria, on the other hand is more vulnerable than Gram negative, because of thinner membrane [82]. Graphene can also enter the cell by endocytosis and increase production of reactive oxygen species, which leads to changes in mitochondrial membrane potential [82]. Graphene may also accept electrons from the surrounding cells, which interrupts the membrane respiratory chain and decreases the cellular ATP level [82]. The production of reactive oxygen species also induce DNA damage which leads to inflammation [82]. DNA damage, oxidative stress and inflammation can lead to apoptosis or programmed cell death [82].

Foreign body sarcomas are a possibility with graphene because of graphene's smooth and continuous surface and large surface area [27]. Foreign body sarcomas and inflammation can be prevented by folding the graphene sheet in order to increase roughness of the layer, covering graphene with a fibrous capsule or covering the surface with different molecules [27]. Different polymer coatings also improves biocompatibility and decreases toxicity [82]. Inhaled graphene flakes may cause granulomas and fibrosis in the alveolar area because the large surface area and size resemble to asbestos fibres [27]. Exposure to inhalation may occur *e.g.* during fabrication. The health hazard research of graphene, since it is a fairly recently discovered electrode material, is at an early stage and the risks needs to be properly evaluated before the possibility of a clinical use.

5.3 Fabrication

Small amounts of graphene can be relatively inexpensively fabricated because of low material cost and high accessibility of graphite. Low material cost is a significant benefit over other electrochemical sensor materials such as widely used CNTs [3].

However cost effective production method of high quality graphene should be carefully selected because even slight variations in the characteristics lead to significant changes in the electrochemical properties. On the other hand large quantities of graphene are required when producing electrodes for electrochemical applications which excludes some of the fabrication methods. Graphene can be fabricated by top-down or bottom-up methods. Top-down method uses natural or synthetic (*e.g.* HOPG) graphite as a source material. Natural graphite has purity levels between 80-98 % while purity of synthetic graphite can be as high as 99.9 % [65, 84]. Top-down methods are exfoliation of graphite by mechanical, chemical or electrochemical techniques or CNT dismantling. Top-down methods are based on weakening of the van der Waal forces between the layers whereas bottom-up methods are based on building graphene from smaller pieces catalytically with *e.g.* chemical vapor deposition (CVD) on a metal substrate or thermally with *e.g.* epitaxial growth on an insulating substrate such as silicon carbide (SiC).

5.3.1 Exfoliation

Exfoliation is based on disruption of the van der Waals forces between the graphene layers in bulk graphite [63]. Exfoliation is commonly done mechanically, chemically or electrochemically. Mechanical exfoliation is done with an adhesive tape to peal the graphite into layers. Adhesive tape is placed on the surface of a graphite sample (*e.g.* HOPG) and thin graphite flakes are peeled off until graphene sheets are obtained [68, 84, 65]. The pealed graphene flakes can be transferred onto another surface (*e.g.* SiO_2 wafer) [68, 84]. The method is referred to as a micromechanical exfoliation or cleavage or as a scotch-tape technique. The method is practical for fundamental study because the samples gained are high quality and the surface is clean [84, 85]. Furthermore the method is simple and does not involve complex and expensive equipment. Although it is not suitable for a large scale production because of the small dimension and lack of scalability for mass-production [84]. Also the electrochemical activity of mechanically exfoliated graphene is rather weak because of high quality *i.e.* low level of defects.

Chemical exfoliation is done by applying ultrasonication to a suspension of graphite powder and a solution. The solvent is usually water [84] but organic solvents such as DMF or NMP can also be used [86, 65]. Ultrasonication separates graphene layers from the graphite solution by weakening the bonds between the layers [84]. Chemical exfoliation is more versatile than mechanical exfoliation and higher volumes with good structural quality can be produced [85, 65]. Although ultrasonication brakes graphene sheets into smaller flakes, may induce impurities and the graphene sheets are mainly multilayered [65]. Also the number of layers formed is not easy to control [65].

Graphite can be exfoliated with electrochemical exfoliation using catodic or anodic potentials or currents in an aqueous or organic electrolyte. Graphite-based working electrode (*e.g.* HOPG) is usually used together with Pt counter electrode and SCE or Ag/AgCl reference electrode [65]. A positive potential oxidizes graphite and the negatively charged ions move from the solution into the layers of graphene. A negative

potential then exfoliates the layers. Oxidizing leads to oxygen functional groups on the surface of the exfoliated graphene, which in turn affects the electrochemical properties of graphene [65]. A negative potential can also be used first, which attracts positive ions, although the formation of oxygen functional groups does not happen [65]. Electrochemical exfoliation produces single or few layer graphene, is environmental friendly, fast and the potential can be easily controlled [65].

The problem with all the previously mentioned exfoliation techniques is that the sheets exfoliated are often multi-layer graphene and the number of layers produced cannot be controlled or even predicted in advance. Also the dimensions of the achieved graphene sheets are limited by the size of the bulk graphite.

5.3.2 Dismantling carbon nanotubes

Graphene can also be fabricated by dismantling CNTs chemically or thermally. The produced graphene is referred as a graphene nanoribbon [65]. The dismantling can be done *e.g.* by hypermanganate chemical oxidation of CNTs, by plasma etching of multi-walled CNTs or with potassium permanganate and sulfuric acid [3, 84, 65]. The band gap of the resulting graphene nanoribbons can be tuned by varying the width of the ribbons which ultimately depends on the dimensions of the CNT [65]. Multi-walled CNTs often contain metallic impurities which affect the electrochemical properties and induce toxicity thus should be avoided in electrochemical detecting [3]. However graphene nanoribbons also include structural defects, which on the other hand increase the electrochemical properties [65].

5.3.3 Epitaxial growth

Epitaxial growth is based on a catalytic decomposition of hydrocarbons or carbon oxide on a metal substrate. The surface is then heated in ultrahigh vacuum which leads to dissolution of hydrogen and oxygen and finally to a formation of a graphene layer [60]. Electrically insulating silicon carbide (SiC) wafer can be used as a substrate [60]. Heating SiC leads to desorption of silicon from the uppermost layers which then exposes some graphene layers on the surface [60]. Afterwards the substrate is removed if necessary by chemical etching [68]. The number of layers can be controlled, unlike during exfoliation techniques, by altering time and temperature of the heating [60]. The use of SiC as a substrate results in high quality and continuous graphene layers but the size of the even region (also called terrace) on the SiC plane ultimately limits the size of the graphene layers [84, 65], although does result in larger area graphene samples than with exfoliation techniques [60]. On the other hand epitaxial growth is more expencive than the exfoliation methods because of the high cost of SiC wafers, need of costly equipment and skilled personnel [84, 65], which limits the use in large-scale fabrication. Also the electrochemical properties are weak because of low electron transfer rate due to high structural quality [65].

5.3.4 Chemical vapor deposition

CVD is based on a deposition of carbon atoms, which forms an sp^2 structured layer on the surface of a metal substrate. Copper (Cu) and nickel (Ni) substrates are commonly used because of their low cost and high availability [87, 65]. The substrate is first heated to about 1000 °C [84] and exposed to a gas mixture (*e.g.* hydrogen/methane or argon/methane) at a high temperature (800 – 1100 °C depending on the substrate) [84, 87, 63]. In case of a Ni substrate, methane is mixed with the gas mixture and carbon from methane adsorbes into the substrate. The Ni/carbon sample is then cooled down which results in the diffusion of carbon atoms from the substrate to form a layer of graphene on the surface. In the case of Cu substrate, carbon atoms decomposes mainly catalytically directly to the surface of the substrate because lesser amount of carbon is dissolved into the substrate [87]. After the formation of the graphene sheet, the layer needs to be transferred to another substrate and the Cu/Ni removed. This can be done with an inert supporting polymer (*e.g.* PMMA or PDMS) and etching or mechanically exfoliating the metal [65]. The transfer process might nevertheless damage or alter the properties of the graphene sheet by inducing metallic impurities or structural damage such as wrinkles and tearing [84].

The choice of the metal substrate affects the electronic and electrochemical properties of the graphene sheet. CVD growth on a Ni substrate produces areas with different number of layers due to grain boundaries on a Ni substrate, which results in higher amount of electroactive edge sites, whereas growth on a Cu substrate is more inexpensive and results more frequently to a single or double layer graphene because of lower solubility of carbon into a Cu substrate [87, 65]. Also the temperature needed for the growth is lower in case of a Cu substrate [84]. The rate of the cooling affects the quality of the graphene sheet and the number of layers formed [87]. Also the concentration of the gas affects the number of layers [63]. Nevertheless the quality of the graphene layer depends more on the transfer prosess of graphene from the substrate than the actual CVD production method [63]. Despite being inexpensive, CVD is not the most usable method to produce large amounts of graphene [84, 87]. However larger dimension graphene sheets can be obtained than with the other fabrication methods (single crystal size up to 0.5 mm [9]).

5.3.5 Comparison of fabrication methods

There are many ways to fabricate graphene but only few of them are practical for electrochemical sensing and biosensing applications because the need of bulk quantities and high amount of edge plane sites. Graphene is hydrophobic and has high surface area, which increases the possibility of restacking due to the van der Waals forces. This is why layers of graphene tend to form a graphite-like multiple layered material. However multiple layers increases the amount of edge plane sites, hence the electron transfer rate increases. Although in many cases the number of layers produced are not easilly controlled. Comparison of the diameters of different sp^2 bonded carbon materials is presented in Figure 20, where L_a is the basal plane width and L_c is the edge plane width. Figure 20 shows approximate values, where pristine graphene referres to a defect free, clean surface layer graphene. CVD method has

been excluded because of the wide variety of dimensions that can be achieved. Figure 20 shows how chemical exfoliation often results in smaller but thicker structures than mechanical exfoliation. L_a for graphene can be from below 50 nm to over 3000 nm, whereas L_c for a monolayer graphene is 0.35 nm [9].

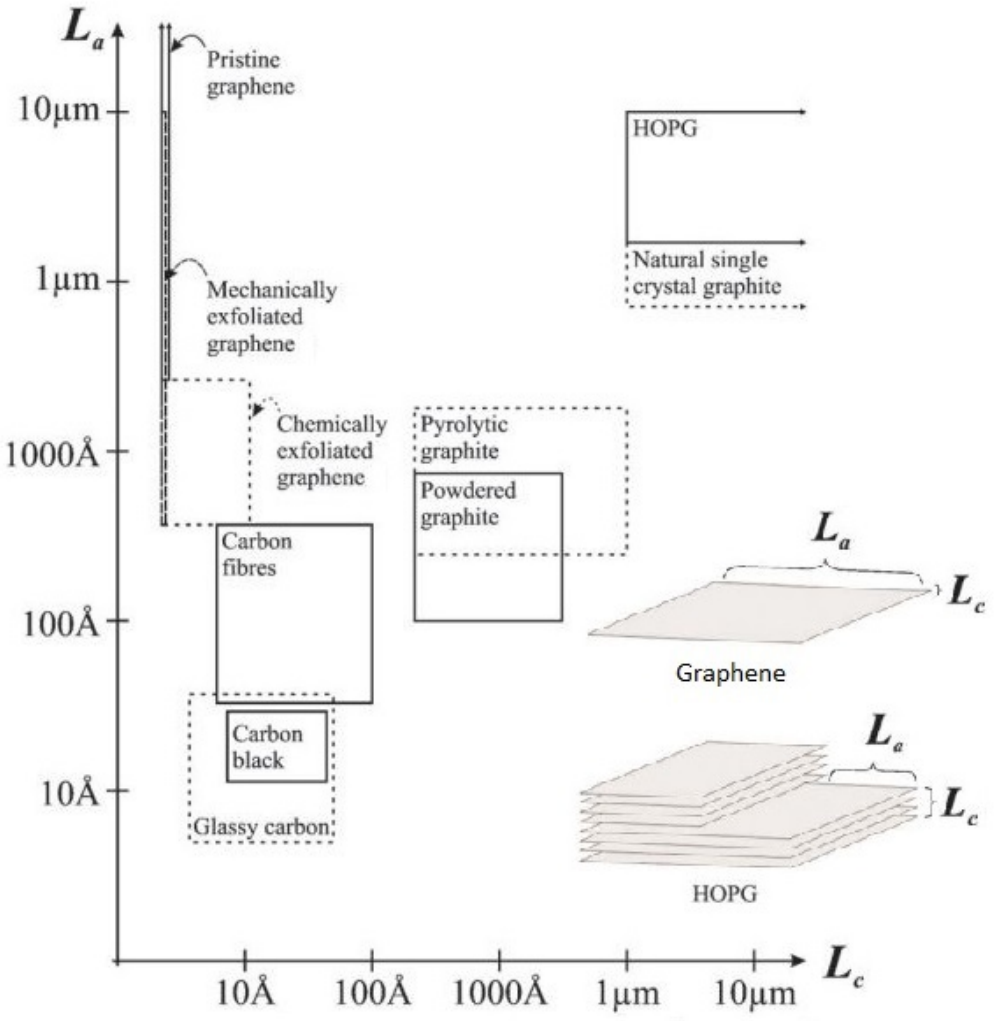

Figure 20: Diameters of different sp^2 bonded carbon materials. L_a is the basal plane width and L_c is the edge plane width. [9]

Each fabrication method presented previosly has advantages and disadvantages that affect the quality and quantity of the produced graphene and there are no single method above all that is suitable fo all purposes or analytes. The main advantages and disadvantages of different fabrication methods are summarized in Figure 21. Before choosing the fabrication method the structural, mechanical and electrochemical characteristics of graphene needs to be properly evaluated. The best approach for evaluating the characteristics of graphene is to combine different techniques such as spectroscopy (Raman or XPS) and microscopy (optical microscopy, STM, AFM, SEM, TEM). Even slight variations in the fabrication methods lead to severe changes in the characteristics. Different fabrication methods induce different

amount of defects and impurities on the surface of the graphene sheets, which results in different electrochemical properties. Depending on the target application, graphene needs to be high quality and closely resembling pristine graphine or include structural defects or functional groups in order to gain the optimal electron transfer rate and thus enhance the electrochemical properties.

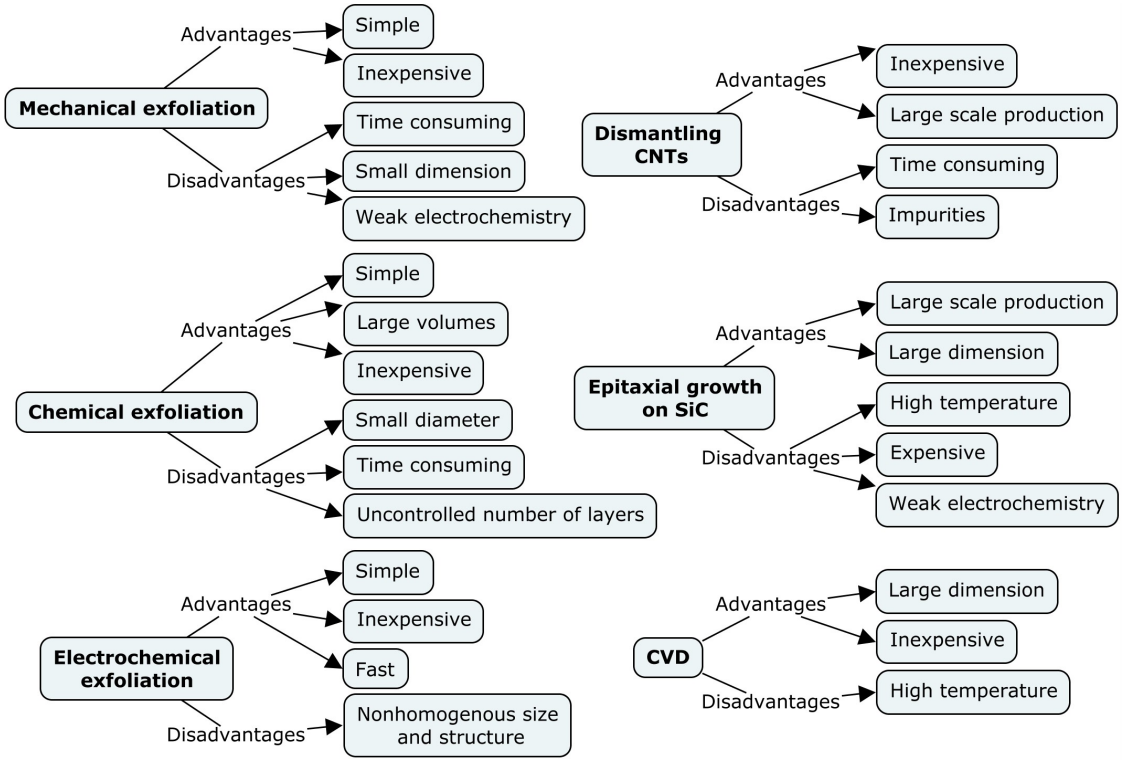

Figure 21: Summary of the advantages and disadvantages of different fabrication methods.

6 Reduced graphene oxide

Since electrochemical detecting in medical applications requires large scale production of electrode material with uniform quality, the before mentioned fabrication methods are not the most suitable. However reduction of oxidized graphene (*i.e.* graphene oxide) is a practical method to produce large amounts of material which has properties such as electrical, thermal and mechanical similar to graphene. The oxidation produces imperfections (*i.e.* oxygen bearing functional groups) and structural defects to the surface of graphene, which results in diminished electrical conductivity [84, 88]. On the other hand oxygen functional groups and defects results in more electroactive sites for electrochemical purposes. The properties of graphene oxide depends on the structure of the material and the number, type and position of the oxygen functional groups. Despite of the diminished electrical conductivity, graphene oxide can be used in electrochemical sensing because the high electrocatalytic activity of the oxygen functional groups, but as stated earlier electrochemical sensors shoud be electrically conductive which is why graphene oxide is usually reduced. Reduction ideally removes the oxygen functional groups and repairs the atomic structure thus restores conductivity. On the other hand, structural, electrical and electrochemical properities are not usually completely retained, because some of the defects and functional groups still remain on the surface of reduced graphene oxide.

6.1 Oxidation

Graphene oxide is usually fabricated by first oxidizing a piece of graphite. Oxidation occurs when graphite is exposed to a mixture of substances. Oxidation inflicts different oxygen bearing functional groups such as hydroxyl (C–OH) and epoxide (C–O–C) to the graphite basal plane and carboxylate functionalities such as carboxyl (COOH), carbonyl (>C=O), phenol, lactone and quinone to the edge planes [89, 26].

Hummers method, which is the most commonly used method to produce graphite oxide [84], involves the use of sodium nitrate ($NaNO_3$), sulfuric acid (H_2SO_4) and potassium permanganate ($KMnO_4$) as an oxidizing mixture [66, 90]. Other common methods are Brodie's method and Staudenmaier's method. Both methods oxidizes with the use of potassium chlorate ($KClO_3$) and nitric acid (HNO_3). For example HNO_3 reacts easily with aromatic carbon surfaces and the reaction results in carboxyls, lactones, and ketones. The characteristics of the oxidized graphite varies strongly depending on the oxidants used, the quality of the graphite and conditions during the reaction. [66]

The degree of oxidation varies along the graphite oxide sheets because the sp^2 bonds in some areas becomes disrupted. Oxygen functional groups changes some of the sp^2 bonds to clusters of sp^3 bonds in the carbon structure. This results in the decrease of charge carrier mobility and concentration which in turn results in diminished conductivity and graphite oxide becomes almost an insulator. [88, 84] The degree of insulation depends on the amount of sp^3 bonded areas [26]. Carboxyl and carbonyl groups at the edges does not have such a strong impact on the conductivity than the hydroxyl and epoxide at the basal plane. [88]

After the oxidation of graphite, single layer or multiple layer graphene oxide can be produced by a variety of thermal and mechanical methods. The layers in graphite oxide are amphiphilic, because the oxygen bearing areas are hydrophilic and the undisturbed areas hydrophobic [27]. Water molecules intercalates between the layers in hydrophilic areas, which is why graphite oxide and graphene oxide are dispersible in water and many solvents. Water molecules weakens the interactions and increases the distance between the layers and thus graphite oxide can be easily further processed (*e.g.* thin film deposition) and mechanically exfoliated [84]. This is usually done by sonicating and stirring the material in water [84, 66]. However sonication in water often results in structural damage, which decreases the dimension of the samples from micrometre to nanometre scale [66]. Exfoliation can also be done by heating the graphite oxide which results in the formation of CO_2 and H_2O between the layers in graphite oxide. The formed gas expands quickly and disconnects the graphene oxide layers. [84]

The exact atomic structure of graphene oxide is not fully discovered because it is partially amorphous, complex and varies according to fabrication method, environment and even between samples, which is why there are several different models to present graphene oxide [66, 88]. One of the widely known model is the Lerf-Klinowski model presented in Figure 22. As can be seen from Figure 22 hydroxyl and epoxide groups are located mainly at the basal plane.

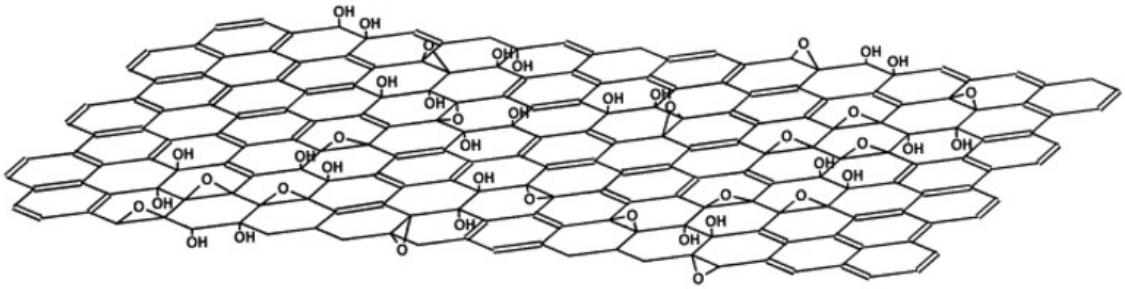

Figure 22: Chemical structure model of a graphene oxide layer by Lerf and Klinowski [91].

Despite the complexity in atomic structure there are some microscopic and spectroscopic methods that can be used in defining the structural properties of graphene oxide. AFM measures the thickness of the graphene oxide and the number of layers. Conductive AFM can be used in evaluating the electrical defects [26]. STM examines the structure of the graphene oxide and gives an estimation of the degree of surface functionalization [26]. High-resolution TEM images atoms in the lattice as well as topological defects. The chemical composition and oxygen functional groups can be detected with spectroscopic techniques such as solid-state nuclear magnetic resonance, X-ray absorption near-edge spectroscopy, Raman spectroscopy, XPS and Fourier transform infrared spectroscopy [26].

6.2 Reduction

Graphite oxide and graphene oxide are both electrically almost insulating because of the changes and defects in sp^2 bonds. In order to use graphene oxide in electrochemical sensing the electrical conductivity has to be retained, which is why graphene oxide is reduced. The reduction of graphene oxide ideally removes the oxygen functional groups from the surface and repairs its disrupted carbon bonds back to C–C and C=C bonds [66, 88]. Reduction hence increases conductivity by restoring charge carrier mobility and concentration [88], increases hydrophobicity of the layer and reduces water dispersibility and surface charge [27]. Graphene oxide can be reduced by a variety of methods such as chemically, thermally or electrochemically.

6.2.1 Basic principle of reduction

Partial reduction of graphene oxide is relatively easy but full reduction to a graphene like material usually involves a combination of methods. Also different reducing methods results in different electrical and mechanical properties because of the varieties in molecular interactions [88]. Different functional groups are connected to the graphene oxide layer with a different binding energy, which also varies according to their location [88, 72]. Epoxy groups are *e.g.* more stable than hydroxyl groups because of higher binding energy [72]. The epoxy and hydroxyl groups, which are located at the non-defected sp^2 bonded areas are easier to remove than from the defected sp^3 bonded areas or from the edges [88]. Groups with higher binding energy at the edge plane *vs.* basal plane tend to migrate to the edges [72]. Controlling the initial oxidation method increases the success and quality of the reduction, because the amount of oxygen groups after the reduction depends on the initial amount of oxygen functional groups [92]. The epoxy groups *e.g.* causes formation of CO and CO_2 which results in holes during the reduction. Diminishing the amount of epoxy groups on the surface of graphene oxide compared to the amount of hydroxyl groups result in more uniform structural quality [92].

At the time of this writing there are no practical methods to directly monitor the reduction process, although there are several methods to measure the effectiveness of the reduction and the easiest are to

- visually observe the solution
- measure the restored electrical conductivity
- observe the HET rate and
- measure the carbon to oxygen atomic ratio (C/O ratio).

During reduction the colour of the graphene oxide sheet changes from darker to lighter and metallic because of improved reflection of light. The improvement in the reflection of light results from the increase in charge carrier concentration and mobility and this change in colour can be visually observed [72]. Electrical conductivity on the other hand is restored by repairing the defected sp^2 carbon structure and removing the oxygen containing functional groups, which ultimately increases the electrical

conductivity. Oxygen functional groups such as the epoxy and hydroxyl groups at the basal plane influence the conductivity more than carboxyl, carbonyl and esters at the edge plane or defected areas of graphene oxide [72]. Reduced graphene oxide is usually still covered with some sp^3 bonded areas which interferes the charge carriers' mobility therefore inducing transport by hopping over the defected sites [92]. sp^3 bonded areas might be able to be further repaired by *e.g.* CVD or doping [72]. Charge transfer resistance can be measured with EIS as mentioned earlier, which corresponds well to the electrochemical properties of reduced graphene oxide. The HET rate is usually evaluated with *e.g.* CV or DPV. C/O ratio principally measures oxygen content and can be determined with *e.g.* XPS [65, 72]. XPS is the main technique to evaluate the degree of oxidation and the effectiveness of the reduction but also the types of oxygen functional groups [65]. Unfortunately XPS is relatively expensive because of the required ultra high vacuum conditions [65]. C/O ratio of graphene oxide is around 2 [65] and C/O ratio higher than 4 (*i.e.* 25 % coverage of oxygen functional groups) is considered a level at which the conductivity is restored but still low [88, 93]. Reduction typically results in C/O ratio between 3 and 15 [65].

6.2.2 Chemical reduction

Chemical reduction is the most commonly used reduction method. Chemical reduction is based on a chemical reaction between reagents and graphene oxide. The reduction can be done at room temperature or by moderate heating so there is no need for a special equipment or environment, making chemical reduction a simple and inexpensive method and suitable for mass production.

Reducing graphene oxide chemically involves the use of strong reductants in a colloidal dispersion [66]. Different reductants are selective towards certain oxygen functional groups [72]. Hydrazine monohydrate ($N_2H_4 \cdot H_2O$) is the most commonly used reducing agent because it does not have a reactivity to water, which is generally used as an exfoliation solvent [66]. The reduction with hydrazine monohydrate is typically done at 80-100 °C [66]. On the other hand hydrazine is highly toxic and explosive when mishandled and for those reasons not the ideal alternative [94]. Sodium borohydride ($NaBH_4$) is an effective reductant for C=O groups but less effective for epoxides and carboxylic acids [66]. AA is another common reductant, which is non-toxic and has higher chemical stability in water than *e.g.* $NaBH_4$ [86, 88]. AA reduction can be done both in water and in organic solvents (*e.g.* DMF or NMP) [86]. Other reductants such as hydroquinone ($C_6H_6O_2$), pyrogallol ($C_6H_6O_3$), potassium hydroxide (KOH), sodium hydroxide ($NaOH$), hydroxylamine (H_3NO), urea (CH_4N_2O) and thiourea (CH_4N_2S) has also been used [86]. However $NaOH$ and KOH are considered toxic [94]. Hydroiodic acid (HI) is also an interesting reductant because it is concidered less toxic than hydrazine [88].

Visible difference between graphene oxide and chemically reduced graphene oxide sheets and solutions is presented in Figure 23. The reduction is easily visible because the reduced graphene oxide solution is darker than graphene oxide. Reduced graphene oxide film on the other hand has a metallic colour compared to slightly transparent and darker film of graphene oxide. The main advantage using chemical reduction is

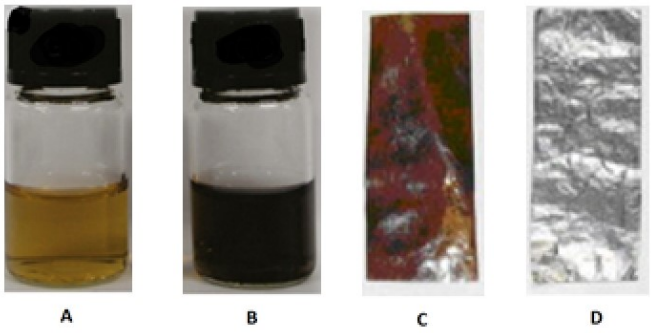

Figure 23: Visible change in colour from graphene oxide solution (A) to chemically reduced graphene oxide solution (B) and from graphene oxide film (C) to chemically reduced graphene oxide film (D) [95].

that the temperature used is not energy consuming and the reductants are easily accessible and inexpensive. However different reductants react differently towards a wide variety of functional groups hence the exact molecular mechanism of the reduction is still unclear. [88]

6.2.3 Thermal reduction

Thermal reducing can be done by heating graphite oxide rapidly (heating rate typically over 2000°C/min [72]) in a furnace [66]. Reduction takes place at temperature above 100°C depending on the type of oxygen functional groups [72]. Carboxyl groups start to slowly desorb in vacuum at 100-150°C, the hydroxyl groups are fully eliminated at 700-1200°C, epoxies above 1200°C and carbonyl groups above 1730°C [72]. Desorbing epoxy groups on the other hand cause structural damage while hydroxyl groups does not alter the structure of the graphene plane [72]. Heating graphite oxide also results in exfoliation of the graphene oxide layers with the help of carbon dioxide (CO_2). CO_2 is generated during the heating process between the layers, creates pressure and detaches the layers [66, 88]. 40 MPa pressure is created at 300°C and 130 MPa at 1000°C [88].

Thermal reduction consumes large amount of energy because of the high temperature needed, causes structural damage due to released CO_2 and is critical for the right heating rate so that the graphite oxide does not fragment uncontrollably [88, 72]. Heating should also be conducted in vacuum or inert atmosphere, because oxygen gas should be excluded during reduction [72]. However it is difficult to completely remove the oxygen functionalities even at high temperatures above 1200°C [88]. The main advantage of thermal reduction is that it simultaneously remowes the oxygen functional groups and exfoliates the graphite oxide layers, unlike chemical reduction, although the energy consumption is higher than with chemical reduction.

6.2.4 Electrochemical reduction

Electrochemical reduction is performed at room temperature and electrodes are placed at both sides of the graphene oxide film deposited on a substrate (*e.g.* glass or plastic) and immersed in *e.g.* a sodium phosphate buffer [66]. A cathodic potential is induced with *e.g.* LSV or CV and the material is reduced [66]. The reduction potential depends on the initial oxidizing method used, because different oxidizing mixtures results in different amount and different types of oxygen functional groups. This can be seen from Figure 24, which compares the electrochemical reduction of graphene oxide produced by different oxidizing methods. Staudenmaier and Hofmann methods uses potassium chlorate, whereas Hummers and Tour methods uses sodium nitrate to oxidize graphene or graphite [65]. Electrochemical reduction can easily

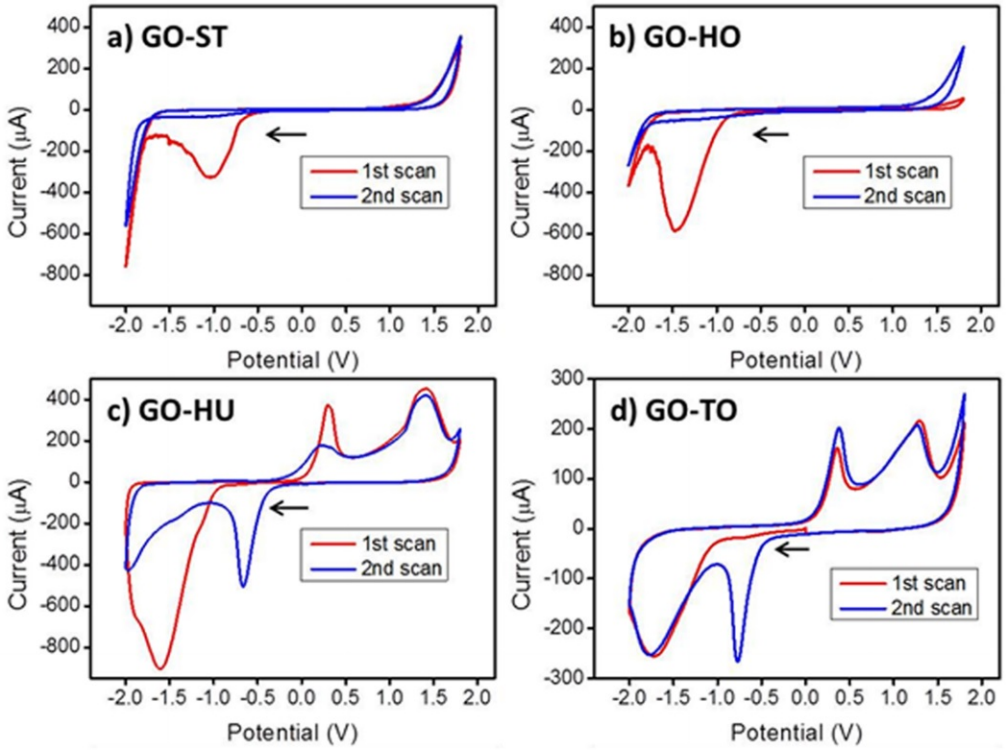

Figure 24: CV during the electrochemical reduction of graphene oxide produced by methods: a) Staudenmaier, b) Hofmann, c) Hummers and d) Tour at 50 mM PBS, pH 7.2, scan rate, 100 mV/s *vs* Ag/AgCl-electrode. Arrow indicates the direction of the first reduction scan marked in red. [96]

reduce oxygen functional groups that are electrochemically active such as quinones, hydroxyls, aldehydes, epoxides, and peroxides [65]. Typical reduction potentials (*vs* Ag/AgCl-electrode) for the peroxides is about -0.7 V, aldehydes about -1.0 V, epoxides about -1.5 V, and carboxyls about -2.0 V [65] as can also be seen from the peaks in Figure 24. Higher amount of carbonyl and carboxylic groups in Hummers and Tour methods compared to Staudenmaier and Hofmann method can be seen from the wider and higher peaks around -2.0 V in Figure 24.

The main advantages of electrochemical reduction are that there is no need for strong and potentially toxic reactants and by-products unlike chemical reduction and lower energy consumption than thermal reduction. It is also a fast, inexpensive and effective method and the applied potential and the time of the reduction can be easily controlled resulting in different C/O ratios [65]. Fast reduction process on the other hand may induce defects, which can be eliminated by annealing or increasing the temperature during the reduction [97]. Electrochemical reduction can also be used in identifying the oxygen functional groups from the graphene oxide surface because the amount of charge can be measured during the reduction [65].

6.2.5 Other reduction methods

There are numerous methods to reduce graphene oxide in addition to the before mentioned. Photocatalytic reduction uses titanium dioxide (TiO_2) as a photocatalyst and ultraviolet irradiation. Irradiation causes separation of charge on the surface of the TiO_2 particles and with ethanol the electrons reduces graphene oxide sheets [88]. Microwave irradiation results in more uniform heating and faster heating rate than normal thermal reduction method with a commercial microwave oven [72]. Flash reduction with a xenon lamp from *e.g.* a camera can also be used. The photo energy is emitted by the lamp and provides higher thermal energy than conventional thermal reduction [72]. On the other hand reduction via bacterial respiration is an environmentally friendly method for reduction. Bacterial respiration uses the ability of Shewanella microbes found *e.g.* from ocean water, spoiled food and sediments to exploit graphene oxide as an electron acceptor for their respiration [98].

6.3 Characteristics of reduced graphene oxide

The following chapters describes the structural, mechanical, electrical and electrochemical properties of reduced graphene oxide obtained by different reducing methods. Different oxidation methods results in differences in the surface chemistry of graphene oxide and different reduction method removes different amount and different type of oxygen functional groups, which is why careful characterization of the properties is important when designing electrochemical devises.

6.3.1 Structure, surface chemistry and mechanical properties

As mentioned earlier the surface area of an electrode is important when designing electrochemical sensors because high surface area provides more electroactive sites and decreases the electrode impedance. Theoretical value for the surface area of a single layer pristine graphene is 2630 m^2/g as stated earlier. Surface area of reduced graphene oxide is substantially smaller regardless of the reduction method. For excample BET surface area for a hydrazine monohydrate reduced graphene oxide is lower than thermally reduced graphene oxide (466 m^2/g *vs.* 600-900 m^2/g) [66].

Raman spectroscopy on the other hand provides information about the structural defects in carbon based electrodes. Structural defects in the sp^2 carbon structure weakens the mechanical properties, which is unfavourable concerning implantable

electrochemical sensors. Electrodes need to be mechanically strong also for long term implantation and flexible enough in order to minimize tissue damage. G and D peaks in the Raman spectra result from the vibrations of the sp^2 bonded carbon, where the D peak corresponds to the amount of defects, *i.e.* higher ratio of the intencity peaks (I_D/I_G), results in higher amount of defects [99]. Figure 25 presents Raman spectra of graphite, graphite oxide, graphene oxide, thermally reduced graphene oxide, electrochemically reduced graphene oxide and chemically reduced graphene oxide. The D-band intensity is the lowest in pristine graphite because of the lowest amount of defects in the carbon structure. The defect density increases during oxidation as can be seen from the small differences in the heights of D band and G band from the Raman spectra of graphite oxide and graphene oxide. The highest amount of defects between differently reduced graphene oxides results from the thermal reduction, because the decomposing oxygen groups divides graphene sheets into smaller pieces by removing carbon atoms from the layer [66, 88]. Figure 25 also indicates that the chemical and electrochemical reduction methods does not completely repair the disrupted carbon structure, which can be seen from the high D-band peak.

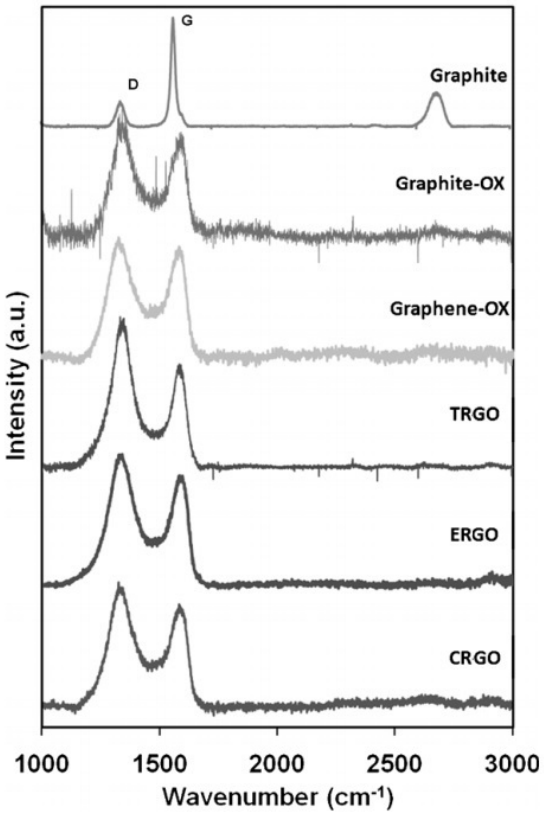

Figure 25: Raman spectra of graphite, graphite oxide, graphene oxide, thermally reduced graphene oxide (TRGO), electrochemically reduced graphene oxide (ERGO), chemically reduced graphene oxide (CRGO) normalized according to the G-band intensity [76].

Surface chemistry and the exact distribution of the oxygen functional groups

are still uncertain because of lack of sensitive characterizing techniques. However, as mentioned earlier, determining the C/O ratio with *e.g.* XPS is a useful tool in evaluating the reduction prosess. Typically C/O ratio of more than 15 is difficult to obtain with any of the chemical reductants [88]. C/O ratio for a hydrazine monohydrate or AA reduced graphene oxide is about 12 [86]. C/O ratio for HI reduced graphene oxide can be a little higher than $NaBH_4$ reduced graphene oxide (15 *vs.* 13) [88, 66]. Electrochemical and thermal reduction usually results in the highest C/O ratios compared to the most common chemical reduction methods (around 23) [66, 100, 101, 76] Higher C/O ratios than these can be obtained by combining different reduction methods, because different reduction steps with different reducing agents or methods can reduce different functional groups. For excample C/O ratios as high as 246 can be obtained by combining chemical and thermal reduction [88]. However clean surface such as pristine graphene without oxygen functional groups is not ideal for electrochemical sensing, which is why typical values obtained by *e.g.* chemical reduction are usually enough.

As stated earlier oxygen bearing functional groups increase the electrochemical response but oxygen functional groups also increase adsorption or desorption of products into the surface of the electrode, which may also decrease the electrochemical reactions [64]. Chemical reduction method, especially with hydrazine monohydrate also results in heteroatomic impurities, which are not easily removed. For excample nitrogen remains covalently bound to the surface of hydrazine monohydrate reduced graphene oxide, which effects the electronic properties. Whereas $NaBH_4$ reduced graphene oxide contains none or only few such heteroatoms but high amount of alcohol impurities. [66]

The structure and surface chemistry of reduced graphene oxide can also be modified by immobilizing other functional groups (*i.e.* functionalization) with a covalent bond to the oxygen group or with a non-covalent bond to the surface of reduced graphene oxide by different chemical reactions [66, 26]. 2D structure, large surface area and oxygen containing functional groups of reduced graphene oxide provides a possibility for the functionalization. Functionalization can improve mechanical, thermal, electrical or electrochemical properties and produces further possibilities for the use of reduced graphene oxide in a variety of applications. Functionalization can be done with *e.g.* NPs, organic compounds and biomaterials [26]. Polymers have also been used to improve reduced graphene oxides characteristics [66]. For excample addition of amines or hydroxyls leads to formation of amides or esters, which results in the covalently bonding of functional groups to the reactive oxygen groups [66].

6.3.2 Electrical properties

As stated earlier ballistic transport in pristine graphene can be almost micrometre distances without scattering, which lead to high conductivity. Oxidation changes graphene from a conductor to almost an insulator and the conductivity needs to be retained by reduction in order to use the material in electrochemical sensing. Conductivity of reduced graphene oxide depends on the chemical and atomic structure, hence the amount of defects and amount and spatial distribution of the oxygen

functional groups on the surface of the material. Oxygen functional groups and defects function as scattering points and decreases the electron transport [72]. However oxygen functional groups are easier to remove than to repair the defects. Due to the incomplete reduction of graphene oxide the conductivity is commonly some orders lower than the pristine graphene.

Electron mobility of pristine graphene can be over 15,000 $cm^2V^{-1}s^{-1}$, whereas electron mobility of graphene oxide is very minimal because of the low conductivity. Electron mobility at different stages of graphene oxide reduction is presented in Figure 26. Darker grey areas are sp^2 carbon bonded areas and lighter grey areas are sp^3 bonded carbon areas with oxygen functional groups presented with light grey dots. At the initial stage (Figure 26 a) sp^2 bonded areas in graphene oxide are isolated by oxygen functional groups, which forms a transport barrier for the electrons. This is why graphene oxide has a very low conductivity. As reduction progresses (Figure 26 b-d) electron transport by hopping and tunnelling gradually increases [102]. New smaller sp^2 bonded carbon areas are formed, which connects the larger sp^2 bonded areas and thus increases mobility. However electron mobility is not fully retained after the reduction because of the remaining defects and oxygen functional groups. For excample electron mobility of chemically reduced graphene oxide is 2-200 $cm^2V^{-1}s^{-1}$ at room temperature [102], which is about two orders of magnitude lower that of pristine graphene.

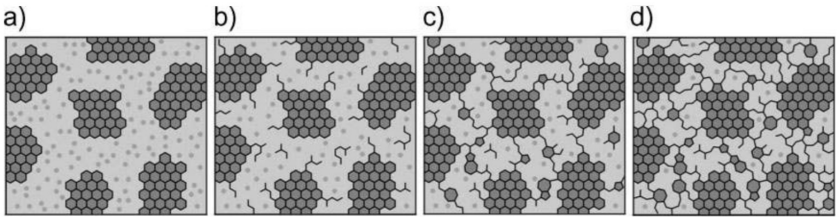

Figure 26: Electron mobility of graphene oxide at different stages of thermal reduction at a) room temperature, b) 100 °C, c) 220 °C and d) 500 °C [102].

Conductivity of graphene oxide prepared by *e.g.* Hummers method is low (0.1-0.5 S/m [103]) because of the disrupted carbon structure and oxygen functional groups. All of the before mentioned reduction methods can restore the conductivities atleast to some extent. The conductivity obtained by hydrazine monohydrate reduced graphene is higher than AA reduced graphene oxide (9960 S/m *vs.* 7700 S/m [86]) The highest electrical conductivity obtained by chemical methods is with HI (30 000 S/m [95]). The conductivity obtained by electrochemical reduction method is comparable to hydrazine monohydrate and AA reduced graphene oxides (8500 S/m [66, 100, 101]). Thermal reduction on the other hand decreases ballistic transport and induces scattering because of defects and structural damage, which is why electrical conductivity is significantly lower (1000-2300 S/m [72]). This leads to the conclusion that reduction does take place also with thermal reduction but only at some extent, despite of the structural defects.

Even higher conductivities can be achieved with a combination of different reduction methods because different reduction methods desorb different oxygen functional

groups. For excample chemical reduction induces less structural damage and thermal reduction desorbs various functional groups, which leads to higher conductivity. Conductivity can also be increased by *e.g.* doping with molecules, ions, functional groups, metal particles or ionic liquids [104]. However adsorption of molecules can either increase or decrease electron mobility by inducing hopping or scattering points [104].

6.3.3 Electrochemical properties

The electrochemical behaviour of reduced graphene oxide depends on the amount of defects and oxygen functional groups remained after the reduction process. The amount and distribution of defects and oxygen functional groups depends both on the oxidation and reduction method. For excample Hummers method of oxidation produces higher amount of carbonyl and carboxylic groups than Staudenmaier method because of different oxidizing mixtures [65]. This is why graphene oxide should be prepared by the same method when comparing different reduction methods, which was clearly visible also from Figure 24.

Reduced graphene oxide typically include structural defects which lead to increased HET rate, which can be tuned by applying different reduction methods [65]. The observed HET rate of graphite oxide produced, *e.g.* by Staudenmaier method, is low (2.92 x 10^{-5} cm/s) because of high amount of oxygen functional groups, low conductivity and electrostatic repulsion [76]. After the exfoliation of graphite oxide to graphene oxide, the HET rate increases slightly to 5.43 x 10^{-5} cm/s, because of higher amount of edge like structure exposed [76]. The highest HET rate between the three most common reduction methods can be obtained by thermal reduction (0.005 cm/s [76]), which is very close to the HET rate of EPPG because of high amount of structural defects. The HET rate of electrochemically reduced graphene oxide on the other hand is higher than chemically reduced graphene oxide, (2.8 x 10^{-3} cm/s *vs.* 3.9 x 10^{-4} cm/s) [76]. All of the before mentioned HET rates were measured with ferro/ferricyanide as a redox probe.

Charge transfer resistance also reflects the electrochemical properties of the material. Figure 27 presents Nyquist diagrams obtained with EIS from graphite, graphite oxide (prepared by Staudenmaier method), graphene oxide, thermally reduced graphene oxide, electrochemically reduced graphene oxide, chemically reduced graphene oxide (with $NaBH_4$), EPPG and GC electrodes. The lowest and smallest curves were obtained with thermally reduced graphene oxide and EPPG, which indicates low charge transfer resistance (3.05 and 2.89 kΩ respectively) and hence high electron transfer rate. The highest charge transfer resistances were obtained with graphite oxide and graphene oxide because of the high amount of oxygen functional groups (14.72 and 11.75 kΩ respectively). Charge transfer resistance of chemically reduced graphene oxide on the other hand is higher than electrochemically reduced graphene oxide also due to higher amount of oxygen functional groups (5.78 *vs.* 4.71 kΩ respectively). The charge transfer resistances and HET rates are summarized in Table 1. As can be seen from Table 1 high HET rate and low charge transfer resistance are directly related.

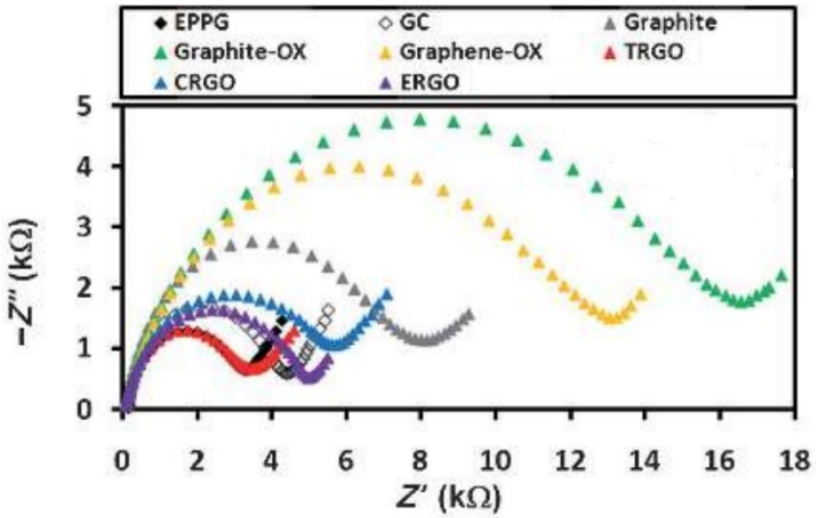

Figure 27: Nyquist diagrams from graphite, graphite oxide, graphene oxide, thermally reduced graphene oxide (TRGO), electrochemically reduced graphene oxide (ERGO), chemically reduced graphene oxide (CRGO), EPPG and GC electrodes. 10 mM $K_3[Fe(CN)_6]/K_3[Fe(CN)_6]$ as a redox probe in 50 mM, pH 7.2 PBS. [76]

Table 1: HET rate constants and charge transfer resistances for different carbon based materials.

Material	**HET rate (cm/s)**	**Charge transfer resistance (kΩ)**	**Ref.**
Graphene (edge plane)	0.01		[64]
Graphene (basal plane)	10^{-9}		[64]
Graphite oxide	2.92 x 10^{-5}	14.72	[76]
Graphene oxide	5.43 x 10^{-5}	11.75	[76]
EPPG	0.005	2.89	[76]
	0.022		[77]
BPPG	2.26 x 10^{-5}		[76]
	$< 10^{-9}$		[77]
GC	0.003		[76]
CRGO ($NaBH_4$)	3.9 x 10^{-4}	5.78	[76]
TRGO	0.005	3.05	[76]
ERGO	2.8 x 10^{-3}	4.71	[76]

Figure 28 presents cyclic voltammetry of graphite, graphite oxide (prepared by Staudenmaier method), graphene oxide, thermally reduced graphene oxide, electrochemically reduced graphene oxide, chemically reduced graphene oxide (with $NaBH_4$), EPPG, BPPG, and GC electrodes. As was seen from Figure 25 earlier, thermally reduced graphene oxide has higher level of defect density than chemically and electrochemically reduced graphene oxide and at the same time rather high C/O

ratio which results in higher electrochemical response. From Figure 28 can be seen that the electrochemical response of thermally reduced graphene oxide has smaller peak separation and lower oxidation potential than chemically or electrochemically reduced graphene oxide. The defect densities of chemically and electrochemically reduced graphene oxide are almost the same (from Figure 25) so the differences in the electrochemical properties observed in Figure 28 are defined mainly by the amount of oxygen functional groups remained. Electrochemical reduction results in a little more distinguished peaks than chemical reduction, which indicates that, as the density of defects are the same, the amount of oxygen functional groups is smaller in electrochemically reduced graphene oxide than chemically reduced graphene oxide resulting in better electrochemical response.

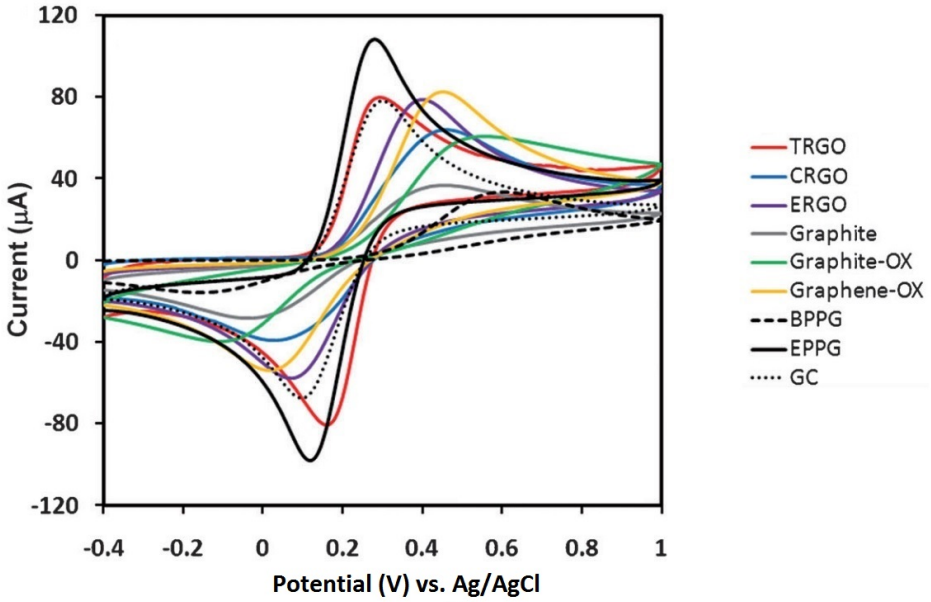

Figure 28: Cyclic voltammetry of graphite, graphite oxide, graphene oxide, thermally reduced graphene oxide (TRGO), electrochemically reduced graphene oxide (ERGO), chemically reduced graphene oxide (CRGO), EPPG, BPPG, and GC electrodes. 10 mM $[Fe(CN)_6]^{4-/3-}$ in 0.1 M KCl electrolyte, scan rate 100 mVs^{-1}. [76]

6.3.4 Biocompatibility

The biocompatibility and cytotoxicity of reduced graphene oxide are highly important concerning electrochemical applications, although very rarely tested in basic electrochemical research. As functionalization of CNT with oxygen groups is believed to decrease the toxicity [105], the same might be expected in case of graphene oxide due to the high amount of oxygen functional groups. Graphene oxide has been proven to slightly decrease the cell viability at high concentration and increase cellular oxidative stress at low concentration, although the cellular oxidative stress is lower than with fullerenes or CNTs. [106]. However graphene oxide does not cause significant toxicity to *e.g.* human lung carcinoma epithelial cells and could even be used as a substrate

for cell growth [106]. On the other hand graphene oxide at high concentration does cause pathological changes when injected in the lung of mice [107]. Biocompatibility of grahene oxide also depends on the size of the sheet, because larger dimension graphene oxide sheets at high concentration are more biocompatible than smaller sheets [106].

Cytotoxicity and biocompatibility of reduced graphene oxide highly depends on the reduction method. Different reduction methods result in different conductivity, size and density of functional groups wich all affect the toxicity [108]. As the most common chemical reducant hydrazine monohydrate has been proven toxic, biocompatibility can be improved and cytotoxicity decreased with different environmentally friendly and nontoxic reductants such as AA. Tissue damage mainly occurs due to the sharp edges of reduced graphene oxide [109]. Reduced graphene oxide platelets seem to induce more cellular damage compared to reduced graphene oxide sheets, indicating high dependence between the lateral dimension of reduced graphene oxide and the cytotoxicity [109].

6.3.5 Comparison of reduction methods and summary

As there are many methods to produce graphene, there are, as discussed earlier, several methods to oxidize graphene or graphite. All of the oxidizing methods result in different surface chemistry, *i.e.* different amount and type of oxygen functional groups attached to the surface of graphene oxide, because of a wide variety of oxidizing agents such as sodium nitrate, potassium permanganate or nitric acid. Nitric acid *e.g.* results in carboxyls lactones and ketones. After the oxidation graphene oxide is almost an insulator and the type and location of the oxygen functional groups affects the conductivity of the material. The purpose of reduction is to restore the electrical conductivity of graphene oxide in order to use it as an electrochemical sensing material. Reduction ideally removes the oxygen functional groups and repairs the structural defects. However different reduction methods result in different outcome.

The main characteristics of reduced graphene oxide in electrochemical sensing is the surface chemistry and the structural defects formed or remained, during and after the oxidation and reduction process. Surface chemistry and the remained defects ultimately determine the surface area, conductivity, C/O ratio, and the HET rate of reduced graphene oxide. As there are no direct method to monitor the reduction process, with the help of these variables, the possible use in electrochemical sensing can be evaluated. Comparison of different reduction methods with the before mentioned characteristics is presented in Table 2.

Chemical reduction of graphene oxide is the most common reduction method despite that C/O ratio of more than 15 is not easy to achieve. Reducing agents can also be highly toxic but promising alternatives have been researched such as AA. Chemical reduction is highly scalable for mass production because the reagents are inexpensive and easily accessible. Different reductants also reduce different oxygen functional groups. The BET surface area is smaller than thermally reduced graphene oxide, but the amount of structural defects is smaller, which results in stronger material to be implanted. The electrical conductivity can be from 7700 to as high as

30 000 S/m. The HET rate on the other hand is the lowest compared to thermal or electrochemical reduction methods, which affect the electrochemical properties.

Thermal reduction method is simple, easy and scalable for mass production but consumes a lot of energy because of the high temperatures. The type of oxygen functional groups reduced can be controlled by changing the reduction temperature. Conductivity is somewhat restored but the larger amount of structural damages and defects affect the mechanical properties. The BET surface area of thermally reduced graphene oxide is larger than *e.g.* chemically reduced graphene oxide with hydrazine monohydrate, which also results in more electroactive sites. The high C/O ratio of thermally reduced graphene oxide indicates an effective reduction process, but the conductivity is low, which results from the structural defects. The HET rate on the other hand is the highest compared to chemical and electrochemical reductions.

Electrochemical reduction method on the other hand is easily controlled with the applied potential. The instrumentation is simple and does not need potentially toxic chemical reagents or ambient environment. Also the C/O ratio obtained is high and the restored conductivity higher than the conductivity of thermally reduced graphene oxide. The HET rate of electrochemically reduced graphene oxide is smaller than thermally reduced graphene oxide but still higher than chemically reduced graphene oxide.

Table 2: Comparison of different reduction methods.

Method (Reductant)	**Conductivity (S/m)**	**C/O ratio**	**HET rate (cm/s)**	**Ref.**
Chemical (AA)	7700	12.5		[86]
	2690	12.5		[86]
Chemical (N_2H_4)	9960	12.5		[86]
	4160	12.5		[86]
Chemical ($NaBH_4$)	0.26-1.55	3.33-5		[86]
		2.9	3.9 x 10^{-4}	[76]
Chemical (HI)	30 000	15		[95]
Chemical (KOH)	0.02-0.19	3.33-5		[86]
Thermal	1000-2300	23.3	0.005	[76]
Electrochemical	8500	23.9		[101]
		5.1	2.8 x 10^{-3}	[76]

There are no single method above all for electrochemical detecting due to the vide variety of ions and molecules to be detected from human body and all of the before mentioned methods have different advantages and disadvantages. However the electrochemical properties can be easily altered with different surface modification methods, which is why basic reduced graphene oxide is rarely used in electrochemical sensing. Selectivity and sensitivity is usually enhanced with stabilizing surfactants, coatings or NPs, which forms different reduced graphene oxide based composite materials.

7 Electrochemical measuring with chemically reduced graphene oxide

The number of research about graphene in electrochemical sensing has been growing exponentially after the 2010 Nobel Prize in Physics. Graphene possess positive characteristics for electrochemical applications such as high electrical conductivity and large surface area. The absence of metallic impurities also favours graphene instead of CNTs since impurities alter the electrochemistry and results in distorted outcome [3]. Low solubility in water and other organic solvents and the lack of large scale, simple and inexpensive fabrication method restricts the use of graphene in electrochemical applications. However reduced graphene oxide provides an ideal solution. Reduced graphene oxide is partially hydrophilic and hydrophobic, therefore dispersible in water and other common solvents, which makes the sensor fabrication easier. Also the diminished electrical conductivity due to the oxidation is restored by reduction which enables electron transfer between a biological analyte and the material. The purpose of this Master's thesis is to evaluate chemically reduced graphene oxide (hence referred as CRGO) in electrochemical sensing for biomedical purposes. According to the previous chapter chemical reduction of graphene oxide (hence referred as GO) is the most common reduction method but not necessary the most suitable method to produce electrochemical sensors for bioapplications because of the toxic reagents. In addition chemical reduction does not usually provide the highest electron transfer rate compared to other reduction methods. However there are numerous surface modification methods to improve the electrochemical properties of CRGO. The following paragraphs introduces different CRGO electrodes and their surface modification methods in the detection of biologically interesting compounds and compares the electrochemical properties. Some interesting environmentally friendly and biocompatible reductants will also be introduced. A summary of the characteristics of CRGO based electrochemical sensors and biosensors are presented after each paragraph and in the appendix Tables A1 and A2.

7.1 Basic principles of measurement

As mentioned earlier electrochemical sensor does not need an additional biological recognition element because graphene based electrochemical sensors can detect the oxidation and reduction of electrochemically active compound directly from the surface of the electrode material. On the other hand large surface area of a graphene based materials provides an ideal platform for the enzymes, antibodies, cells, NPs or probes to be immobilized in order to increase the electrochemical response. Reduced GO combined with surface modification structures can be dispersed directly on the surface of a substrate electrode or with another material such as Nafion or ionic liquids. Nafion and ionic liquids decrease the aggleromation of the NPs, which further increases the surface area. The deposition is commonly performed by drop casting and drying the electrode composite solution to the surface of a substrate electrode. GC and screen printed electrodes (SPE) are commonly used as a substrate. Deposition often results in lower structural quality because of defects and uncontrolled layer

thickness [26]. The density of defects and thickness can be controlled *e.g.* with a spin-coating deposition technique [26]. The thickness and homogeneity depends on the concentration of the graphene based suspension, spinning speed and the number of cycles [26]. Self-assembly technique is another useful method to deposite graphene based material on a substrate electrode, where the thickness of the layer can be controlled as well as the dimension on a nanoscale [26].

During the research of CRGO in electrochemical detecting of biological analytes, C/O ratio, charge transfer resistance, linear concentration range, level of detection (LOD) and sensitivity if often evaluated, which is why this comparative work has also focused on these parameters. C/O ratio is commonly measured with XPS and the amount of defects with the ratios of I_D and I_G bands provided by Raman spectroscopy. The amount of oxygen functional groups and defects can be used in evaluating the amount of electroactive sites, which ultimately affects the elecrochemical properties of CRGO. EIS is used in measuring the charge transfer resistance which indicates the rate of the electron transfer. Charge transfer resistance can be evaluated with the obtained Nyquist plot. Linear concentration range is measured amperometrically by adding increasing amount of analyte at a certain potential and calibrating the linear current *v.s.* concentration curve. LOD is measured the same way but with a decreasing amount of analyte and measuring the lowest still detectable current. Sensitivity is typically presented in $AM^{-1}cm^{-2}$ and reflects to a change in current resulting from a change in concentration per area. Higher sensitivity indicates a better electrochemical result.

7.2 Detection of DA, 5-HT, AA and UA

As mentioned earlier simultaneous detection of DA, 5-HT, UA and AA is important because of their coexistence in biological samples. DA, 5-HT, AA and UA are usually all oxidized at very similar potentials during electrochemical sensing with conventional electrodes and in order to successfully detect these molecules, the electrodes need to be selective enough. It is easier to construct a highly selective sensor to detect one of these, but simultaneous detection of all of the molecules would be less time consuming, simpler and inexpensive. Typical LOD for DA, 5-HT, AA and UA with carbon-based electrodes is between 0.01-1.5 μM [47]. Addition of enzymes on the surface of carbon-based electrodes lowers the typical LOD to 0.003-1.0 μM and MIPs to even lower, starting from 0.01 nM [47].

7.2.1 Without surface functionalization

Electrochemical detection of DA, 5-HT, AA, UA can be done with a simple CRGO sensor without surface functionalization. Sensitivity and LOD can be improved using different reductants. Zhou *et al.* [24] successfully measured the individual oxidation of UA, AA, DA and APAP with a simple CRGO sensor with no additional surface modifications. They prepared GO from graphite by modified Hummers method. Chemical reduction was performed with hydrazine and the CRGO suspension was dried on the surface of a GC electrode. The thickness of the CRGO layer changed

from 1.2 nm to 0.8 nm during reduction and was measured with AFM, which indicates a successful reduction with some additional oxygen functional groups. I_D/I_G ratio measured with Raman spectroscopy was 1.38 which results from high level of defects on the surface of CRGO. C/O ratio changed during reduction from 1.4 to 11.8. Charge transfer resistance of CRGO/GC electrode was 160.8 Ω, which was lower than graphite/GC (about 400 Ω) and GC (about 200 Ω) indicating higher electron transfer rate. CRGO/GC electrodes required lower potential and induced larger current for the oxidation (and reduction) prosess compared to graphite/GC and GC electrodes The sensor fabricated by Zhou *et al.* is very simple, but unfortunaltely the stability, reproducibility, LOD and sensitivity of the sensor was not tested. Also the sensor was only tested in PBS instead of biological samples. The effect of interfering subtances was not tested, which would be highly important because of the similar oxidizing potentials. However the sensor was versatile and could be used in detecting other biological compounds such as free DNA bases, NADH and H_2O_2 as will be described later.

Kim *et al.* [110] also prepared an unmodified CRGO sensor and tested different reductants during the detection of 5-HT and also in the presence of DA and AA. They used improved Hummers method to oxidize graphite and compared three chemical reductants: 1. hydrazine monohydrate with ammonium hydroxide, 2. hydrazine monohydrate and 3. hydroxylamine hydrochloride ($NH_2OH \cdot H_2O$) with ammonium hydroxide. The CRGO solutions were dried on a GC electrode. The lowest electron transfer resistance measured with EIS was at hydrazine monohydrate with ammonium hydroxide reduced GO, indicating a positive effect of the ammonium hydroxide on the reduction prosess. The C/O ratio of hydrazine with ammonia reduced GO the other hand was 4.23, which was lower than hydrazine monohydrate reduced GO (4.98) but higher than hydroxylamine hydrochloride with ammonium hydroxide reduced GO (4.17). The amount of oxygen functional groups were high with all of the different reductants compared to Zhou *et al.* (11.8), which presumably results from the differencies in the fabrication prosess.

The CV of 100 μM 5-HT in 0.1 M pH 7.4 PBS showed superior electrochemical responce for hydrazine monohydrate with ammonia reduced GO and the peak current for oxidation of 5-HT was at 0.36 V. All of the reductants showed distinquished oxidation peaks for both 5-HT and DA also in the presence of high amount of AA. The hydrazine with ammonia reduced GO/GC showed very minimal sensitivity towards the oxidation of AA, although AA did interfere the detection of DA by increasing the oxidation peak current of DA. The peak oxidation potential for 5-HT was slightly shifted with hydrazine monohydrate and hydroxyl amine and ammonia as reductants in the presence of DA and AA. However the addition of AA did not interfere the oxidation of DA with hydrazine monohydrate as a reductant, which indicates that hydrazine monohydrate is more selective in detecting DA and 5-HT in the presence of interfering substances. On the other hand the oxidation peak currents are smaller with hydrazine monohydrate as a reductant. Linear ranges for 5-HT, DA and AA were 1-100 μM with all of the sensors. LOD for hydrazine with ammonia reduced GO/GC electrode for 5-HT was the lowest compared to hydrazine reduced GO/GC and hydroxyl amine and ammonia reduced GO/GC (32 nM *vs.* 46

nM and 52 nM respectively). Hydrazine with ammonia reduced GO/GC electrode also showed highest sensitivity (20.152 mA$mM^{-1}cm^{-2}$) between the three electrodes.

The sensitivity of the sensor towards the fabrication prosess can be seen from Figure 29. Zhou *et al.* and Kim *et al.* both used hydrazine and hydrazine monohydrate as reductants and modified/improved Hummers method as an oxidizing method. However the sensor produced by Kim *et al.* was not significantly interferred by AA during the detection of DA due to the slight difference in the oxidizing potentials (Figure 29C, green line), whereas the sensor by Zhou *et al.* would probably be due to the similar oxidizing potentials, although it was not measured (Figure 29A and B). The reverse voltage axel in Figure 29C from positive to negative should also be noted and the negative oxidizing current (*vs.* positive in Figures 29A and B).

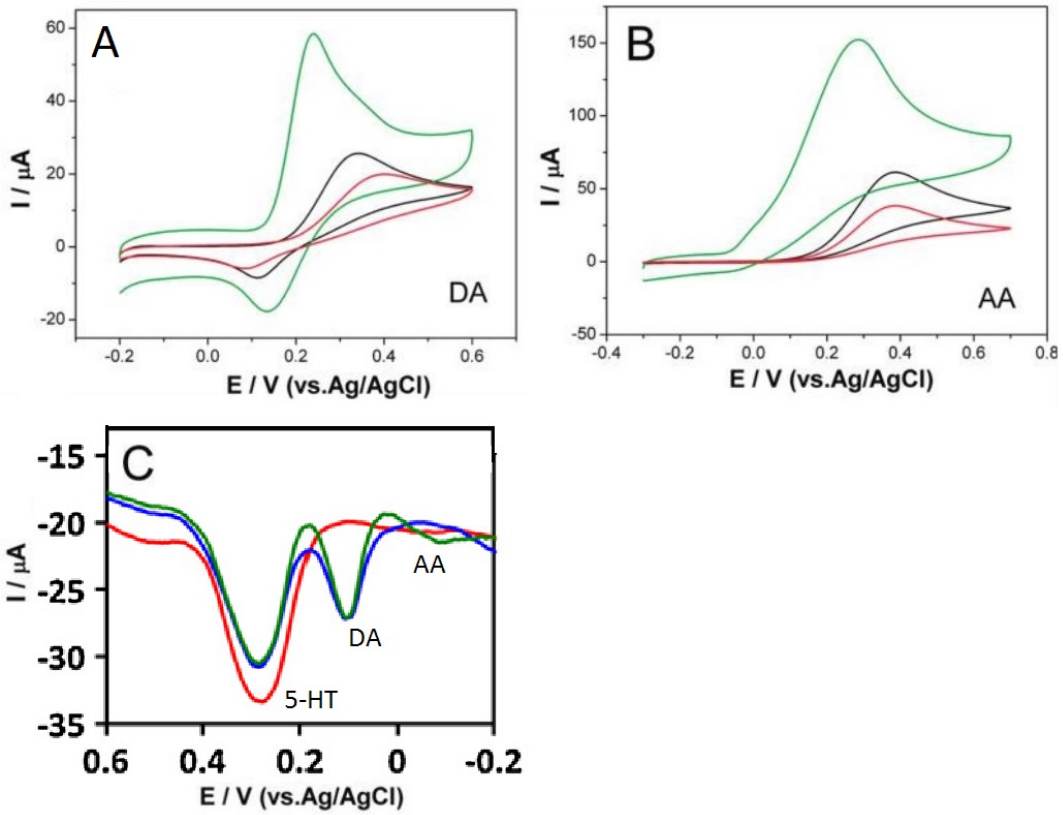

Figure 29: CV of the individual oxidation of A) 3 mM AA and B) 3 mM DA with hydrazine monohydrate reduced GO/GC electrode by Zhou *et al.* in 0.1 M pH 7.0 PBS, scan rate 50 mV/s [24] and C) DPV of 20 μM 5-HT without interfering substances (red line), in the presence of 20 μM DA (blue line) and in the presence of 20 μM DA and 200 μM AA (green line) with hydrazine reduced GO/GC by Kim *et al.* in 0.1 M pH 7.4 PBS, scan rate 25 mV/s [110].

A summary of the properties of the previously mentioned sensors is presented in Table 3. The most significant advantage of unmodified CRGO based electrochemical sensors is the simplicity of the electrode design. Different reductants result in different electrochemical properties and finding the right reductant for a particular analyte

results in LOD in nanomolar scale. The problem for unmodified sensors is usually the selectivity. Substances present in biological samples may interfere the detection because there are no recognition elements to improve selectivity or stabilizing layers to decrease foaling, which is why unmodified CRGO is mainly used in research purposes when comparing the electrochemical properties of different reductants.

Table 3: Unmodified CRGO based electrochemical sensors.

Molecule	**Reductant**	**C/O**	**Linear range (μM)**	**LOD (μM)**	**Sensitivity ($AM^{-1}cm^{-2}$)**	**Ref.**
DA	$N_2H_4 \cdot H_2O$	11.8				[24]
5-HT	$N_2H_4 \cdot H_2O$, ammonia	4.23	1-100	0.032	20.152	[110]
	$N_2H_4 \cdot H_2O$	4.98	1-100	0.046	9.533	[110]
	$NH_2OH \cdot HCl$, ammonia	4.17	1-100	0.052	6.773	[110]
AA	$N_2H_4 \cdot H_2O$	11.8				[24]
UA	$N_2H_4 \cdot H_2O$	11.8				[24]

7.2.2 Platinum and palladium nanoparticles

As mentioned earlier metallic NPs have many advantages in electrochemical sensing. NPs increases surface area, improves stability, sensitivity, selectivity, conductivity and increases the electron transfer rate [16]. Chitosan and Poly(diallyldimethylammonium chloride) (PDDA) are common stabilizing agents used with different NPs. Xu *et al.* [34] detected the oxidation of DA and UA selectively in the presence of high concentration of AA with platinum (Pt) NP decorated CRGO electrode with chitosan as a stabilizer, whereas Yan *et al.* [111] combined Pt and palladium (Pd) NPs with PDDA and successfully detected DA, UA as well as AA. Combining different metallic NPs was used in order to increase surface area, biocompatibility and electron transfer rate. Both research used modified Hummers method for the oxidation. However Xu *et al.* used $NaBH_4$ and Yan *et al.* NaOH as reductants. Both electrode materials were dried on a GC electrode.

The oxidation currents for the individual detection of DA and UA were significantly higher with Pt NPs than without the NPs, which indicates higher electrical conductivity and electron transfer mobility. Also the Pt NPs increase the oxidation peak potential separation between DA and UA. However the oxidation of AA was blocked with the NPs by Xu *et al.* because Pt NPs reduced at the oxidation potential of DA and UA, but not at the oxidation potential of AA, which resulted in the oxidation of only DA and UA. Simultaneous detection of DA and UA in the presence of AA with Pt/chitosan/CRGO/GC electrode is presented in Figure 30A. Pt/PDDA/CRGO/GC electrode on the other hand did successfully detect also AA unlike the Pt/chitosan/CRGO/GC electrode by Xu *et al.* This results either from the effect of PDDA *vs.* chitosan or different reductans used, which is why further studies should be conducted. The redox peak potentials were significantly higher with PdPt/PDDA/CRGO/GC compared to Pt/PDDA/CRGO/GC electrode indicating increased electron transfer rate of bimetallic NPs. Simultaneous detection of DA, UA and AA with PdPt/PDDA/CRGO/GC electrode is presented in Figure 30B.

Linear concentration range for DA was wider with PdPt/PDDA/CRGO/GC than with Pt/chitosan/CRGO/GC by Xu *et al.* (4-200 μM *vs.* 5.0-150.0 μM) and for UA significantly wider (4-400 μM *vs.* 10.0-130.0 μM). Linear range for AA with PdPt/PDDA/CRGO/GC electrode was 40-1200 μM. LOD for DA was lower with PdPt/PDDA/CRGO/GC (0.04 μM *vs.* 0.45 μM) and also for UA (0.1 μM *vs.* 0.70 μM, S/N=3). LOD for AA was 0.61 μM.

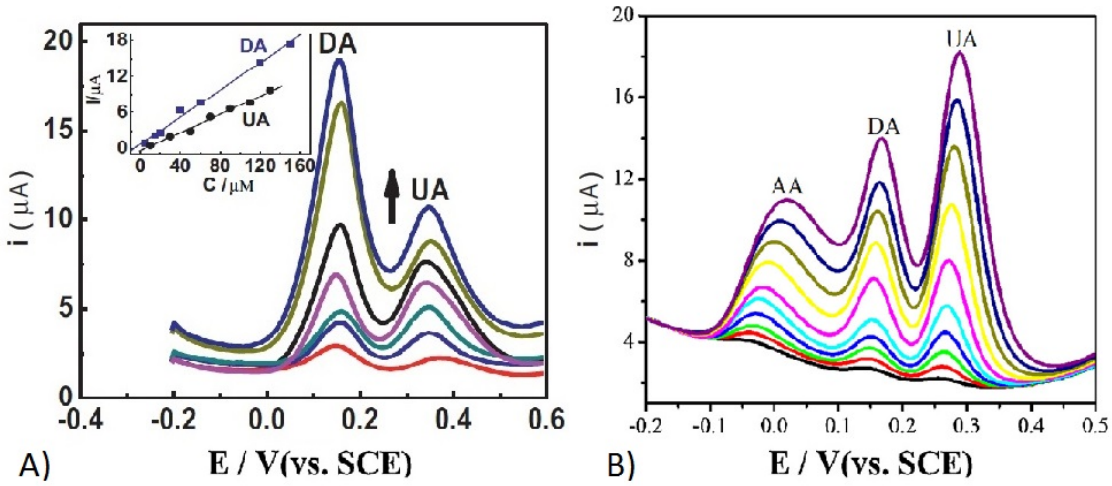

Figure 30: DPV of simultaneous detection of various concentration of DA and UA in the presence of 1.0 mM AA with Pt/chitosan/CRGO/GC electrode in 0.1 M PBS [34]. B) DPV of simultaneous detection of AA, DA and UA with PdPt/PDDA/CRGO/GC electrode in 0.1 M pH 7.4 PBS [111].

A summary of the properties of the previously mentioned sensors is presented in Table 4. Based on these values PdPt/PDDA/CRGO/GC electrode seems to result in more favourable outcome, which is due to the increased surface area with bimetallic NPs combined with the benefit gained either from the PDDA or the reduction with NaOH. Yan *et al.* also successfully tested the PdPt/PDDA/CRGO/GC electrode in human blood serum and urine samples with a recovery test unlike Xu *et al.*

Table 4: Pt and Pd NP modified CRGO based electrochemical sensors.

Molecule	**Electrode**	**Reductant**	**Linear range (μM)**	**LOD (μM)**	**Ref.**
DA	PtNP/chitosan/CRGO/GC	$NaBH_4$	5.0-150.0	0.45	[34]
	PtPdNP/PDDA/CRGO/GC	NaOH	4-200	0.04	[111]
AA	PtPdNP/PDDA/CRGO/GC	NaOH	40-1200	0.61	[111]
UA	PtNP/chitosan/CRGO/GC	$NaBH_4$	10.0-130.0	0.70	[34]
	PtPdNP/PDDA/CRGO/GC	NaOH	4-400	0.1	[111]

7.2.3 Gold nanoparticles

Gold (Au) NPs can be used with *e.g.* PAMAM dendrimers or MIPs. PAMAM is a branched macromolecules referred as a dendrimer, which can be used with metallic

NPs to increase selectivity and sensitivity. PAMAM dendrimers encapsulate the Au NPs and prevent them from accumulating. Accumulutation results in decreased electrochemical responce due to decreased surface area. On the other hand Au NPs can be used in improving the conductivity and catalytic activity of MIP, which are highly selective and can function as an artificial antibody for target molecules.

Liu *et al*. [111] and Wang *et al*. [18] both used Au NPs and PAMAM dendrimers in the simultaneous detection of DA and UA. Liu *et al*. functionalized with polysodium 4-styrenesulfonate (PSS) and used PDDA as a stabilizer. Wang *et al*. on the other hand also added MWCNTs and succesfully detected AA among DA and UA. Liu *et al*. used hydrazine and Wang *et al*. AA as a reductant. MWCNTs were used in preventing the CRGO sheets from restacking. Liu *et al*. oxidized with modified Hummers method, whereas the oxidation method was not mentioned by Wang *et al*. MWCNT and Au NPs were added to the mixture and the solution was drop casted and dried to a GC electrode. Liu *et al*. on the other hand used layer-by-layer self-assembly technique, because it was believed to result in more controlled composition, thickness and structure of the material.

Figure 31A presents the simultaneous oxidation of varying concentrations of DA and UA with hydrazine reduced GO/PSS/PDDA/PAMAM/AuNP by Liu *et al*. and Figure 31B presents the simultaneous oxidation of DA, UA, and AA with AA reduced GO/PAMAM/MWCNT/AuNP electrode by Wang *et al*. DPV in Figure

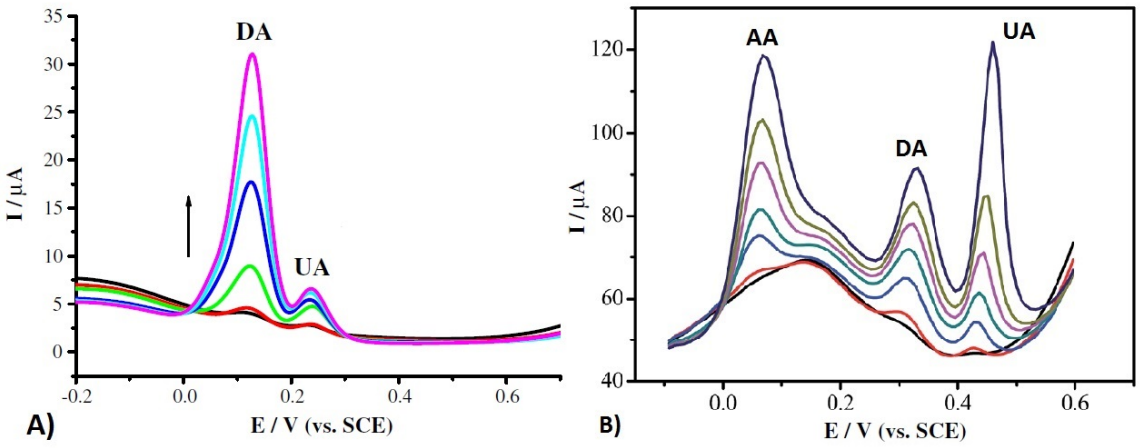

Figure 31: A) DPV of CRGO/PSS/PDDA/PAMAM/AuNP with varying concentrations of DA and UA in 0.1 M, pH 7.4 PBS [111]. B) DPV of CRGO/PAMAM/MWCNT/AuNP with varying concentratioons of DA, UA and AA in 0.1 M, pH 4.0 PBS. [18]

31B shows distinct peaks with CRGO/PAMAM/MWCNT/AuNP electrode by Wang *et al*. for all of the molecules during simultaneous detection, whereas the oxidation peak potentials with CRGO/PAMAM/AuNP by Liu *et al*. were smaller, although Liu *et al*. did not provide DPV in the presence of AA. On the other hand pH 4.0 as a measurement condition by Wang *et al*. does not correspond to natural conditions in human body, but was chosen because of the improved electrochemical

responce. Selectivity of the electrode was believed by Wang *et al.* to be due to PAMAM dendrimers containing carboxylic functional groups that may react with proton donating groups of DA, UA and AA via hydrogen bonds. The porousity of the electrode obtained by MWCNTs was also thought to increase selectivity towards different analytes oxidizing at similar potentials, which can also be seen from Figure 31B. MWCNTs also increases the electrochemically active surface area. The effect of hydrazine *vs.* AA reductants was not evaluated in either of the research. Linear concentration range by Liu *et al.* for DA was narrower compared to Wang *et al.* (1-60 μM *vs.* 10-320 μM) and slightly at a higher range for UA (10-120 μM *vs.* 1-114 μM). The LOD were slightly lower by Liu *et al.* compared to Wang *et al.* but were measured in the absence of AA (for DA 0.02 μM *vs.* 3.3 μM and for UA 0.27 μM *vs.* 0.33 μM). Low LOD was believed to result from the layer-by-layer assemply technique rather than the reductant. However Liu *et al.* measured the interfering effect of AA and glucose (among other substances) and concluded that the peak current changed very little in the presence of glucose but more in the presence of AA, which indicates a negative effect during the simultaneous detection of DA, UA and AA.

Xue *et al.* [112] on the other hand combined MIPs with Au NPs. Xue *et al.* fabricated a AuNP/MIP/polyaniline(PANI)/CRGO nanocomposite electrode for the detection of 5-HT. PANI acted as a surface coating for the CRGO to increase sensitivity because of high conductivity of PANI. Modified Hummers method was used and the reduction was done with hydrazine hydrate. AuNP/MIP membrane was fabricated by electro-polymerization and 5-HT were used as a template molecule and p-aminothiophenol as a cross-linker. The electrode signal for the 5-HT oxidation was not interferred with AA, DA, UA or epinephrine and 5-HT can be selectively detected with an artificial recognition element such as MIP in the presence of these molecules. Linear concentration range for the detection of 5-HT was 0.2-10 μM and LOD was 11.7 nM (S/N=3), which is low compared to other 5-HT detection sensors. However MIPs usually have slow responce times [112]. The sensor was also succesfully tested in human serum sample. A summary of the properties of the previously mentioned sensors is presented in Table 5.

Table 5: Au NP modified CRGO based electrochemical sensors.

Molecule	**Electrode**	**Reductant**	**Linear range (μM)**	**LOD (μM)**	**Ref.**
DA	PSS/AuNP/PDDA/PAMAM/CRGO/GC	$N_2H_4 \cdot H_2O$	1-60	0.02	[111]
	AuNP/PAMAM/MWCNT/CRGO/GC	AA	10-320	3.3	[18]
AA	AuNP/PAMAM/MWCNT/CRGO/GC	AA	20-1800	6.7	[18]
UA	PSS/AuNP/PDDA/PAMAM/CRGO/GC	$N_2H_4 \cdot H_2O$	10-120	0.27	[111]
	AuNP/PAMAM/MWCNT/CRGO/GC	AA	1-114	0.33	[18]
5-HT	AuNP/MIP/PANI/CRGO/GC	$N_2H_4 \cdot H_2O$	0.2-10	0.0117	[112]

7.2.4 Metalloporphyrins

Porphyrin is a 2D structure, consists of 18 π-electrons and is electrocatalytically active, thermally stable and chemically inert [113]. Porphyrins can behave as mediators for electron transfer with metal cations because hydrogen bond in the porphyrin reacts with proton-donating group of DA, AA and UA [113]. Deng *et al.* [113] used tetraphenylporphyrin (TPP) with cobalt (Co) and Karuppiah *et al.* [114] with copper (Cu). Karuppiah *et al.* and Deng *et al.* both oxidized with modified Hummers method and used hydrazine hydrate and ammonia as reductants. After the reduction metal-tetraphenylporphyrin solution was added to the CRGO solution and the formed solution was dried on a GC electrode. The metallic TPP molecules attach to the surface of CRGO via π-π interaction and provides larger surface area than CRGO. Deng *et al.* simultaneously detected DA, AA and UA whereas Karuppiah *et al.* detected DA selectively in the presence of AA and UA.

Figure 32A present DPV of CuTPP/CRGO/GC electrode with varying concentrations of DA and Figure 32B presents DPV of CoTPP/CRGO/GC electrode with varying concentrations of DA, UA and AA. All three molecules can be simultaneously detected with the CoTPP/CRGO/GC electrode, whereas the oxidation potential for DA with CuTPP/CRGO/GC electrode was smaller. Cu showed a blocking effect towards UA and AA, which was believed to result from the negatively charged environment repulsing UA and AA molecules, however the peak current from the oxidation of DA increased in the presence of AA and UA.

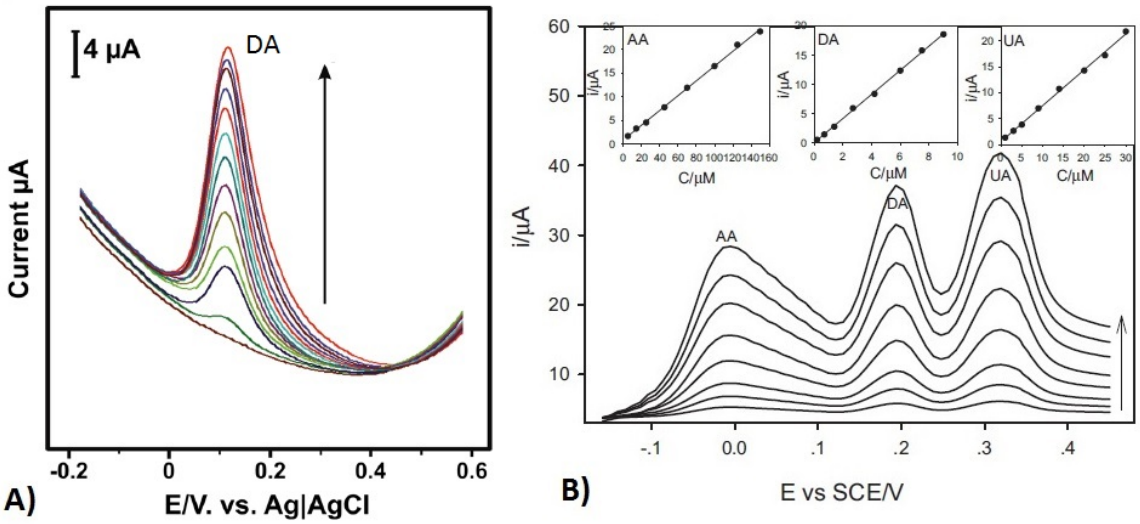

Figure 32: A) DPV of CuTPP/CRGO/GC electrode with varying concentrations of DA in pH 7.0 PBS [114]. B) DPV of CoTPP/CRGO/GC electrode with varying concentrations of DA, UA and AA in 0.1 M, pH 6.5 PBS [113].

Based on the results obtained by Deng *et al.* and Karuppiah *et al.* Co seems to be more suitable NP to be used with TPP because of the ability to simultaneously detect DA, AA and UA, the LOD for DA was lower (0.03 μM *vs.* 0.76 μM) and linear range covers the normal concentration range of DA better (0.1-12.0 μM *vs.*

2-200 μM). Deng *et al.* also measured the LOD for AA 1.2 μM and for UA 0.15 μM. Linear range for AA was 5.0-200.0 μM and for UA 0.5-40 μM. Both electrodes were successfully tested in natural environment with a recovery test, the electrode with Co in human urine and serum samples, whereas the sensor with Cu in human urine and saliva samples. A summary of the properties of both of the sensors is presented in Table 6.

Table 6: Metalloporphyrin modified CRGO based electrochemical sensors.

Molecule	**Electrode**	**Reductant**	**Linear range (μM)**	**LOD (μM)**	**Sensitivity ($AM^{-1}cm^{-2}$)**	**Ref.**
DA	Cu-TPP/CRGO/GC	$N_2H_4 \cdot H_2O$, ammonia	2-200	0.76	2.46	[114]
	Co-TPP/CRGO/GC	$N_2H_4 \cdot H_2O$, ammonia	0.1-12.0	0.03		[113]
AA	Co-TPP/CRGO/GC	$N_2H_4 \cdot H_2O$, ammonia	5-200	1.2		[113]
UA	Co-TPP/CRGO/GC	$N_2H_4 \cdot H_2O$, ammonia	0.5-40	0.15		[113]

7.2.5 Iron Oxide nanoparticles

Fe_3O_4 is a magnetic NP, which is biocompatible, low toxic, chemically stable and catalytically active [115]. The preparation of the NPs is simple because of the simultaneous reduction of graphene oxide and NP synthesis via chemical reaction. Fe_3O_4 increases the surface area and conductivity of CRGO by preventing the CRGO sheets from restacking, whereas CRGO provides a platform for Fe_3O_4 nanoparticles to evenly distribute via strong interaction [116, 117].

Bagheri *et al.* [116] measured the simultaneous oxidation of DA and melatonin with Fe_3O_4 decorated CRGO on the surface of carbon paste electrode (CPE) in the presence of AA and UA. They used Hummers method for the oxidation and AA and hydrazine hydrate as reductants. Peik-See *et al.* [118] on the other hand used simplified Hummers method for the oxidation, ammonium hydroxide (NH_4OH) as a reductant and the solution was dried on a GC electrode. They measured DA in the presence of AA. Fe_3O_4 nanoparticles were also used by Teymourian *et al.* [117]. They simultaneously detected DA, AA and UA and used modified Hummers method for the oxidation and hydrazine hydrate and ammonia solution for the reduction. The Fe_3O_4/CRGO solution was dried on a GC electrode.

Figure 33A presents the square wave voltammogram of simultaneous detection of DA and melatonin in the presence of varying concentrations of AA by Bagheri *et al.* AA even at higher concentrations have little effect on the oxidation of DA or melatonin, although the concentration of AA was only at micromolar range. On the other hand increasing the amount of DA did increase the oxidation current of melatonin. The peak oxidation potential for UA was about 0.57 V *vs.* SCE and 5-HT was about 0.3 V *vs.* SCE, which succests that the oxidation of UA and 5-HT might also be simultaneously possible because of the enough separation in the peak potentials. However tryptophan did severely interfere with the detection of melatonin. On the other hand pH for the measurement was 5.0 which does not correspond to the natural human sample environment. Figure 33B presents DPV of Fe_3O_4/CRGO/GC

with varying concentrations of AA in the presence of DA by Peik-See *et al.* High amount of AA shifted the peak potential of DA, which Peik-See *et al.* believed to be due to change in pH of the solution, which results from the acidic nature of AA. The same effect was not visible in the research by Bagheri *et al.* because of smaller amount of AA used. Figure 33C presents the DPV at Fe_3O_4/CRGO/GC electrode with varying concentrations of DA, AA and UA by Teymourian *et al.*. The simultaneous detection was possible, although the charge transfer resistance of the electrode was higher than obtained by Peik-See *et al.* (37.6 Ω *vs.* 3.7 x 10^{-3} Ω) indicating weaker electrochemical properties.

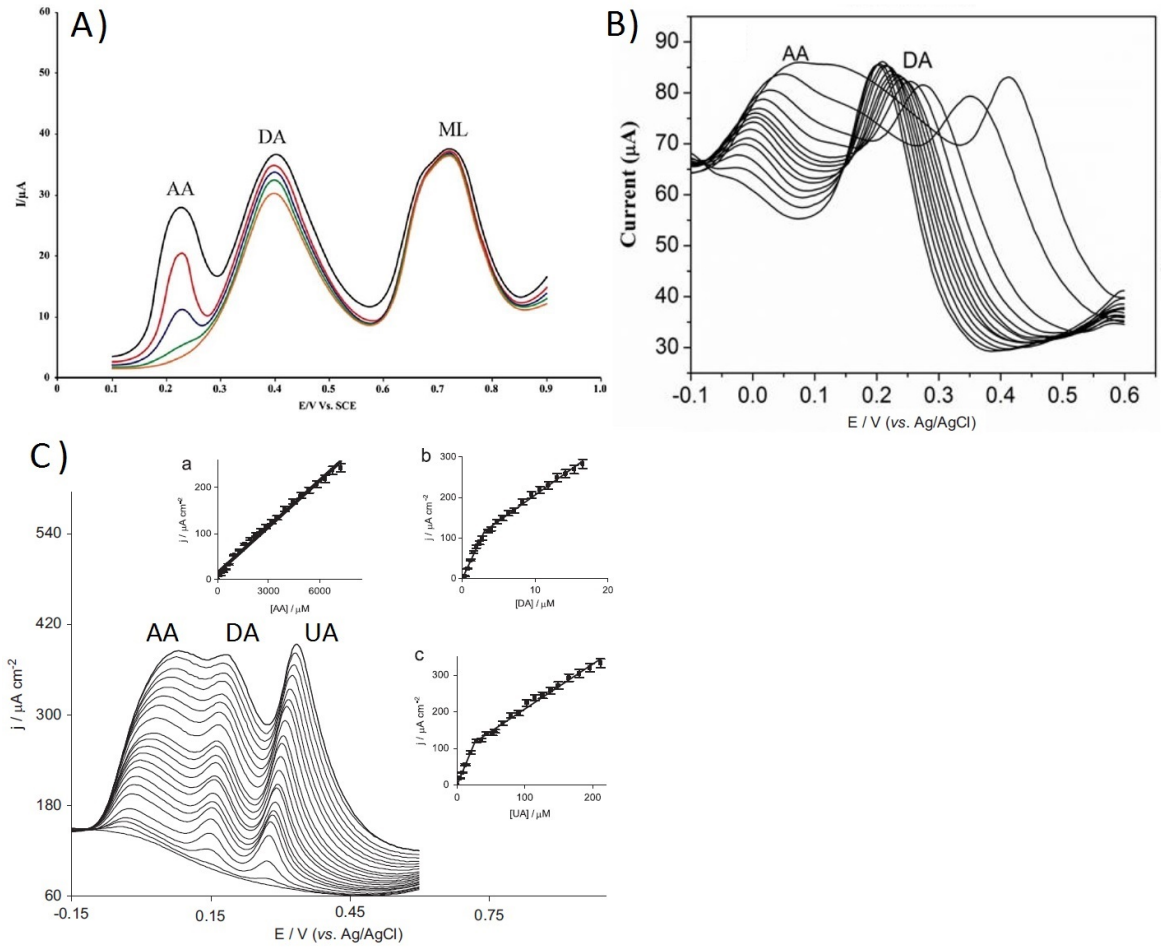

Figure 33: A) Square wave voltammogram of Fe_3O_4/CRGO/CPE with varying concentrations of AA (5-15 μM) in the presence of DA and melatonin [116]. B) DPV of Fe_3O_4/CRGO/GC with varying concentrations of AA (1-25 mM) in the presence of 0.1 mM DA [118]. C) DPV of Fe_3O_4/CRGO/GC electrode with varying concentrations of AA (a), DA (b) and UA (c) [117].

LOD for DA was 6.50 nM and for melatonin 8.4 nM by Bagheri *et al.*, which are both rather low. Linear range for the simultaneous detection of DA and melatonin was measured for 0.05-5.80 μM for both. Sensitivity, reproducibility and stability of

the sensor was not tested. Linear range for DA by Peik-See *et al.* was significantly higher compared to Bagheri *et al.* (0.5-100 μM *vs.* 0.05-5.80 μM) and for AA 1-9 mM. LOD for DA was also higher than obtained by Bagheri *et al.* (0.12 μM *vs.* 6.50 nM). LOD for AA was 0.42 μM, whereas the effect of UA was not measured. LOD for DA by Teymourian *et al.* was higher than obtained by Bagheri *et al.* (0.08 μM *vs.* 6.50 nM) and for AA higher than obtained by Peik-See *et al.* (20.0 μM *vs.* 0.42 μM). LOD for UA was 0.5 μM. Linear concentration ranges for DA and AA were rather narrow compared to the other research by Bagheri *et al.* and Peik-See *et al.* (0.4-3.5 μM for DA and 0.16-7.2 mM for AA). However they measured the effect of UA unlike Peik-See *et al.* and the same electrode was also successfully used for the detection of H_2O_2, NADH and nitrite.

Based on the before mentioned research, Fe_3O_4 nanoparticles combined with hydrazine hydrate and AA as reductants seems to result in lowest LOD and high selectivity during simultaneous detection of various analytes. However the oxidation potential of *e.g.* DA was significantly higher, which usually results in higher interference from other compounds. On the other hand the reference electrode used (SCE) was different than used in the other research (Ag/AgCl), which does affect the comparison. In addition the fabrication methods were not completely comparable, which results in differencies in the electrochemical properties. In order to evaluate the effect of the reductants an additional research ought to be conducted as well as stability and reproducibility should be measured. A summary of the properties of the previously mentioned sensors is presented in Table 7.

Table 7: Fe_3O_4 modified CRGO based electrochemical sensors.

Molecule	**Electrode**	**Reductant**	**Linear range (μM)**	**LOD (μM)**	**Sensitivity ($AM^{-1}cm^{-2}$)**	**Ref.**
DA	Fe_3O_4/CRGO/GC	$N_2H_4 \cdot H_2O$, ammonia	0.4 -3.5	0.08	38.8	[117]
	Fe_3O_4/CRGO/CPE	$N_2H_4 \cdot H_2O$, AA	0.02-5.80	6.5		[116]
	Fe_3O_4/CRGO/GC	NH_4OH	0.5-100	0.12		[118]
AA	Fe_3O_4/CRGO/GC	$N_2H_4 \cdot H_2O$, ammonia	160-7200	20	33.5 x 10^{-3}	[117]
	Fe_3O_4/CRGO/GC	NH_4OH	1000-9000	0.42		[118]
UA	Fe_3O_4/CRGO/GC	$N_2H_4 \cdot H_2O$, ammonia	4-20	0.5	4.50	[117]

7.3 Detection of glucose

The most common method to detect glucose is with a GluOx enzyme. The GluOx enzyme reacts with oxygen and forms H_2O_2 which can be electrochemically detected. Increasing the amount of glucose results in degreasing electrochemical signal due to the O_2 consumption. As mentioned earlier normal blood glucose concentration is between 4-6 mM. Enzymes can be covalently or non-covalently attached to the surface of an electrochemical biosensor. Covalent interaction results from the chemical reaction between an enzyme and a functional group of CRGO during the fabrication prosess [20]. Non-covalent binding is weaker and can occur *e.g.* via van der Waals forces, hydrogen bonding or $\pi - \pi$ interaction between the layers of CRGO [20]. Enzyme based biosensors are usually unstable, which is why stability results are also

mentioned if conducted. However glucose can also be detected nonenzymatically and selectivity, sensitivity and stability can be improved with *e.g.* different NPs. A summary of different CRGO based electrochemical sensors and biosensors for the detection of glucose is presented in Table A2.

7.3.1 Enzyme based biosensors

GluOx enzyme can be used with a simple CRGO sensor without additional surface functionalization as well as with carbon nitrite dots (CND), Fe_3O_4 NPs and chemical doping with nitrogen. CND can be used because of their stabilizing effect on CRGO, Fe_3O_4 NPs to increase the electron transfer between the CRGO and GluOx enzyme and nitrogen doping in order to enhance the charge carrier density and electrical conductivity. Also different ionic liquid stabilizers can be used in order to increase the otherwise unstable enzymes.

Zhou *et al.* [24] prepared a simple hydrazine monohydrate reduced GO/GC electrode as described earlier and detected glucose with GluOx enzyme. Linear range of the GluOx/CRGO/GC electrode towards the detection of glucose was 0.01-10 mM, which covers the normal concentration range. Sensitivity was 20.21 $\mu \mathrm{Am} M^{-1} \mathrm{c} m^{-2}$ and the LOD 2.00 μM at -2.0 V *vs.* Ag/AgCl electrode (S/N=3). The oxidation of AA, UA, DA and APAP did not interfere with the signal because the applied potential was low (-2.0 V). GluOx/CRGO/GC electrode also showed good stability after 1 month of storage because only 7.0 % of the signal was lost in the presence of 10 M glucose.

Qin *et al.* [119] combined CND with GluOx/CRGO electrode. Oxidation was performed by Hummers method and the reduction was done with a solution of hydrazine hydrate and ammonia. GluOx/CND/CRGO solution was dried on a GC electrode. CNDs were several nanometers in size and stable in aqueous media which results in a stabilizing effect on the CRGO solution. CNDs also bind strongly to CRGO via π-π interactions and covalently to the carboxyl groups at the edges of CRGO. The carboxylic groups on the surface of GluOx bind to CND/CRGO and formed a 3D structure. I_D/I_G ratio changed from 0.84 to 0.96, which indicates a recovery of the carbon structure. However the amount of defects is smaller compared to Zhou *et al.* (I_D/I_G ratio 1.38) indicating weaker electrochemical properties. C/O ratio of CRGO increased after the addition of CND and the amount of oxygen functional groups was higher than obtained by Zhou *et al.* (7.87 *vs.* 11.8). The reduction peak potential of O_2 with CND/CRGO/GC electrode shifts to more positive compared to CRGO/GC electrode, which indicates an increase in the electrocatalytic activity of CNDs. The same occured with H_2O_2 but with a smaller peak reduction current. After the addition of GluOx enzyme, the reduction peak current decreased as the concentration of glucose increased as can be seen from Figure 34A. CND/CRGO/GC electrode without the enzyme on the other hand was not sensitive to the amount of glucose. Based on the results, the addition of CND did enhance the electrochemical properties compared to CRGO by Zhou *et al.* and increased the linear range (40 μM-20 mM *vs.* 10 μM-10 mM) but LOD was still weaker than Zhou *et al.* (40 μM *vs.* 2.00 μM). The stability of the sensor was weak and lost 19 % from its initial

value in only 5 days, which was believed to result from the decrease of the GluOx enzyme activity. The sensor was also successfully tested in human blood serum sample. Further research would be needed to understand the reasons for the higher LOD, but as mentioned earlier even slight variations in the fabrication prosess lead to changes in the electrochemical properties.

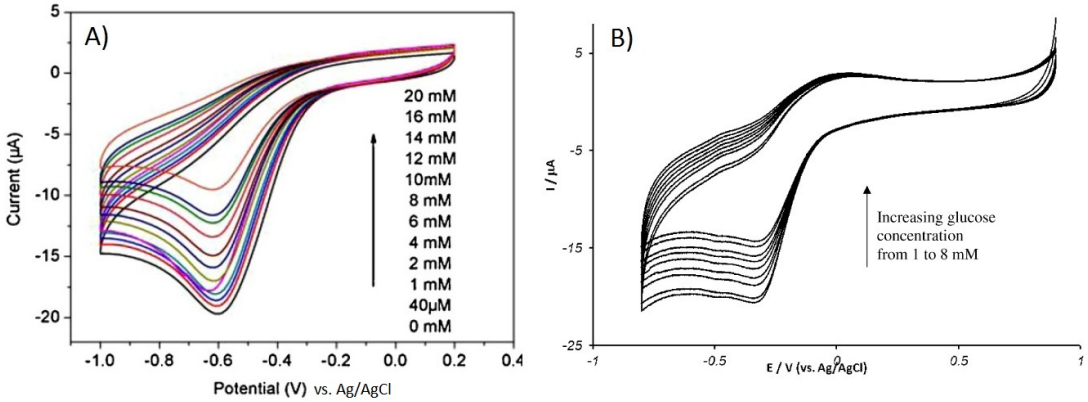

Figure 34: A) CV of the reduction of O_2 with CND/CRGO/GC/GluOx electrode in the presence of various concentrations of glucose in 0.2 M PBS at pH 7.4, scan rate 20 mV/s [119]. B) CV of the reduction of O_2 with Fe_3O_4/CRGO/GC/GluOx electrode in the presence of various concentrations of glucose in 0.1 M PBS at pH 7.0 [120].

Teymorian *et al.* [120] used Fe_3O_4 decorated hydrazine reduced GO/GC electrode with GluOx enzyme. Oxidation was done with modified Hummers method. The electrochemical signal in O_2-saturated PBS decreased with increasing amount of glucose as can be seen from Figure 34B. The reduction potential was more positive and the reduction peak current higher than with CND/CRGO/GC/GluOx electrode by Qin *et al.* (Figure 34A *vs.* B), indicating better electrochemical responce. The linear concentration range for the detection of glucose was 0.5-12 mM. The LOD was higher than obtained with the basic CR-GO/GC electrode by Zhou *et al.* (50 μM *vs.* 2.00 μM) and comparable to CND electrode, but the same Fe_3O_4/CRGO/GC sensor could also be used in detecting all free DNA bases and IgE, as will be described later. The stability of the sensor was tested with 100 repetitive measurements and the peak current decreased only 10 %. Based on the LOD, Fe_3O_4 seems to bring no additional benefit to the detection of glucose, on the other hand the stability of the sensor might be significantly higher.

Wang *et al.* [121] used chemical doping with nitrogen because of its appropriate size and ability to strongly bond with carbon atoms. Hummers method was used as an oxidation method and reduction was done with hydrazine. CRGO and chitosan polymer solution was dried on a GC electrode. Chitosan was used in immobolizing the GluOx enzyme to the surface of the electrode. It was realized that N-doping decreased the C/O ratio from 5.4-5.9 to 2.5-2.7 because N-doping almost doubled the oxygen content. The reduction current of H_2O_2 increased with N-doped CRGO

compared to CRGO and GC electrodes and shifted to more positive compared to GC electrode. This was believed to be due to breaking of the O-O bonds in H_2O_2 more easily at the surface of N-doped graphene. N-doping also increased the DOS of the material, which resulted in higher electronic conductivity. Higher electrochemical responce with N-doping can also been seen with GluOx enzyme. Linear concentration range for the detection of glucose was 0.1-1.1 mM, which does not cover the normal concentration range of glucose. LOD was 10 μM, indicating better ability of the sensor to detect small concentrations. The GluOx/N-doped/CRGO/GC electrode lost 4 % of the signal in three days and the electrode showed no interference in the presence of 5mM AA and UA.

Gu *et al.* [122] used sulfonic acid to prevent the CRGO layers from restacking and amine-terminated ionic liquid as a stabilizer. Graphene based composite material consisted of positively charged ionic liquid CRGO (IL-CRGO) and negatively charged sulfonic acid CRGO (S-CRGO) assembled layer-by-layer. The composite material provided a suitable platform for the GluOx enzyme to be attached. The oxidation was done with modified Hummers method and the reduction with hydrazine solution. The electrode was also coated with a Nafion layer. IL/S-CRGO/Nafion/GluOx/GC electrode showed an increased reduction current in the presence of H_2O_2. The *in vitro* linear range for the detection of glucose was 10-500 μM, sensitivity 0.0718 nAμM^{-1} and LOD was 3.33 μM. 0.1 mM AA, 10 μ DA and 50 μ UA showed no interference during the detection of glucose. 17 % of the signal was lost during 14 days of storage. Gu *et al.* also successfully measured the basal concentration of glucose *in vivo* from the rat striatum with injection of insulin via microdialysis probe. Especially the low linear range indicates that the sensor would be more suitable in measuring the small concentrations from rats than from human samples with higher concentrations.

Shan *et al.* [123] used polyvinylpyrrolidone protected CRGO, which was added to a solution of polyethylenimine-functionalized ionic liquid (PFIL) because of its good solubility, stability and ionic conductivity. Anions in PHIL also reacts easily with negatively charged GluOx. Oxidation was performed by Hummers method and the reduction was done with a solution of hydrazine hydrate and ammonia. PHIL/CRGO was dried on a GC electrode. Reduction current of O_2 with PHIL/CRGO was observed at about 0.3 V which was more positive compared to PHIL/GC and graphite/PHIL/GC. More positive reduction potential was also observed towards H_2O_2. During the reduction of O_2 with GluOx/PHIL/CRGO electrode the reduction peak current decreases as the concentration of glucose increases, which was thought to be due to the consumption of O_2 during the reaction. Linear range for the detection of glucose was 2-14 mM, which indicates that the sensor is more suitable in detecting higher concentrations. The signal decreased 4.9 % during 7 days.

Based on the before mentioned research a simple hydrazine reduced graphene oxide sensor with a GluOx enzyme provides fairly low LOD and suitable linear range within normal glucose concentration in human body. Better stability of the sensor can be obtained with Fe_3O_4. Fe_3O_4 NPs provide more positive reduction peak potential than CND, which was also used as a stabilizing structure. Lower concentrations on the other hand can be measured with layer-by-layer assembled

ionic liquid/CRGO composite, which was also suitable for *in vivo* measuring. A summary of the properties of the previously mentioned biosensors for the detection of glucose is presented in Table 8.

Table 8: CRGO and GluOx enzyme based electrochemical biosensors for the detection of glucose.

Electrode	**Reductant**	**C/O**	**Linear range (μM)**	**LOD (μM)**	**Sensitivity ($AM^{-1}cm^{-2}$)**	**Ref.**
CRGO/GC	$N_2H_4 \cdot H_2O$	11.8	10-10000	2.0	20.21 x 10^{-3}	[24]
Fe_3O_4/CRGO/GC	$N_2H_4 \cdot H_2O$		500-12000	50		[120]
CND/CRGO/GC	$N_2H_4 \cdot H_2O$, ammonia	7.87	40-20000	40		[119]
N-doped/CRGO/GC	$N_2H_4 \cdot H_2O$	2.6	100-1100	10		[121]
PHIL/CRGO	$N_2H_4 \cdot H_2O$		2000-14000			[123]
IL/S-CRGO/Nafion/GC	$N_2H_4 \cdot H_2O$		10-500	3.33	71.8 x 10^{-6} AM^{-1}	[122]

7.3.2 Nonenzymatic sensors

The nonenzymatic detection of glucose mainly relies on the enhanced electrochemical properties of metallic NPs such as Pt, Pd, Au, copper oxide (CuO) and nickel oxide (NiO). NPs increase the surface area as well as level of defects and combining metal NPs with metal oxides increase the electrochemical responce compared to using only one element. Dhara *et al.* [124] used a nonenzymatic sensor with Pt nanocubes and CuO nanoflowers in the detection of glucose. CuO was used in catalysing the glucose oxidation reaction and Pt NPs further increases the electron transfer by decreasing the charge transfer resistance. GO was fabricated by Hummers method, Pt/Cu/GO solution was reduced with $NaBH_4$ and dried on a screen printed electrode (SPE). LSV presented a distinqued oxidation peaks for glucose with CuO/CRGO/SPE and Pt/CuO/CRGO/SPE. However the oxidation current was higher with Pt/CuO/CRGO/SPE. No oxidation current was observed with Pt/CRGO/SPE. This indicates that the CuO was nesessary for the oxidation but Pt increased the sensitivity of the sensor. The sensor was also highly selective towards the oxidation of glucose in the presence of DA, AA, UA and APAP. Pt NPs were also tested with NiO by Wang *et al.* [125]. Pt NPs were believed to increase the catalytic activity of NiO. Modified Hummers method was used and the reduction was environmentally friendly conducted with urea. Dhara *et al.* [126] on the other hand used Au and CuO nanoparticles on a $NaBH_4$ reduced GO. Oxidation was done with modified Hummers method. The sensor showed good selectivity in the presence of *e.g.* DA, AA, UA, APAP. Dhara *et al.* [127] also tested the CRGO produced the same way with Pd/CuO nanoparticles. CuO NPs were used because of their electrocatalytic activity and Pd NPs because of their low charge transfer resistance. The Pd/CuO decorated sensor showed good selectivity in the presence of *e.g.* DA, AA, UA, APAP.

The oxidation with Pt/CuO/CRGO/SPE, Au/CuO/CRGO/SPE and Pd/CuO /CRGO/SPE with increasing amount of glucose is presented in Figure 35. As can

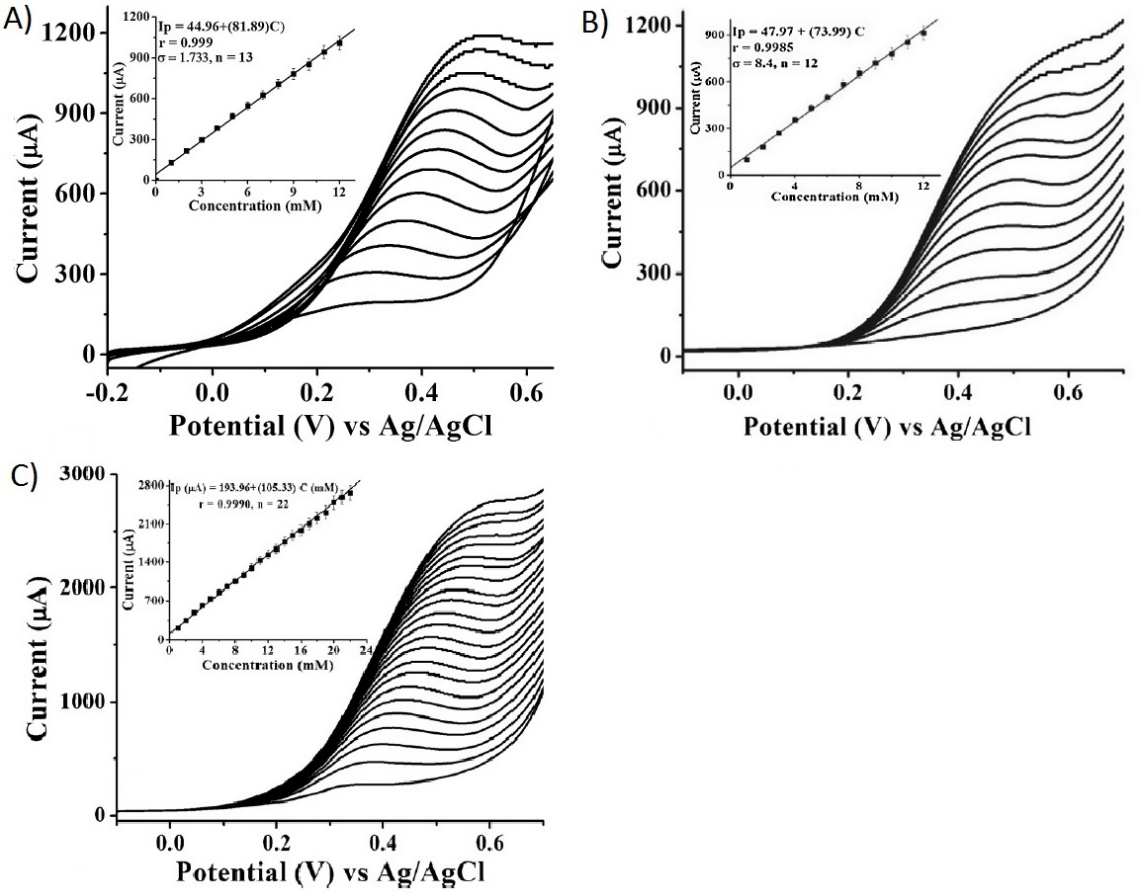

Figure 35: LSV of increasing amount of glucose with A) Pt/CuO/CRGO/SPE [124], B) Au/CuO/CRGO/SPE [126] and C) Pd/CuO/CRGO/SPE [127] in 0.1 M NaOH, scan rate 0.1 V/s.

be seen from the Figure 35 the oxidation peak potential is the lowest with Pt NPs, however the oxidation peak current is substantially higher with Pd NPs than with Au or Pt NPs. Linear range is the widest with Pd NPs compared to Au and Pt NPs (6 μM-22 mM *vs.* 1-12 mM and $<$ 12 mM). LOD with Pd NPs is lower than with Au NPs and comparable to the LOD with Pt NPs (0.03 μM, 0.1 μM and 0.01 μM respectively). Also the sensitivity is higher with Pd NPs than with Au NPs and almost the same as with Pt NPs (3355 $\mu A m M^{-1} cm^{-2}$, 2356 $\mu A m M^{-1} cm^{-2}$ and 3577 $\mu \mathrm{Am} M^{-1} cm^{-2}$ respectively). LOD and sensitivity with PtNP/NiO were both weaker than with PtNP/CuO (2.67 μM *vs.* 0.01 μM and 832.95 $\mu A m M^{-1} cm^{-2}$ *vs.* 3577 $\mu \mathrm{Am} M^{-1} cm^{-2}$ respectively). Linear concentration range on the other hand was wider (8 μM-14.5 mM *vs.* $<$ 12 mM). The research however did prove that the reduction with urea was successful via an environmentally safe method. Based on these results Pd NPs would be the most suitable NP to be used with CuO during nonenzymatic detection of glucose. However all of the before mentioned results were obtained in NaOH, which does not correspond to the natural environment in human body. A summary of the properties of the previously mentioned nonenzymatic sensors

for the detection of glucose is presented in Table 9.

Table 9: CRGO based nonenzymatic electrochemical sensors for the detection of glucose.

Electrode	**Reductant**	**Linear range (μM)**	**LOD (μM)**	**Sensitivity ($AM^{-1}cm^{-2}$)**	**Ref.**
Pt/CuO/CRGO/SPE	$NaBH_4$	< 12000	0.01	3.577	[124]
Au/CuO/CRGO/SPE	$NaBH_4$	1000-12000	0.1	2.356	[126]
Pd/CuO/CRGO/SPE	$NaBH_4$	6-22000	0.03	3.355	[127]
Pt/NiO/CRGO/GC	urea	8-14500	2.67	832.95 x 10^{-6}	[125]

7.4 Detection of NADH

As mentioned earlier, an obstacle concerning the oxidation of NADH is the required high overpotential with traditional carbon or GC electrodes. The overpotential can be decreased with CRGO because of the increased electron transfer rate. The detection of NADH can be done without surface modification or with metallic NPs. A summary of different CRGO based electrochemical sensors and biosensors for the detection of NADH is presented in Table A2.

7.4.1 Without surface functionalization

Zhou *et al.* [24] prepared a basic CRGO/GC electrode with hydrazine monohydrate as a reductant for the detection of NADH. The redox current was increased and the potential decreased compared to both graphite/GC and GC electrodes. Linear range for NADH was 40-800 μM, LOD 10 μM and sensitivity 2.68 μA$m M^{-1}cm^{-2}$. The sensor lost 14 % from the signal in 1 hour in the presence of NADH, indicating some resitance to fouling. However the sensor was not tested in the presence of interfering compounds.

Tabrizi *et al.* [128] and Tabrizi *et al.* [129] used interesting environmental friendly options for the reduction of graphene oxide. Tabrizi *et al.* [128] used fenolic compound from malt solution (nonalcoholic barley malt from Tuborg) as a reductant and Tabrizi *et al.* [129] used NADH as a reductant. Both researches used modified Hummers method for the oxidation. Tabrizi *et al.* [128] added malt solution to the GO solution and phenolic compound (*i.e.* antioxidant in malt) oxidized to guinone during the reduction and the electrons released reduced the GO. During the reduction I_D/I_G ratio increased from 0.91 to 1.21, which indicates a dimished amount of oxygen functional groups and increased amount of defects. Figure 36A presents CV of the oxidation of NADH with GC electrode and malt reduced GO/GC electrode. The oxidation potential significantly decreased, which was believed to be due to higher conductivity, surface area and hydrogen bonding between OH and COH groups of CRGO and OH and NH_2 groups of NADH. Tabrizi *et al.* [129] on the other hand retained electrical conductivity and high surface area with NADH reduction. The effectiveness of the NADH reduction was noticed from the decreased thickness. Figure

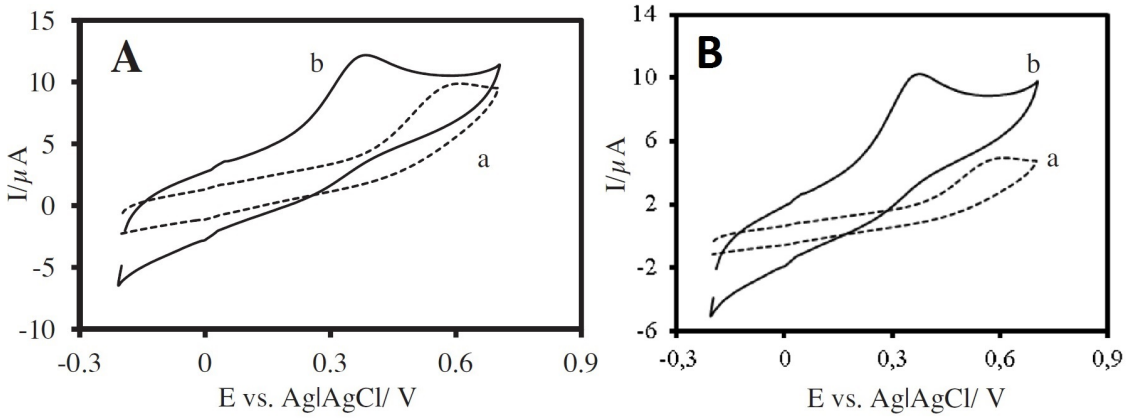

Figure 36: A) CV of the oxidation of 0.2 mM NADH with GC electrode (a) and malt reduced GO/GC electrode (b) in 0.1 M pH 7.0 PBS, scan rate 50 mV/s [128]. B) CV of the oxidation of 0.2 mM NADH with GC electrode (a) and NADH reduced GO/GC electrode (b) in 0.1 M pH 7.0 PBS, scan rate 25 mV/s [129].

36B presents CV of the oxidation of NADH with GC electrode and NADH reduced GO/GC electrode. The oxidation current increased and the peak potential decreased. As can be seen from the Figure 36 very similar result can be obtained with both of the reductans, although malt reduced GO resulted in slightly increased oxidation current. However the scan rate was higher, which does affect the results. Linear concentration range with NADH as a reductant was narrower than with malt reduction (0-400 μM *vs.* 10-600 μM) and LOD higher (0.6 μM *vs.* 0.33 μM). However the simultaneous detection of NADH and AA was also tested and the separation in the oxidation peaks was enough for the simultaneous detection of these two common analytes. Based on these result malt as a reductant seems to result in superior electrochemical properties compared to NADH or hydrazine monohydrate in addition to the environmentally friendly nature of the reductant. A summary of the properties of the previously mentioned unmodified sensors for the detection of NADH is presented in Table 10.

Table 10: CRGO based unmodified electrochemical sensors for the detection of NADH.

Electrode	**Reductant**	**Linear range (μM)**	**LOD (μM)**	**Sensitivity ($AM^{-1}cm^{-2}$)**	**Ref.**
CRGO/GC	$N_2H_4 \cdot H_2O$	40-800	10	2.68 x 10^{-6}	[24]
CRGO/GC	malt	10-600	0.33		[128]
CRGO/GC	NADH	0-400	0.6		[129]

7.4.2 Nanoparticles

Different NPs or nanostructures are mainly used in order to increase electron transfer rate and surface area as mentioned previously. For excample Fe_3O_4 and Au NPs can be used in detecting NADH. Teymourian *et al.* [117] used the same

Fe_3O_4/CRGO/GC electrode as mentioned previously. Figure 37A presents the CV in the absence and in the presence of NADH with Fe_3O_4/GC electrode, CRGO/GC electrode and Fe_3O_4/CRGO/GC electrode. The oxidation potential of NADH decreased and the current increased with Fe_3O_4/CGO/GC electrode because of the electrocatalytic activity of Fe_3O_4 NPs. The linear concentration range for the detection of NADH was 2-15 μM, LOD 0.40 μM (S/N=3) and sensitivity 0.113 A$M^{-1}cm^{-2}$. The sensor has shown high versatility with different analytes and could also be used in detecting H_2O_2 in addition to the before mentioned DA, AA and glucose.

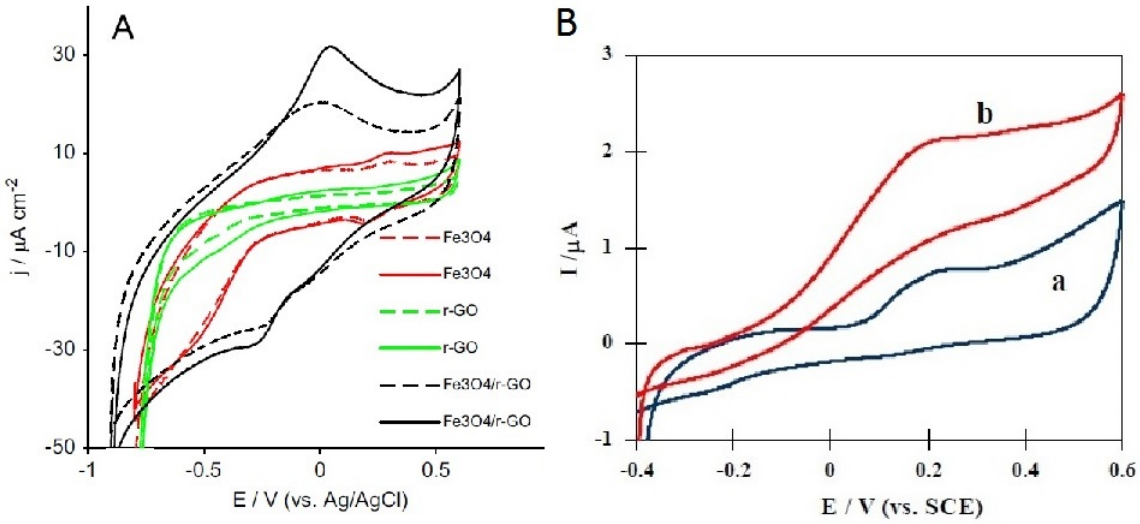

Figure 37: A) CV of the oxidation of 0.5 mM NADH (solid line) and in the absence of NADH (dashed line) with Fe_3O_4/GC electrode, CRGO/GC electrode and Fe_3O_4/CRGO/GC electrode in 0.1 M pH 7.0 PBS, scan rate 20 mV/s [117]. B) CV of the oxidation of 1 mM NADH (b, red line) and in the absence of NADH (a, blue line) with AuNPs/PDRGO/GC electrode in N_2-saturated 0.1 M pH 7.0 PBS, scan rate 1 mV/s [130].

Tian *et al.* [130] on the other hand used Au NPs. The reduction was done with oxidative polymerization of DA to polydopamine (PD). PD simultaneously reduced GO and formed a surface layer in which Au NPs could be attached in order to increase surface area. An additional reduction was done with $NaBH_4$. The oxidation peak current increased and the potential decreased after the addition of AuNPs, which indicates a significant impact of the AuNPs on the oxidation of NADH. The increased electrochemical responce was also thought to result from the oxidation of NADH by cathecols in PD. Figure 37B presents the oxidation of NADH with AuNPs/PDRGO/GC electrode. The oxidation potential was higher with Au NPs than with Fe_3O_4, although the reference electrode was not the same. Also the scan rate differed, which does not make the comparison possible. Linear concentration range for the detection of NADH was 50 nM-42 μM, which was significantly lower at the small concentration range than with Fe_3O_4, indicating also lower LOD. However LOD and sensitivity was not tested. The same electrode could also be used as an ethanol biosensor with an additional alcohol dehydrogenase enzyme attached to the

surface. A summary of the properties of the previously mentioned NP modified sensors for the detection of NADH is presented in Table 11.

Table 11: CRGO based NP modified electrochemical sensors for the detection of NADH.

Electrode	**Reductant**	**Linear range (μM)**	**LOD (μM)**	**Sensitivity ($AM^{-1}cm^{-2}$)**	**Ref.**
Fe_3O_4/CRGO/GC	$N_2H_4 \cdot H_2O$	2-150	0.4	0.133	[117]
AuNP/CRGO/GC	DA, $NaBH_4$	0.050-42			[130]

7.4.3 Other

Also other structures such as SWCNTs can be used in order to increase the electrode surface area during the detection of NADH. SWCNTs can also be used in increasing the conductivity and decreasing the charge transfer barrier of the CRGO layer. DNA on the other hand can be used in providing a platform for the immobilization of methylene blue (MB). MB is a redox indicator, which is concidered to be electrocatalytically active towards the oxidation of NADH.

Huang *et al*. [131] used SWCNTs with CRGO. GO was fabricated with modified Hummers method, GO/SWCNT solution was reduced with hydrazine and dried to a GC electrode. The oxidation and reduction currents of NADH both increased and shifted to more negative potential values compared to GC, SWCNT/GC and CRGO/GC electrode. Ferreira *et al*. [132] used DNA with MB. Graphene was also oxidized with modified Hummers method and GO/dsDNA solution reduced with hydrazine. DNA/CRGO was then mixed with MB and dried on a GC electrode. Linear concentration range for the detection of NADH was wider than with SWCNTs (10 μM-1.50 mM *vs*. 20-400 μM) whereas LOD was higher (1.0 μM *vs*. 0.078 μM). DNA combined with MB decreased the NADH oxidation overpotential significantly. However increasing the concentration of DNA above 1.2 mg/ml increased the charge transfer resistance. In addition, increasing the concentration of MB above 3 mM decreased the current responce. In conclusion, using moderate concentrations of both, DNA and MB, provided the highest electrochemical responce. However based on these and the before mentioned results, SWCNTs seems to be the most suitable choise for electrochemical sensing of NADH with the lowest LOD, if the toxicity of hydrazine willl not be concidered. A summary of the properties of the previously mentioned sensors for the detection of NADH is presented in Table 12.

Table 12: CRGO based modified electrochemical sensors for the detection of NADH.

Electrode	**Reductant**	**Linear range (μM)**	**LOD (μM)**	**Sensitivity ($AM^{-1}cm^{-2}$)**	**Ref.**
SWCNT/CRGO/GC	N_2H_4	20-400	0.078	0.204	[131]
MB/DNA/CRGO/GC	$N_2H_4 \cdot H_2O$	10-1500	1.0	12.75 AM^{-1}	[132]

7.5 Other interesting biomolecules

Almost any biological compound or an ion can be oxidized with the right electrode and potential. However the challenge is to find the right composite material and a recognition element to selectively detect only the desired one or simultaneously some of them. In addition to the before mentioned biomolecules, there are vast amount of research on other interesting analytes and few are presented here.

As H_2O_2 is usually detected with a GluOx enzyme during the detection of glucose, it can also be detected nonenzymatically and even selectively in the presence of glucose. Zhou *et al.* [24] prepared a basic CRGO/GC electrode with hydrazine monohydrate as a reductant for the detection of H_2O_2. The detection of H_2O_2 showed lower overpotential for CRGO/GC electrode than graphite/GC and GC electrodes. Lower overpotential usually results in higher selectivity which was also successfully tested in the presence of AA, UA and DA. However the selectivity was not tested in the presence of glucose. Linear range for H_2O_2 was 0.05-1500 μM and the detection limit 0.05 μM at -0.2 V *vs* Ag/AgCl electrode. Dhara *et al.* [133] constructed a $NaBH_4$ reduced GO sensor with Au nanoparticles. The detection of H_2O_2 with Au nanoparticles showed high selectivity in the presence of glucose, DA, AA UA and APAP. Linear concentration range was 20 μM-10 mM, which is more suitable detecting higher concentrations than the sensor by Zhou *et al.* LOD was 0.1 μM, which was also higher and sensitivity 1238 $\mu A m M^{-1} cm^{-2}$. Another interesting nonenzymatic H_2O_2 electrode was prepared by Wang *et al.* [134]. The reduction was done environmentally friendly with tyrosine. C/O ratio changed from 2.03 to 6.07 during the reduction, which indicated a successful reduction. Linear range was 100 μM-2.1 mM, LOD 80 μM (S/N=3) and sensitivity 69.07 $\mu A m M^{-1} cm^{-2}$. All of them weaker than by Zhou *et al.* and Dhara *et al.* However the sensor was also selective in the presence of DA, AA, UA and glucose. Huang *et al.* [131] used SWCNTs also for the detection of H_2O_2. Modified Hummers method was used and the reduction was done with hydrazine solution. Linear concentration range for the detection of H_2O_2 was 0.5-5 M, which is only suitable for large concentrations. Sensitivity for H_2O_2 was 2732.4 $\mu \mathrm{Am} M^{-1} cm^{-2}$, which is rather high. LOD was 1.3 μM (S/N=3). The reduction current of H_2O_2 increased significantly with SWCNT/CRGO/GC electrode compared to GC, SWCNT/GC and CRGO/GC electrode. Also the addition of AA, UA and DA did not interfere with the detection of H_2O_2. Teymourian *et al.* [117] used the same Fe_3O_4/CRGO/GC electrode as mentioned previously in the detection of H_2O_2. Linear range for H_2O_2 was 0.02-19 μM, which is more suitable in detecting small concentrations than *e.g.* the sensor by Zhou *et al.* The LOD was 6 nM (S/N=3) which is the lowest compared to the before mentioned results. Also the sensitivity is the highest with Fe_3O_4 (29.18 $\mathrm{Am} M^{-1} cm^{-2}$). A summary of the properties of the previously mentioned sensors for the detection of H_2O_2 is presented in Table 13.

Free DNA bases can be detected either directly with an electrochemical sensor or with a DNA probe immobilized on the surface of an electrochemical biosensor. DNA probes are usually immobilized on the surface of reduced graphene oxide by physical adsorption or chemical binding [135]. Physical adsorption occurs via $\pi - \pi$ interaction between the aromatic ring of DNA probe and the hexagonal structure of graphene

Table 13: CRGO based modified and unmodified electrochemical sensors for the detection of H_2O_2.

Electrode	**Reductant**	**Linear range (μM)**	**LOD (μM)**	**Sensitivity (A$M^{-1}cm^{-2}$)**	**Ref.**
CRGO/GC	$N_2H_4 \cdot H_2O$	0.05-1500	0.05		[24]
AuNP/CRGO/SPE	$NaBH_4$	20-10000	0.1	1.238	[133]
CRGO/GC	Tyrosine	100-2100	80	0.0691	[134]
SWCNT/CRGO/GC	N_2H_4	0.5 x 10^6-5 x 10^6	1.3	2.7324	[131]
Fe_3O_4/CRGO/GC	$N_2H_4 \cdot H_2O$	0.02-19	0.006	29.18	[117]

[135]. Chemical binding consists of a covalent attachment between the DNA probe and the carboxylic group [135]. Electrochemical reduction is a more frequently used method with DNA detection, although some interesting research have been conducted with CRGO. Zhou *et al.* [24] prepared a simple hydrazine monohydrate reduced GO electrode as described earlier. The direct oxidation and simultaneous detection of DNA bases G, A, T and C was reported with the CRGO/GC electrode. DPV was measured from G, A, T and C, ssDNA and dsDNA and showed distinguished oxidation peaks for all four DNA bases. Although the oxidation peaks from ssDNA and dsDNA shifts to more positive values. Zhou *et al.* [24] also successfully measured single-nucleotide polymorphisms without hybridization or labeling with CRGO. Teymourian *et al.* [120] also detected the free bases of DNA, but with a Fe_3O_4 decorated hydrazine reduced GO/GC electrode. Oxidation was done with modified Hummers method. The electrode could detect all four DNA bases individually but the simultaneous detection was only possible with G and A. This was believed to result from the high oxidation potential (>1.4 V) affecting the Fe_3O_4 NPs. LOD for G was 0.3 μM and for A 0.8 μM.

Electrochemical immunosensors can be used in detecting multiple tumor markers as was successfully done by Zhao *et al.* [136]. PPy microspheres were used as an immunoprobe together with Au NPs on a $NaBH_4$ reduced GO. Carcinoembryonic antigen (CEA) and alpha-fetoprotein (AFP) was detected with adriamycin and thionine as a signal tags on the surface of PPy immunoprobes. PPy and Au NPs provided a platform for a large number of adriamycin and thionine to be immobilized, which increased the electrochemical responce for CEA and AFP. Also the antibodies for CEA and AFP were immobilised on the surface of PPy. The electrochemical oxidation current increased as the concentration of CEA and AFP increased. Linear range for the simultaneous detection of CEA and AFP was 1.0 pg/ml-50 ng/ml, LOD for CEA was 0.40 pg/ml and for AFP 0.33 pg/ml (S/N=3). The sensor also showed selectivity in the presence of IgG, PSA, HCG and HSA. The peak current decreased 9.7 % in 20 days, which indicates good stability. Immunosensor for the detection of CEA was also fabricated by Qiumei *et al.* [137] using ferrocene grafted polyethyleneimine (PEI) as a conducting polymer. PEI was chosen because of it's low cost and ability to prevent the CRGO layer from restacking. HRP labeled antibody was used for CEA detection and the antibody was immobilized with concanavalin A lectin monolayer. The sensor was fabricated with layer-by-layer technique because of the ability to efficiently and simply immobilize antibodies to the surface of a

sensor material. CRGO was prepared with modified Hummers method and hydrazine and the layer-by-layer fabricated PEI/CRGO composite material was fabricated on a Au electrode. The electrochemical signal decreased after the fabrication of the concanavalin A layer and after the immobilization of the antibody. Addition of CEA also further decreased the signal, which indicated a successive detection of CEA. Linear range for the detection of CEA was 0.1-120 ng/ml and LOD 60 pg/ml. The sensor showed selectivity in the presence of PSA, bovine serum albumin and HRP and the signal decreased 5.2 % in 14 days. The results obtained by Zhao *et al.* and Qiumei *et al.* indicates a superior detection ability of PPy/AuNP/CRGO compared to layer-by-layer assembled PEI/CRGO electrode, although the PEI/CRGO electrode might present better stability.

Wang *et al.* [138] produced an aptamer (*i.e.* DNA sequence) based electrochemical biosensor for the detection of lysozyme. PPy was used in increasing the amount of aptamer absorbed on the surface of CRGO. TiO_2 nanoballs were used because of the low electrochemical properties of PPy to increase the electron transfer rate. The aptamer was 5'-ATCAGGGCTAAAGAGTGCAGAGTTACTTAG-3' and reduction was done with hydrazine hydrate. The composite material was deposited on the surface of a Au electrode. The detection of lysozyme was based on the inhibiting signal caused by the lysozyme absorption on the surface of the electrode, which is why increasing amount of lysozyme decreases the detection current. LOD was as low as 5.5 pM (S/N=3) and linear range 0.007-3.5 nM. The sensor also showed high selectivity in the presence of other proteins such as thrombin, bovine serum albumin and bovine hemoglobin.

Mazloum-Ardakani *et al.* [139] fabricated another aptasensor for the detection of a protein biomarker tumor necrosis factor-alpha (TNF-α). TNF-α is a cytokine related to *e.g.* autoimmune disorders, cancer, atherosclerosis and osteoporosis [140]. The aptamer used was SH-5'-TTTT TTT TTT TTT TTT GGT GGA TGG CGC AGT CGG CGA CAA-3'. The oxidation was done with modified Hummers method and he reduction with $NaBH_4$. CRGO was covered with Ag/Pt NPs and the composite was deposited on a gold SPE. Ag NPs were used because of their conductivity and Pt NPs because of their biocompatibility and electrocatalytic activity. Ag NPs bind to the surface of GO via electrostatic interaction with the oxygen functional groups and Pt nanoparticles bind to the surface of Ag NPs because of stronger bond between two metals, than between metal and carbon [139]. The oxidation of cathecol was blocked in the presence of increasing amount of TNF-α, because TNF-α binds to the aptamer and covers the surface of the electrode. Linear range for the detection of TNF-α was 0.0 pg/ml-60 pg/ml and LOD 2.07 pg/ml. The signal decreased only 4 % in 15 days, indicating high stability. The sensor also showed selectivity in the presence of *e.g.* bovine serum albumin and Hb.

Aptamers can also be used in detecting IgE as was successfully done by Teymourian *et al.* [120] with D17:4ext aptamer (5'GCG CGG GGC ACG TTT ATC CGT CCC TCC TAG TGG CGT GCC CCG CGC-3'). IgE is an antibody related to immune reactions such as allergy, asthma and AIDS. The sensor was the same Fe_3O_4 decorated CRGO/GC as described earlier. The binding of increasing amount of IgE to the aptamer resulted in decrease of the electrochemical signal.

Estradiol is the main female estrogen hormone produced in the ovaries and related to diseases such as osteoporosis. Estradiol was detected by Janegitz *et al.* [141] without any recognition elements. Dihexadecylphosphate (DHP) was used as a stabilizing surfactant. DHP is a hydrophobic molecule consisting of a phosphate group and hydrocarbon chains [142]. Modified Hummers method was used for the oxidation and the reduction was done with $NaBH_4$. Electron transfer resistance changed from 30.5 kΩ to 2.73 kΩ after reduction indicating an increase in the electron transfer rate. Linear range for the detection of estradiol was 0.4-10 μM and LOD was 77 nM. The current decreased 10 % in 15 days. Selectivity of the sensor was successfully tested among common compounds found from human urine such as urea, glucose and NaCl. A summary of the properties of the previously mentioned sensors and biosensors is presented in Table 14.

Table 14: CRGO based modified electrochemical sensors and biosensors for the detection of different analytes.

Molecule	**Electrode, recognition element**	**Reductant**	**Linear range**	**LOD**	**Ref.**
DNA base G	Fe_3O_4/CRGO/GC	$N_2H_4 \cdot H_2O$		0.3 μM	[120]
DNA base A	Fe_3O_4/CRGO/GC	$N_2H_4 \cdot H_2O$		0.8 μM	[120]
Tumor marker CEA	PPy/AuNP/CRGO/GC	$NaBH_4$	1.0 pg/ml-50 ng/ml	0.40 pg/ml	[136]
Tumor marker CEA	PEI/CRGO/Au	$NaBH_4$	0.1-120 ng/ml	60 pg/ml	[137]
Tumor marker AFP	PPy/AuNP/CRGO/GC	$NaBH_4$	1.0 pg/ml-50 ng/ml	0.33 pg/ml	[136]
Lysozyme	PPy/TiO_2/CRGO/Au, aptamer	$N_2H_4 \cdot H_2O$	7 pM-3.5 nM	5.5 pM	[138]
Protein marker TNF-α	Ag/Pt/CRGO/SPE, aptamer	$NaBH_4$	0.0-60 pg/ml	2.07 pg/ml	[139]
Estradiol hormone	DHP/CRGO/GC	$NaBH_4$	0.4-10 μM	0.077 μM	[141]

7.6 Summary and reflection

The most frequently used electrochemical measuring methods are CV and DPV. CV and DPV are suitable for *in vitro* studies but are concidered too slow for the *in vivo* measuring [47]. For excample FSCV might provide a possible solution for that, although rarely used in basic research. The scan rate can also be optimized during the voltammetric measurement in order to gain the most distinguished redox reaction, which leads to difficulties in comparing the different electrode materials. GC or SPE were mainly used as a substrate electrode, however both of them are too large for implantation. Also the reference electrode used in the measurement plays a significant role in the ability to compare the results. The oxidizing current and applied potential is measured *vs.* the reference electrode, which is why the oxidizing potential and current are not comparable between different reference electrodes. PBS was used in most of the studies, which is ideal when comparing the electrochemical responces, although does not contain the interfering substances found in real serum, urin or saliva samples. In some of the researches, pH was optimized in order to gain the highest electrochemical responces, which is not ideal for further use in biological samples. Variations in pH usually lead to significant changes in the oxidizing

potential and current, which also leads to difficulties in comparing the properties of different electrode composite materials. In biomedical applications the reusability or disposability of the sensor needs to be properly evaluated. If the sensor is diposable, the design of the sensor should be simple and fabrication inexpensive and rapid. More complex structure should result in better electrochemical properties such as lower LOD or higher sensitivity and selectivity. However complex electrode design usually results in higher cost, which limits the use in only reasearch purposes instead of clinical diagnosis or monitoring. Reusable sensors on the other hand needs to be able to clean from the adsorbed compounds and still retain the electrochemical properties. Reproducibility and repeatability are extremely important in electrochemical sensing because similar results should be obtained with every sensor or measurement. The lower the LOD the more significant is to obtain accurate results. However both reproducibility and repeatability are very rarely measured. Stability of the sensor during continous monitoring is also important and should not result in toxicity or tissue damage. Stability tests should be conducted especially with otherwise unstable enzymes. However stability test during storage are rarely presented in research not to mention the stability in biological solution or human body.

The main problem in comparing different electrochemical sensors and biosensors based on CRGO is that the oxidation or reduction method was not always mentioned. Also terms graphene-like, chemically modified graphene and reduced graphene oxide were all used for CRGO, even though the fabrication method is the main aspect defining the electrochemical characteristics of graphene-based materials. Hummers method or a modification of the Hummers method are the most common method to produce graphene oxide as could be seen from the reseach indroduced here. The most common method for reduction is to use chemical reductants during mild heating. Chemical reduction might not be the most effective method to remove oxygen functional groups but it is inexpensive, simple and with some reductants such as AA and malt even environmentally friendly. Hydrazine hydrate is the most common reductant. Hydrazine hydrate is effective in restoring the conductivity and the electrochemical properties of hydrazine reduced graphene oxide can be further improved with *e.g.* ammonia solution. Another interesting combination would be double-step reduction with hydrazine hydrate and AA, which also seems to enhance the electrochemical properites compared to plain hydrazine reduction. However very little emphasis has been put to the biocompatibility and cytotoxicity of hydrazine hydrate reduced graphene oxide.

Large surface area and restored conductivity of CRGO provides ideal characteristics for CRGO to be used as an electrochemical sensor and biosensor material. Large surface area of CRGO provides an ideal platform for surface functionalization. Surface functionalization further increases sensitivity and the obtained lower redox potential increases selectivity for different analytes. During the fabrication of CRGO, single layer is usually more desirable than multiple layer structure. Single layer results in higher surface area, which results in better electrochemical properties, even though multiple layer structure increases the amount of electroactive edge sites. Higher surface area also provides more sites for surface functionalization. Higher surface area results in higher amount of recognition elements or NPs immobilized on

the surface of the electrode, which increases the electrochemical responce. Recognition elements such as NPs can also be used in preventing the CRGO sheets from restacking. Restacking of the CRGO layers can also be prevented with stabilizing layers such as PDDA or DHP. NPs may also aggregate because the NPs are usually deposited simultaneously with the chemical reduction prosess. Surface area of the aggregated NPs are smaller than uniformly distributed NPs, which leads to decreased electrochemical responce. Aggregation of NPs can also be avoided with *e.g.* a stabilizing layer. However stabilizing surfactants and layers affect the electrochemical signal, which can be either benefitial or dedrimental. Surface film might increase the electron transfer rate by decreasing the charge transfer resistance or decrease the electron transfer rate due to tunneling, which results in increased responce time.

Nonenzymatic sensors mainly rely on bimetallic systems decorated on the surface of CRGO. Bimetallic systems can be *e.g.* nanoflowers compared with nanoparticles. Pt/CuO, Au/CuO, Pd/CuO, Pt/NiO or Pd/Pt are common combinations. Combinations are used in enhancing the electrochemical responce and selectivity, increasing the responce time and degreasing the charge transfer resistance. Electrochemical responce highly depends on the size and shape of the nanostructures because more complex structure ressults in higher surface area. Bi-metallic nanostructures are more stabile than enzyme based sensors and also lowers the cost of the sensor, because enzymes are usually expensive. However bi-metallic nanostructures can be used with enzymes to further lower the LOD. Especially Fe_3O_4 is an interesting compound because of it's high versatility. Fe_3O_4 was used in electrochemical detection of DA, AA, UA, NADH, H_2O_2 and DNA bases as well as could be used with a GluOx enzyme to detect glucose with a comparable LOD and linear range in most of the cases.

The highest selectivity and sensitivity, lowest LOD and widest linear concentration range can be obtained with highly specific sensors towards a single analyte. However as was presented previously also simultaneous detection of multiple analytes is possible with CRGO based modified composite materials. The future goal might be to construct a highly versatile sensor with a changeable recognition element, which would yield the highest selectivity towards a variety of analytes. Some excamples of the multifunctional electrode based on CRGO already exists such as Huang *et al.* [143]. However more focus needs to be addressed to the biocompatibility, cytotoxicity and selectivity during *in vivo* tests, since very few of the before mentioned electrodes were tested *in vivo* or even in real human samples.

8 Conclusions

The aim for electrochemical sensing industry is to fabricate sensing devices which are inexpensive, small, selective, sensitive and fast for the purpose of rapidly expanding field of biomedical applications such as *e.g.* personalized medicine, bed-side diagnostics and drug delivery. Accurate electrochemical sensing will provide details about the functions of human body and information about some of the most common diseases, which are yet to be cured. For excample monitoring blood glucose concentrations will be an interesting field also for electrochemical sensing, since the number of diabetic patiens are predicted to increase.

Electrochemical properites of an electrochemical sensor or biosensor is mainly related to the surface structure and chemistry of the electrode material. Graphene has raised excessive interest among researchers because of the excellent mechanical and electrical properties. Graphene is extremely strong and at the same time flexible, which makes it an ideal material for an implantable sensor. Electrical conductivity is also high due to the fast electron mobility, which is essential for electrochemical sensors. Electron transfer rate on the other hand is an important indicator for the electrochemical properties of an electrode material. Electron transfer rate at defect free basal plane of graphene is very low. However defects at the basal plane and higher amount of edge plane sites increases the electron transfer rate and results in higher electrochemical responce. The main problem in using graphene for electrochemical sensing purposes is the lack of simple, inexpensive, homogeneous and reproducible fabrication method for mass production, since even small changes in the fabrication prosess lead to significant differencies in the electrochemical properties of graphene.

The reduction of oxidized graphene is an effective method to produce large amount of pristine like graphene, although even at its best, does not solve all the problems concerning homogeneity and repeatability. Chemical reduction of graphene oxide is however simple and inexpensive and the electrochemical properties can be easily improved with different surface modification methods. Chemically reduced graphene oxide is often modified with surfactants or stabilizers in order to prevent the layers from restacking, which also provides a platform for metallic nanoparticles or nanostructures to evenly distribute. High surface area of graphene based materials also results in higher amount of nanoparticles or recognition elements to be attached, which leads to higher electrochemical responce. Nanoparticles are also used in order to even further increase the surface area, since higher surface area results in lower impedance.

On the other hand more complex electrode structure does not necessarily result in lower LOD, higher sensitivity or superior electrochemical responce. Comparison of different sensors merely based on the published research is also problematic due to the wide variety of chemical reductants as well as differencies in the oxidation and fabrication prosess, which is why a comparative research on different reductants and surface modification methods with more than only a few sensors to test the repeatability would be essential. Comparative study about the effect of the commonly used reductants during chemical reduction of graphene oxide on biocompatibility and cytotoxicity is also lacking and would be highly interesting for medical purposes,

since some of the reductants are concidered highly toxic. An interesting comparative research would be to evaluate the electrochemical properties resulted from diffrent environmentally friendly, nontoxic and biocompatible reductants such as ascorbic acid, malt or bacterial respiration. The effect of stabilizers such as PDDA and chitosan *vs.* stabilizing structures such as MWCNTs, SWCNTs or CNDs would also be interesting to compare. Finally a comparative research in real human sample between Fe_3O_4 *vs.* simple bimetallic nanopatricles such as PdPt *vs.* without any surface functionalization would answer questions about the benefit of complex surface functionalization. Future work has to be addressed also towards the overall biocompatibility and toxicity of graphene based materials in electrochemical sensing applications. The health hazard research of chemically reduced graphene oxide as well as other graphene based materials is rarely conducted during electrochemical measuring and needs to be properly evaluated before clinical use.

References

[1] R. M. Wightman, "Probing cellular chemistry in biological systems with microelectrodes," *Science*, vol. 311, no. 5767, pp. 1570–1574, 2006. DOI: 10.1126/science.1120027.

[2] A. C. Michael and L. Borland, *Electrochemical methods for neuroscience*. CRC Press, 2006. ISBN-10: 0-8493-4075-6.

[3] M. Pumera, A. Ambrosi, A. Bonanni, E. L. K. Chng, and H. L. Poh, "Graphene for electrochemical sensing and biosensing," *TrAC Trends in Analytical Chemistry*, vol. 29, pp. 954–965, 10 2010. DOI: 10.1016/j.trac.2010.05.011.

[4] A. J. Bard and L. R. Faulkner, *Electrochemical methods: fundamentals and applications*, vol. 2. Wiley New York, 1980. ISBN: 978-0-471-04372-0.

[5] R. G. Compton and C. E. Banks, *Understanding voltammetry*, vol. 2. World Scientific, 2007. ISBN: 978-1-84816-585-4.

[6] D. Grieshaber, R. MacKenzie, J. Vörös, and E. Reimhult, "Electrochemical biosensors - sensor principles and architectures," *Sensors*, vol. 8, no. 3, pp. 1400–1458, 2008. ISSN: 14243210.

[7] J. G. Webster, *Medical Instrumentation-Application and Design.* John Wiley & sons, Inc., 4 ed., 1978. pp. 189-234. ISBN: 0471676004.

[8] D. L. Robinson, A. Hermans, A. T. Seipel, and R. M. Wightman, "Monitoring rapid chemical communication in the brain," *Chemical reviews*, vol. 108, no. 7, pp. 2554–2584, 2008. DOI: 10.1021/cr068081q.

[9] D. A. C. Brownson, D. K. Kampouris, and C. E. Banks, "Graphene electrochemistry: Fundamental concepts through to prominent applications," *Chemical Society Reviews*, vol. 41, no. 21, pp. 6944–6976, 2012. DOI: 10.1039/c2cs35105f.

[10] N. Dale, S. Hatz, F. Tian, and E. Llaudet, "Listening to the brain: microelectrode biosensors for neurochemicals," *Trends in biotechnology*, vol. 23, pp. 420–428, 8 2005. DOI: 10.1016/j.tibtech.2005.05.010.

[11] J. Cazes, *Analytical instrumentation handbook*. CRC Press, 3 ed., 2004. ISBN: 9780824753481.

[12] J. Janata, "Electrochemical sensors and their impedances: A tutorial," *Critical Reviews in Analytical Chemistry*, vol. 32, no. 2, pp. 109–120, 2002. DOI: 10.1080/10408340290765470.

[13] S. Chandra and D.K.Y.Wongn, *Electrochemical detection of neurotransmitters at structurally small electrodes*, pp. 317–338. Nanostructured Materials for Electrochemical Biosensors, Nova Science Publishers, Inc., 2009. ISBN: 978-160741706-4.

[14] R. A. S. Luz, R. M. Iost, and F. N. Crespilho, *Nanomaterials for biosensors and implantable biodevices*, pp. 27–48. Nanobioelectrochemistry: From Implantable Biosensors to Green Power Generation, 2013. DOI: 10.1007/978-3-642-29250-7-2.

[15] D. W. Kimmel, G. Leblanc, M. E. Meschievitz, and D. E. Cliffel, "Electrochemical sensors and biosensors," *Analytical Chemistry*, vol. 84, no. 2, pp. 685–707, 2012. DOI: 10.1021/ac202878q.

[16] X. Luo, A. Morrin, A. J. Killard, and M. R. Smyth, "Application of nanoparticles in electrochemical sensors and biosensors," *Electroanalysis*, vol. 18, no. 4, pp. 319–326, 2006. DOI: 10.1002/elan.200503415.

[17] D. Astruc, E. Boisselier, and C. Ornelas, "Dendrimers designed for functions: From physical, photophysical, and supramolecular properties to applications in sensing, catalysis, molecular electronics, photonics, and nanomedicine," *Chemical reviews*, vol. 110, no. 4, pp. 1857–1959, 2010. DOI: 10.1021/cr900327d.

[18] S. Wang, W. Zhang, X. Zhong, Y. Chai, and R. Yuan, "Simultaneous determination of dopamine, ascorbic acid and uric acid using a multi-walled carbon nanotube and reduced graphene oxide hybrid functionalized by pamam and au nanoparticles," *Analytical Methods*, vol. 7, no. 4, pp. 1471–1477, 2015. DOI: 10.1039/c4ay02086c.

[19] Y. Song, Y. Luo, C. Zhu, H. Li, D. Du, and Y. Lin, "Recent advances in electrochemical biosensors based on graphene two-dimensional nanomaterials," *Biosensors and Bioelectronics*, vol. 76, pp. 195–212, 2/15 2016. DOI: 10.1016/j.bios.2015.07.002.

[20] E. B. Bahadır and M. K. Sezgintürk, "Applications of graphene in electrochemical sensing and biosensing," *TrAC Trends in Analytical Chemistry*, vol. 76, pp. 1–14, 2 2016. DOI: 10.1016/j.trac.2015.07.008.

[21] T. Kuila, S. Bose, P. Khanra, A. K. Mishra, N. H. Kim, and J. H. Lee, "Recent advances in graphene-based biosensors," *Biosensors and Bioelectronics*, vol. 26, pp. 4637–4648, 8/15 2011. DOI: 10.1016/j.bios.2011.05.039.

[22] A. T. Lawal, "Synthesis and utilisation of graphene for fabrication of electrochemical sensors," *Talanta*, vol. 131, pp. 424–443, 2015. DOI: 10.1016/j.talanta.2014.07.019.

[23] X. Zhang, H. Ju, and J. Wang, *Electrochemical sensors, biosensors and their biomedical applications*. Academic Press, 2011. ISBN: 978-0-12-373738-0.

[24] M. Zhou, Y. Zhai, and S. Dong, "Electrochemical sensing and biosensing platform based on chemically reduced graphene oxide," *Analytical Chemistry*, vol. 81, no. 14, pp. 5603–5613, 2009. DOI: 10.1021/ac900136z.

[25] A. Merkoçi and S. Alegret, "New materials for electrochemical sensing iv. molecular imprinted polymers," *TrAC - Trends in Analytical Chemistry*, vol. 21, no. 11, pp. 717–725, 2002. DOI: 10.1016/S0165-9936(02)01119-6.

[26] D. Chen, H. Feng, and J. Li, "Graphene oxide: Preparation, functionalization, and electrochemical applications," *Chemical reviews*, vol. 112, no. 11, pp. 6027–6053, 2012. DOI: 10.1021/cr300115g.

[27] V. C. Sanchez, A. Jachak, R. H. Hurt, and A. B. Kane, "Biological interactions of graphene-family nanomaterials: An interdisciplinary review," *Chemical research in toxicology*, vol. 25, no. 1, pp. 15–34, 2012. DOI: 10.1021/tx200339h.

[28] R. L. McCreery, "Advanced carbon electrode materials for molecular electrochemistry," *Chemical reviews*, vol. 108, no. 7, pp. 2646–2687, 2008. DOI: 10.1021/cr068076m.

[29] A. Jaquins-Gerstl and A. C. Michael, "A review of the effects of fscv and microdialysis measurements on dopamine release in the surrounding tissue," *Analyst*, vol. 140, no. 11, pp. 3696–3708, 2015. DOI: 10.1039/c4an02065k.

[30] M. Bear, B. W. Connors, M. Paradiso, M. Bear, B. Connors, and M. Neuroscience, *Exploring the brain*, vol. 3. Neuroscience: Williams and Wilkins, 1996. ISBN: 978-0781760034.

[31] C. B. Jacobs, M. J. Peairs, and B. J. Venton, "Review: Carbon nanotube based electrochemical sensors for biomolecules," *Analytica Chimica Acta*, vol. 662, pp. 105–127, 3/10 2010. DOI: 10.1016/j.aca.2010.01.009.

[32] Y. Li, M. Liu, C. Xiang, Q. Xie, and S. Yao, "Electrochemical quartz crystal microbalance study on growth and property of the polymer deposit at gold electrodes during oxidation of dopamine in aqueous solutions," *Thin Solid Films*, vol. 497, no. 1-2, pp. 270–278, 2006. DOI: 10.1016/j.tsf.2005.10.048.

[33] X. L. Wen, Y. H. Jia, and Z. L. Liu, "Micellar effects on the electrochemistry of dopamine and its selective detection in the presence of ascorbic acid," *Talanta*, vol. 50, no. 5, pp. 1027–1033, 1999. DOI: 10.1016/S0039-9140(99)00207-6.

[34] T. Q. Xu, Q. L. Zhang, J. N. Zheng, Z. Y. Lv, J. Wei, A. J. Wang, and J. J. Feng, "Simultaneous determination of dopamine and uric acid in the presence of ascorbic acid using pt nanoparticles supported on reduced graphene oxide," *Electrochimica Acta*, vol. 115, pp. 109–115, 2014. DOI: 10.1016/j.electacta.2013.10.147.

[35] M. V. Bezrukov, Y. E. Shilov, N. V. Shestakova, and T. P. Klyushnik, "Biological evaluation of the severity of depression – a new method for assaying platelet serotonin concentrations," *Neuroscience and behavioral physiology*, pp. 1–6, 2016. DOI: 10.1007/s11055-016-0238-5.

[36] E. W. Boyer and M. Shannon, "Current concepts: The serotonin syndrome," *New England Journal of Medicine*, vol. 352, no. 11, pp. 1112–1120, 2005. DOI: 10.1056/NEJMra041867.

[37] B. E. K. Swamy and B. J. Venton, "Carbon nanotube-modified microelectrodes for simultaneous detection of dopamine and serotonin in vivo," *Analyst*, vol. 132, no. 9, pp. 876–884, 2007. DOI: 10.1039/b705552h.

[38] B. V. Sarada, T. N. Rao, D. A. Tryk, and A. Fujishima, "Electrochemical detection of serotonin using conductive diamond electrodes," *Chemistry Letters*, no. 11, pp. 1213–1214, 1999. ISSN: 03667022.

[39] J. N. Stuart, A. B. Hummon, and J. V. Sweedler, "The chemistry of thought: Neurotransmitters in the brain," *Analytical Chemistry*, vol. 76, no. 7, pp. 120A–128A+107A, 2004. ISSN: 00032700.

[40] E. P. D. Oliveira and R. C. Burini, "High plasma uric acid concentration: Causes and consequences," *Diabetology and Metabolic Syndrome*, vol. 4, no. 1, 2012. DOI: 10.1186/1758-5996-4-12.

[41] A. Dehghan, A. Köttgen, Q. Yang, S.-J. Hwang, W. L. Kao, F. Rivadeneira, E. Boerwinkle, D. Levy, A. Hofman, B. C. Astor, E. J. Benjamin, C. M. van Duijn, J. C. Witteman, J. Coresh, and C. S. Fox, "Association of three genetic loci with uric acid concentration and risk of gout: a genome-wide association study," *The Lancet*, vol. 372, pp. 1953–1961, 12/6–12 2008. DOI: 10.1016/S0140-6736(08)61343-4.

[42] H. Vuorinen-Markkola and H. Yki-Järvinen, "Hyperuricemia and insulin resistance.," *The Journal of Clinical Endocrinology & Metabolism*, vol. 78, no. 1, pp. 25–29, 1994. DOI: 10.1210/jc.78.1.25.

[43] Z. Yan, J. R. Zhang, and H. Q. Fang, "Electrocatalytic oxidation of uric acid at cysteine modified glassy carbon electrode," *Analytical Letters*, vol. 32, no. 2, pp. 223–234, 1999. ISSN: 00032719.

[44] G. Fabregat, J. Casanovas, E. Redondo, E. Armelin, and C. Alemán, "A rational design for the selective detection of dopamine using conducting polymers," *Physical Chemistry Chemical Physics*, vol. 16, no. 17, pp. 7850–7861, 2014. DOI: 10.1039/c4cp00234b.

[45] S. Eskelinen, "Glukoosi." DUODECIM Terveyskirjasto, 2012. Cited: 2016/01/11. Accessed: http://www.terveyskirjasto.fi/terveyskirjasto/tk.koti?p_artikkeli=snk03091.

[46] "Diabetes." WHO Media centre, 2015. Cited: 2016/01/11. Accessed: http://www.who.int/mediacentre/factsheets/fs312/en/.

[47] C. Yang, M. E. Denno, P. Pyakurel, and B. J. Venton, "Recent trends in carbon nanomaterial-based electrochemical sensors for biomolecules: A review," *Analytica Chimica Acta*, vol. 887, pp. 17–37, 2015. DOI: 10.1016/j.aca.2015.05.049.

[48] M. Baghayeri, A. Amiri, and S. Farhadi, "Development of non-enzymatic glucose sensor based on efficient loading ag nanoparticles on functionalized carbon nanotubes," *Sensors and Actuators, B: Chemical*, vol. 225, pp. 354–362, 2016. DOI: 10.1016/j.snb.2015.11.003.

[49] N. German, A. Ramanavicius, and A. Ramanaviciene, "Electrochemical deposition of gold nanoparticles on graphite rod for glucose biosensing," *Sensors and Actuators, B: Chemical*, vol. 203, pp. 25–34, 2014. DOI: 10.1016/j.snb.2014.06.021.

[50] P. Belenky, K. L. Bogan, and C. Brenner, "Nad+ metabolism in health and disease," *Trends in biochemical sciences*, vol. 32, no. 1, pp. 12–19, 2007. DOI: 10.1016/j.tibs.2006.11.006.

[51] W. J. Blaedel and R. A. Jenkins, "Study of the electrochemical oxidation of reduced nicotinamide adenine dinucleotide.," *Analytical Chemistry*, vol. 47, no. 8, pp. 1337–1343, 1975. ISSN: 00032700.

[52] G. N. Vemuri, M. A. Eiteman, J. E. McEwen, L. Olsson, and J. Nielsen, "Increasing nadh oxidation reduces overflow metabolism in saccharomyces cerevisiae," *Proceedings of the National Academy of Sciences of the United States of America*, vol. 104, no. 7, pp. 2402–2407, 2007. DOI: 10.1073/pnas.0607469104.

[53] H. R. Zare, N. Nasirizadeh, M. Mazloum-Ardakani, and M. Namazian, "Electrochemical properties and electrocatalytic activity of hematoxylin modified carbon paste electrode toward the oxidation of reduced nicotinamide adenine dinucleotide (nadh)," *Sensors and Actuators, B: Chemical*, vol. 120, no. 1, pp. 288–294, 2006. DOI: 10.1016/j.snb.2006.02.043.

[54] T. G. Drummond, M. G. Hill, and J. K. Barton, "Electrochemical dna sensors," *Nature biotechnology*, vol. 21, no. 10, pp. 1192–1199, 2003. DOI: 10.1038/nbt873.

[55] S. Eskelinen, "Perusverenkuva (b-pvk)." DUODECIM Terveyskirjasto, 2012. Cited: 2016/01/11. Accessed: http://www.terveyskirjasto.fi/terveyskirjasto/tk.koti?p_artikkeli=snk03030.

[56] Y. He, Q. Sheng, J. Zheng, M. Wang, and B. Liu, "Magnetite-graphene for the direct electrochemistry of hemoglobin and its biosensing application," *Electrochimica Acta*, vol. 56, no. 5, pp. 2471–2476, 2011. DOI: 10.1016/j.electacta.2010.11.020.

[57] G. Martínez-García, L. Agüí, P. Yáñez-Sedeño, and J. M. Pingarrón, "Multiplexed electrochemical immunosensing of obesity-related hormones at grafted

graphene-modified electrodes," *Electrochimica Acta*, vol. 202, pp. 209–215, 2016. DOI: 10.1016/j.electacta.2016.03.140.

[58] C. Zhu and S. Dong, "Energetic graphene-based electrochemical analytical devices in nucleic acid, protein and cancer diagnostics and detection," *Electroanalysis*, vol. 26, no. 1, pp. 14–29, 2014. DOI: 10.1002/elan.201300056.

[59] A. K. Geim and K. S. Novoselov, "The rise of graphene," *Nature Materials*, vol. 6, no. 3, pp. 183–191, 2007. DOI: 10.1038/nmat1849.

[60] A. H. C. Neto, F. Guinea, N. M. R. Peres, K. S. Novoselov, and A. K. Geim, "The electronic properties of graphene," *Reviews of Modern Physics*, vol. 81, no. 1, pp. 109–162, 2009. DOI: 10.1103/RevModPhys.81.109.

[61] A. K. Geim, "Random walk to graphene (nobel lecture)," *Angewandte Chemie - International Edition*, vol. 50, no. 31, pp. 6966–6985, 2011. DOI: 10.1002/anie.201101174.

[62] "The nobel prize in physics 2010." Nobel Media AB, 2014. Cited: 2015/12/16. Accessed: http://www.nobelprize.org/nobel_prizes/physics/laureates/2010/.

[63] S. K. Vashist and J. H. T. Luong, "Recent advances in electrochemical biosensing schemes using graphene and graphene-based nanocomposites," *Carbon*, vol. 84, no. 1, pp. 519–550, 2015. DOI: 10.1016/j.carbon.2014.12.052.

[64] M. Pumera, "Graphene-based nanomaterials and their electrochemistry," *Chemical Society Reviews*, vol. 39, pp. 4146–4157, 2010. DOI: 10.1039/c002690p.

[65] A. Ambrosi, C. K. Chua, A. Bonanni, and M. Pumera, "Electrochemistry of graphene and related materials," *Chemical reviews*, vol. 114, no. 14, pp. 7150–7188, 2014. DOI: 10.1021/cr500023c.

[66] D. R. Dreyer, S. Park, C. W. Bielawski, and R. S. Ruoff, "The chemistry of graphene oxide," *Chemical Society Reviews*, vol. 39, no. 1, pp. 228–240, 2010. DOI: 10.1039/b917103g.

[67] M. Pumera, "Graphene in biosensing," *Materials Today*, vol. 14, pp. 308–315, 0 2011. DOI: 10.1016/S1369-7021(11)70160-2.

[68] A. K. Geim, "Graphene: Status and prospects," *Science*, vol. 324, no. 5934, pp. 1530–1534, 2009. DOI: 10.1126/science.1158877.

[69] A. A. Balandin, S. Ghosh, W. Bao, I. Calizo, D. Teweldebrhan, F. Miao, and C. N. Lau, "Superior thermal conductivity of single-layer graphene," *Nano Letters*, vol. 8, no. 3, pp. 902–907, 2008. DOI: 10.1021/nl0731872.

[70] C. Lee, X. Wei, J. W. Kysar, and J. Hone, "Measurement of the elastic properties and intrinsic strength of monolayer graphene," *Science*, vol. 321, no. 5887, pp. 385–388, 2008. DOI: 10.1126/science.1157996.

[71] D. Chen, L. Tang, and J. Li, "Graphene-based materials in electrochemistry," *Chemical Society Reviews*, vol. 39, no. 8, pp. 3157–3180, 2010. DOI: 10.1039/b923596e.

[72] S. Pei and H. M. Cheng, "The reduction of graphene oxide," *Carbon*, vol. 50, no. 9, pp. 3210–3228, 2012. DOI: 10.1016/j.carbon.2011.11.010.

[73] Y. Shao, J. Wang, H. Wu, J. Liu, I. A. Aksay, and Y. Lin, "Graphene based electrochemical sensors and biosensors: A review," *Electroanalysis*, vol. 22, no. 10, pp. 1027–1036, 2010. DOI: 10.1002/elan.200900571.

[74] I. I. Suni, "Impedance methods for electrochemical sensors using nanomaterials," *TrAC - Trends in Analytical Chemistry*, vol. 27, no. 7, pp. 604–611, 2008. DOI: 10.1016/j.trac.2008.03.012.

[75] A. Ambrosi and M. Pumera, "Stacked graphene nanofibers for electrochemical oxidation of dna bases," *Physical Chemistry Chemical Physics*, vol. 12, no. 31, pp. 8943–8947, 2010. DOI: 10.1039/c0cp00213e.

[76] A. Ambrosi, A. Bonanni, Z. Sofer, J. S. Cross, and M. Pumera, "Electrochemistry at chemically modified graphenes," *Chemistry - A European Journal*, vol. 17, no. 38, pp. 10763–10770, 2011. DOI: 10.1002/chem.201101117.

[77] T. J. Davies, M. E. Hyde, and R. G. Compton, "Nanotrench arrays reveal insight into graphite electrochemistry," *Angewandte Chemie - International Edition*, vol. 44, no. 32, pp. 5121–5126, 2005. DOI: 10.1002/anie.200462750.

[78] D. K. Kampouris and C. E. Banks, "Exploring the physicoelectrochemical properties of graphene," *Chemical Communications*, vol. 46, no. 47, pp. 8986–8988, 2010. DOI: 10.1039/c0cc02860f.

[79] D. A. C. Brownson, C. W. Foster, and C. E. Banks, "The electrochemical performance of graphene modified electrodes: An analytical perspective," *Analyst*, vol. 137, no. 8, pp. 1815–1823, 2012. DOI: 10.1039/c2an16279b.

[80] D. A. C. Brownson, L. J. Munro, D. K. Kampouris, and C. E. Banks, "Electrochemistry of graphene: Not such a beneficial electrode material?," *RSC Advances*, vol. 1, no. 6, pp. 978–988, 2011. DOI: 10.1039/c1ra00393c.

[81] M. Pumera, R. Scipioni, H. Iwai, T. Ohno, Y. Miyahara, and M. Boero, "A mechanism of adsorption of β-nicotinamide adenine dinucleotide on graphene sheets: Experiment and theory," *Chemistry - A European Journal*, vol. 15, no. 41, pp. 10851–10856, 2009. DOI: 10.1002/chem.200900399.

[82] S. Syama and P. V. Mohanan, "Safety and biocompatibility of graphene: A new generation nanomaterial for biomedical application," *International journal of biological macromolecules*, vol. 86, pp. 546–555, 2016. DOI: 10.1016/j.ijbiomac.2016.01.116.

[83] W. Hu, C. Peng, W. Luo, M. Lv, X. Li, D. Li, Q. Huang, and C. Fan, "Graphene-based antibacterial paper," *ACS Nano*, vol. 4, no. 7, pp. 4317–4323, 2010. DOI: 10.1021/nn101097v.

[84] K. E. Whitener and P. E. Sheehan, "Graphene synthesis," *Diamond and Related Materials*, vol. 46, pp. 25–34, 2014. DOI: 10.1016/j.diamond.2014.04.006.

[85] S. Park and R. S. Ruoff, "Chemical methods for the production of graphenes.," *Nature nanotechnology*, vol. 4, no. 4, pp. 217–224, 2009. DOI: 10.1038/nnano.2009.58.

[86] M. J. Fernández-Merino, L. Guardia, J. I. Paredes, S. Villar-Rodil, P. Solís-Fernández, A. Martínez-Alonso, and J. M. D. Tascón, "Vitamin c is an ideal substitute for hydrazine in the reduction of graphene oxide suspensions," *Journal of Physical Chemistry C*, vol. 114, no. 14, pp. 6426–6432, 2010. DOI: 10.1021/jp100603h.

[87] Y. Zhang, L. Zhang, and C. Zhou, "Review of chemical vapor deposition of graphene and related applications," *Accounts of Chemical Research*, vol. 46, no. 10, pp. 2329–2339, 2013. DOI: 10.1021/ar300203n.

[88] S. Pei and H. M. Cheng, "The reduction of graphene oxide," *Carbon*, vol. 50, no. 9, pp. 3210–3228, 2012. DOI: 10.1016/j.carbon.2011.11.010.

[89] Y. Zhu, "Graphene and graphene oxide: Synthesis, properties, and applications," *Advanced Materials*, vol. 22, no. 35, pp. 3906–3924. DOI: 10.1002/adma.201001068.

[90] W. S. H. Jr. and R. E. Offeman, "Preparation of graphitic oxide," *Journal of the American Chemical Society*, vol. 80, no. 6, p. 1339, 1958. ISSN: 00027863.

[91] H. He, J. Klinowski, M. Forster, and A. Lerf, "A new structural model for graphite oxide," *Chemical Physics Letters*, vol. 287, no. 1-2, pp. 53–56, 1998. ISSN: 00092614.

[92] A. Bagri, C. Mattevi, M. Acik, Y. J. Chabal, M. Chhowalla, and V. B. Shenoy, "Structural evolution during the reduction of chemically derived graphene oxide," *Nature Chemistry*, vol. 2, no. 7, pp. 581–587, 2010. DOI: 10.1038/nchem.686.

[93] D. W. Boukhvalov and M. I. Katsnelson, "Modeling of graphite oxide," *Journal of the American Chemical Society*, vol. 130, no. 32, pp. 10697–10701, 2008. DOI: 10.1021/ja8021686.

[94] "Kansainväliset kemikaalikortit." Työterveyslaitos, 2012. Cited: 2015/12/30. Accessed: http://kappa.ttl.fi/kemikaalikortit/index.php?page=info.html.

[95] S. Pei, J. Zhao, J. Du, W. Ren, and H. M. Cheng, "Direct reduction of graphene oxide films into highly conductive and flexible graphene films by hydrohalic acids," *Carbon*, vol. 48, no. 15, pp. 4466–4474, 2010. DOI: 10.1016/j.carbon.2010.08.006.

[96] A. Y. S. Eng, A. Ambrosi, C. K. Chua, F. Šanek, Z. Sofer, and M. Pumera, "Unusual inherent electrochemistry of graphene oxides prepared using permanganate oxidants," *Chemistry - A European Journal*, vol. 19, no. 38, pp. 12673–12683, 2013. DOI: 10.1002/chem.201301889.

[97] H. L. Guo, X. F. Wang, Q. Y. Qian, F. B. Wang, and X. H. Xia, "A green approach to the synthesis of graphene nanosheets," *ACS Nano*, vol. 3, no. 9, pp. 2653–2659, 2009. DOI: 10.1021/nn900227d.

[98] E. C. Salas, Z. Sun, A. Lüttge, and J. M. Tour, "Reduction of graphene oxide via bacterial respiration," *ACS Nano*, vol. 4, no. 8, pp. 4852–4856, 2010. DOI: 10.1021/nn101081t.

[99] A. C. Ferrari and J. Robertson, "Interpretation of raman spectra of disordered and amorphous carbon," *Physical Review B - Condensed Matter and Materials Physics*, vol. 61, no. 20, pp. 14095–14107, 2000. ISSN: 01631829.

[100] M. Zhou, Y. Wang, Y. Zhai, J. Zhai, W. Ren, F. Wang, and S. Dong, "Controlled synthesis of large-area and patterned electrochemically reduced graphene oxide films," *Chemistry - A European Journal*, vol. 15, no. 25, pp. 6116–6120, 2009. DOI: 10.1002/chem.200900596.

[101] M. Zhou, Y. Wang, Y. Zhai, J. Zhai, W. Ren, F. Wang, and S. Dong, "Controlled synthesis of large-area and patterned electrochemically reduced graphene oxide films," *Chemistry - A European Journal*, vol. 15, no. 25, pp. 6116–6120, 2009. DOI: 10.1002/chem.200900596.

[102] C. Mattevi, G. Eda, S. Agnoli, S. Miller, K. A. Mkhoyan, O. Celik, D. Mastrogiovanni, C. Cranozzi, E. Carfunkel, and M. Chhowalla, "Evolution of electrical, chemical, and structural properties of transparent and conducting chemically derived craphene thin films," *Advanced Functional Materials*, vol. 19, no. 16, pp. 2577–2583, 2009. DOI: 10.1002/adfm.200900166.

[103] C. Gómez-Navarro, R. T. Weitz, A. M. Bittner, M. Scolari, A. Mews, M. Burghard, and K. Kern, "Electronic transport properties of individual chemically reduced graphene oxide sheets," *Nano Letters*, vol. 7, no. 11, pp. 3499–3503, 2007. DOI: 10.1021/nl072090c.

[104] G. Eda and M. Chhowalla, "Chemically derived graphene oxide: Towards large-area thin-film electronics and optoelectronics," *Advanced Materials*, vol. 22, no. 22, pp. 2392–2415, 2010. DOI: 10.1002/adma.200903689.

[105] C. M. Sayes, F. Liang, J. L. Hudson, J. Mendez, W. Guo, J. M. Beach, V. C. Moore, C. D. Doyle, J. L. West, W. E. Billups, K. D. Ausman, and V. L. Colvin, "Functionalization density dependence of single-walled carbon nanotubes cytotoxicity in vitro," *Toxicology letters*, vol. 161, no. 2, pp. 135–142, 2006. DOI: 10.1016/j.toxlet.2005.08.011.

[106] Y. Chang, S. T. Yang, J. H. Liu, E. Dong, Y. Wang, A. Cao, Y. Liu, and H. Wang, "In vitro toxicity evaluation of graphene oxide on a549 cells," *Toxicology letters*, vol. 200, no. 3, pp. 201–210, 2011. DOI: 10.1016/j.toxlet.2010.11.016.

[107] X. Zhang, J. Yin, C. Peng, W. Hu, Z. Zhu, W. Li, C. Fan, and Q. Huang, "Distribution and biocompatibility studies of graphene oxide in mice after intravenous administration," *Carbon*, vol. 49, no. 3, pp. 986–995, 2011. DOI: 10.1016/j.carbon.2010.11.005.

[108] S. Gurunathan, J. W. Han, V. Eppakayala, and J. H. Kim, "Green synthesis of graphene and its cytotoxic effects in human breast cancer cells," *International Journal of Nanomedicine*, vol. 8, pp. 1015–1027, 2013. DOI: 10.2147/IJN.S42047.

[109] O. Akhavan, E. Ghaderi, and A. Akhavan, "Size-dependent genotoxicity of graphene nanoplatelets in human stem cells," *Biomaterials*, vol. 33, no. 32, pp. 8017–8025, 2012. DOI: 10.1016/j.biomaterials.2012.07.040.

[110] S. K. Kim, D. Kim, and S. Jeon, "Electrochemical determination of serotonin on glassy carbon electrode modified with various graphene nanomaterials," *Sensors and Actuators, B: Chemical*, vol. 174, pp. 285–291, 2012. DOI: 10.1016/j.snb.2012.08.034.

[111] S. Liu, J. Yan, G. He, D. Zhong, J. Chen, L. Shi, X. Zhou, and H. Jiang, "Layer-by-layer assembled multilayer films of reduced graphene oxide/gold nanoparticles for the electrochemical detection of dopamine," *Journal of Electroanalytical Chemistry*, vol. 672, pp. 40–44, 2012. DOI: 10.1016/j.jelechem.2012.03.007.

[112] C. Xue, X. Wang, W. Zhu, Q. Han, C. Zhu, J. Hong, X. Zhou, and H. Jiang, "Electrochemical serotonin sensing interface based on double-layered membrane of reduced graphene oxide/polyaniline nanocomposites and molecularly imprinted polymers embedded with gold nanoparticles," *Sensors and Actuators, B: Chemical*, vol. 196, pp. 57–63, 2014. DOI: 10.1016/j.snb.2014.01.100.

[113] K. Deng, J. Zhou, and X. Li, "Noncovalent nanohybrid of cobalt tetraphenylporphyrin with graphene for simultaneous detection of ascorbic acid, dopamine, and uric acid," *Electrochimica Acta*, vol. 114, pp. 341–346, 2013. DOI: 10.1016/j.electacta.2013.09.164.

[114] C. Karuppiah, S. Sakthinathan, S. M. Chen, K. Manibalan, S. M. Chen, and S. T. Huang, "A non-covalent functionalization of copper tetraphenylporphyrin/chemically reduced graphene oxide nanocomposite for the selective

determination of dopamine," *Applied Organometallic Chemistry*, vol. 30, no. 1, pp. 40–46, 2016. DOI: 10.1002/aoc.3397.

[115] A. H. Lu, E. L. Salabas, and F. Schüth, "Magnetic nanoparticles: Synthesis, protection, functionalization, and application," *Angewandte Chemie - International Edition*, vol. 46, no. 8, pp. 1222–1244, 2007. DOI: 10.1002/anie.200602866.

[116] H. Bagheri, A. Afkhami, P. Hashemi, and M. Ghanei, "Simultaneous and sensitive determination of melatonin and dopamine with fe3o4 nanoparticle-decorated reduced graphene oxide modified electrode," *RSC Advances*, vol. 5, no. 28, pp. 21659–21669, 2015. DOI: 10.1039/c4ra16802j.

[117] H. Teymourian, A. Salimi, and S. Khezrian, "Fe3o4 magnetic nanoparticles/reduced graphene oxide nanosheets as a novel electrochemical and bioeletrochemical sensing platform," *Biosensors and Bioelectronics*, vol. 49, pp. 1–8, 2013. DOI: 10.1016/j.bios.2013.04.034.

[118] T. Peik-See, A. Pandikumar, H. Nay-Ming, L. Hong-Ngee, and Y. Sulaiman, "Simultaneous electrochemical detection of dopamine and ascorbic acid using an iron oxide/reduced graphene oxide modified glassy carbon electrode," *Sensors (Switzerland)*, vol. 14, no. 8, pp. 15227–15243, 2014. DOI: 10.3390/s140815227.

[119] X. Qin, A. M. Asiri, K. A. Alamry, A. O. Al-Youbi, and X. Sun, "Carbon nitride dots can serve as an effective stabilizing agent for reduced graphene oxide and help in subsequent assembly with glucose oxidase into hybrids for glucose detection application," *Electrochimica Acta*, vol. 95, pp. 260–267, 2013. DOI: 10.1016/j.electacta.2013.02.014.

[120] H. Teymourian, A. Salimi, and S. Firoozi, "A high performance electrochemical biosensing platform for glucose detection and ige aptasensing based on fe3o4/reduced graphene oxide nanocomposite," *Electroanalysis*, vol. 26, no. 1, pp. 129–138, 2014. DOI: 10.1002/elan.201300496.

[121] Y. Wang, Y. Shao, D. W. Matson, J. Li, and Y. Lin, "Nitrogen-doped graphene and its application in electrochemical biosensing," *ACS Nano*, vol. 4, no. 4, pp. 1790–1798, 2010. DOI: 10.1016/j.snb.2014.01.044.

[122] H. Gu, Y. Yu, X. Liu, B. Ni, T. Zhou, and G. Shi, "Layer-by-layer self-assembly of functionalized graphene nanoplates for glucose sensing in vivo integrated with on-line microdialysis system," *Biosensors and Bioelectronics*, vol. 32, no. 1, pp. 118–126, 2012. DOI: 10.1016/j.bios.2011.11.044.

[123] C. Shan, H. Yang, J. Song, D. Han, A. Ivaska, and L. Niu, "Direct electrochemistry of glucose oxidase and biosensing for glucose based on graphene," *Analytical Chemistry*, vol. 81, no. 6, pp. 2378–2382, 2009. DOI: 10.1021/ac802193c.

[124] K. Dhara, J. Stanley, T. Ramachandran, B. G. Nair, and S. B. T.g, "Pt-cuo nanoparticles decorated reduced graphene oxide for the fabrication of highly sensitive non-enzymatic disposable glucose sensor," *Sensors and Actuators, B: Chemical*, vol. 195, pp. 197–205, 2014. DOI: 10.1016/j.snb.2014.01.044.

[125] L. Wang, X. Lu, C. Wen, Y. Xie, L. Miao, S. Chen, H. Li, P. Li, and Y. Song, "One-step synthesis of pt-nio nanoplate array/reduced graphene oxide nanocomposites for nonenzymatic glucose sensing," *Journal of Materials Chemistry A*, vol. 3, no. 2, pp. 608–616, 2015. DOI: 10.1039/c4ta04724a.

[126] K. Dhara, T. Ramachandran, B. G. Nair, and T. G. S. Babu, "Single step synthesis of au-cuo nanoparticles decorated reduced graphene oxide for high performance disposable nonenzymatic glucose sensor," *Journal of Electroanalytical Chemistry*, vol. 743, pp. 1–9, 2015. DOI: 10.1016/j.jelechem.2015.02.005.

[127] K. Dhara, R. Thiagarajan, B. G. Nair, and G. S. B. Thekkedath, "Highly sensitive and wide-range nonenzymatic disposable glucose sensor based on a screen printed carbon electrode modified with reduced graphene oxide and pd-cuo nanoparticles," *Microchimica Acta*, vol. 182, no. 13-14, pp. 2183–2192, 2015. DOI: 10.1007/s00604-015-1549-x.

[128] M. A. Tabrizi, S. J. Azar, and J. N. Varkani, "Eco-synthesis of graphene and its use in dihydronicotinamide adenine dinucleotide sensing," *Analytical Biochemistry*, vol. 460, pp. 29–35, 2014. DOI: 10.1016/j.ab.2014.05.002.

[129] M. A. Tabrizi and Z. Zand, "A facile one-step method for the synthesis of reduced graphene oxide nanocomposites by nadh as reducing agent and its application in nadh sensing," *Electroanalysis*, vol. 26, no. 1, pp. 171–177, 2014. DOI: 10.1002/elan.201300370.

[130] J. Tian, S. Y. Deng, D. L. Li, D. Shan, W. He, X. J. Zhang, and Y. Shi, "Bioinspired polydopamine as the scaffold for the active aunps anchoring and the chemical simultaneously reduced graphene oxide: Characterization and the enhanced biosensing application," *Biosensors and Bioelectronics*, vol. 49, pp. 466–471, 2013. DOI: 10.1016/j.bios.2013.06.009.

[131] T. Y. Huang, J. H. Huang, H. Y. Wei, K. C. Ho, and C. W. Chu, "Rgo/swcnt composites as novel electrode materials for electrochemical biosensing," *Biosensors and Bioelectronics*, vol. 43, no. 1, pp. 173–179, 2013. DOI: 10.1016/j.bios.2012.10.047.

[132] G. M. M. Ferreira, F. M. D. Oliveira, F. R. F. Leite, C. M. Maroneze, L. T. Kubota, F. S. Damos, and R. D. C. S. Luz, "Dna and graphene as a new efficient platform for entrapment of methylene blue (mb): Studies of the electrocatalytic oxidation of β-nicotinamide adenine dinucleotide," *Electrochimica Acta*, vol. 111, pp. 543–551, 2013. DOI: 10.1016/j.electacta.2013.08.037.

[133] K. Dhara, T. Ramachandran, B. G. Nair, and T. G. S. Babu, "Au nanoparticles decorated reduced graphene oxide for the fabrication of disposable nonenzymatic hydrogen peroxide sensor," *Journal of Electroanalytical Chemistry*, vol. 764, pp. 64–70, 2016. DOI: 10.1016/j.jelechem.2016.01.011.

[134] Q. Wang, M. Li, S. Szunerits, and R. Boukherroub, "Environmentally friendly reduction of graphene oxide using tyrosine for nonenzymatic amperometric h2o2 detection," *Electroanalysis*, vol. 26, no. 1, pp. 156–163, 2014. DOI: 10.1002/elan.201300356.

[135] A. Bonanni, A. H. Loo, and M. Pumera, "Graphene for impedimetric biosensing," *TrAC - Trends in Analytical Chemistry*, vol. 37, pp. 12–21, 2012. DOI: 10.1016/j.trac.2012.02.011.

[136] J. Zhao, Z. Guo, J. Guo, J. Wang, and Y. Zhang, "Electrochemical detection of two tumor markers based on functionalized polypyrrole microspheres as immunoprobes," *RSC Advances*, vol. 6, no. 37, pp. 31448–31453, 2016. DOI: 10.1039/c6ra01773h.

[137] C. Qiumei, B. Hongmei, Y. Zhaoxia, J. Liu, and F. Xi, "A reagentless electrochemical immunosensor based on probe immobilization and the layer-by-layer assembly technique for sensitive detection of tumor markers," *Analytical Methods*, vol. 7, no. 22, pp. 9655–9662, 2015. DOI: 10.1039/c5ay01871d.

[138] M. Wang, S. Zhai, Z. Ye, L. He, D. Peng, X. Feng, Y. Yang, S. Fang, H. Zhang, and Z. Zhang, "An electrochemical aptasensor based on a tio2/three-dimensional reduced graphene oxide/ppy nanocomposite for the sensitive detection of lysozyme," *Dalton Transactions*, vol. 44, no. 14, pp. 6473–6479, 2015. DOI: 10.1039/c5dt00168d.

[139] M. Mazloum-Ardakani, L. Hosseinzadeh, and Z. Taleat, "Synthesis and electrocatalytic effect of ag@pt core-shell nanoparticles supported on reduced graphene oxide for sensitive and simple label-free electrochemical aptasensor," *Biosensors and Bioelectronics*, vol. 74, pp. 30–36, 2015. DOI: 10.1016/j.bios.2015.05.072.

[140] R. M. Locksley, N. Killeen, and M. J. Lenardo, "The tnf and tnf receptor superfamilies: Integrating mammalian biology," *Cell*, vol. 104, no. 4, pp. 487–501, 2001. DOI: 10.1016/S0092-8674(01)00237-9.

[141] B. C. Janegitz, F. A. D. Santos, R. C. Faria, and V. Zucolotto, "Electrochemical determination of estradiol using a thin film containing reduced graphene oxide and dihexadecylphosphate," *Materials Science and Engineering C*, vol. 37, no. 1, pp. 14–19, 2014. DOI: 10.1016/j.msec.2013.12.026.

[142] B. C. Janegitz, M. Baccarin, P. A. Raymundo-Pereira, F. A. D. Santos, G. G. Oliveira, S. A. S. Machado, M. R. V. Lanza, O. Fatibello-Filho, and V. Zucolotto, "The use of dihexadecylphosphate in sensing and biosensing," *Sensors and Actuators, B: Chemical*, vol. 220, pp. 805–813, 2015. DOI: 10.1016/j.snb.2015.06.020.

[143] N. Huang, S. Zhang, L. Yang, M. Liu, H. Li, Y. Zhang, and S. Yao, "Multifunctional electrochemical platforms based on the michael addition/schiff base reaction of polydopamine modified reduced graphene oxide: Construction and application," *ACS Applied Materials and Interfaces*, vol. 7, no. 32, pp. 17935–17946, 2015. DOI: 10.1021/acsami.5b04597.

[144] T. Qian, C. Yu, X. Zhou, S. Wu, and J. Shen, "Au nanoparticles decorated polypyrrole/reduced graphene oxide hybrid sheets for ultrasensitive dopamine detection," *Sensors and Actuators, B: Chemical*, vol. 193, pp. 759–763, 2014. DOI: 10.1016/j.snb.2013.12.055.

[145] X. Liu, L. Xie, and H. Li, "Electrochemical biosensor based on reduced graphene oxide and au nanoparticles entrapped in chitosan/silica sol-gel hybrid membranes for determination of dopamine and uric acid," *Journal of Electroanalytical Chemistry*, vol. 682, pp. 158–163, 2012. DOI: 10.1016/j.jelechem.2012.07.031.

[146] J. Zhou, M. Chen, and G. Diao, "Calix[4,6,8]arenesulfonates functionalized reduced graphene oxide with high supramolecular recognition capability: Fabrication and application for enhanced host-guest electrochemical recognition," *ACS Applied Materials and Interfaces*, vol. 5, no. 3, pp. 828–836, 2013. DOI: 10.1021/am302289v.

[147] H. F. Ma, T. T. Chen, Y. Luo, F. Y. Kong, D. H. Fan, H. L. Fang, and W. Wang, "Electrochemical determination of dopamine using octahedral sno2 nanocrystals bound to reduced graphene oxide nanosheets," *Microchimica Acta*, vol. 182, no. 11-12, pp. 2001–2007, 2015. DOI: 10.1007/s00604-015-1521-9.

[148] L. X. Chen, J. N. Zheng, A. J. Wang, L. J. Wu, J. R. Chen, and J. J. Feng, "Facile synthesis of porous bimetallic alloyed pdag nanoflowers supported on reduced graphene oxide for simultaneous detection of ascorbic acid, dopamine, and uric acid," *Analyst*, vol. 140, no. 9, pp. 3183–3192, 2015. DOI: 10.1039/c4an02200a.

A Summary of chemically reduced graphene oxide in electrochemical sensing and biosensing

Table A1: Chemically reduced graphene oxide in electrochemical sensing and biosensing.

Molecule	**Electrode**	**Reductant**	**C/O**	**Method**	**Linear range (μM)**	**LOD (μM)**	**Sensitivity ($AM^{-1}cm^{-2}$)**	**Ref.**
DA	CRGO/GC	$N_2H_4 \cdot H_2O$	11.8	CV				[24]
	PtNP/chitosan/CRGO/GC	$NaBH_4$		DPV	5.0-150.0	0.45		[34]
	PtPdNP/PDDA/CRGO/GC	NaOH		DPV	4-200	0.04		[111]
	AuNP/PAMAM/MWCNT/CRGO/GC	AA		DPV	10-320	3.3		[18]
	PSS/AuNP/PDDA/PAMAM/CRGO/GC	$N_2H_4 \cdot H_2O$		DPV	1-60	0.02		[111]
	Au/PPy/CRGO/GC	$N_2H_4 \cdot H_2O$		CV	10^{-4}–5	18.29 x 10^{-6}	16.40 AM^{-1}	[144]
	AuNP/CSHM/CRGO/GC	$N_2H_4 \cdot H_2O$		CV	1.0-200	0.3		[145]
	Cu-TPP/CRGO/GC	$N_2H_4 \cdot H_2O$, ammonia		CV	2-200	0.76	2.46	[114]
	Co-TPP/CRGO/GC	$N_2H_4 \cdot H_2O$, ammonia		CV	0.1-12.0	0.03		[113]
	Fe_3O_4/CRGO/GC	$N_2H_4 \cdot H_2O$, ammonia		DPV	0.4 -3.5	0.08	38.8	[117]
	Fe_3O_4/CRGO/CPE	$N_2H_4 \cdot H_2O$, AA		SWV	0.02-5.80	6.5		[116]
	Fe_3O_4/CRGO/GC	NH_4OH		DPV	0.5-100	0.12		[118]
	SC8/CRGO/GC	$N_2H_4 \cdot H_2O$		CV	0.01-21	0.008		[146]
	SnO_2/CRGO/GC	AA		DPV	0.08-30	0.006		[147]
	PdAgNF/CRGO/GC	AA		DPV	0.4-96.0	0.048		[148]
5-HT	CRGO/GC	$N_2H_4 \cdot H_2O$, ammonia	4.23	DPV	1-100	0.032	20.152	[110]
	CRGO/GC	$N_2H_4 \cdot H_2O$	4.98	DPV	1-100	0.046	9.533	[110]
	CRGO/GC	$NH_2OH \cdot HCl$, ammonia	4.17	DPV	1-100	0.052	6.773	[110]
	AuNP/MIP/PANI/CRGO/GC	$N_2H_4 \cdot H_2O$		DPV	0.2-10	0.0117		[112]
AA	CRGO/GC	$N_2H_4 \cdot H_2O$	11.8	CV				[24]
	PtPdNP/PDDA/CRGO/GC	NaOH		DPV	40-1200	0.61		[111]
	AuNP/PAMAM/MWCNT/CRGO/GC	AA		DPV	20-1800	6.7		[18]
	Co-TPP/CRGO/GC	$N_2H_4 \cdot H_2O$, ammonia		CV	5-200	1.2		[113]
	PdAgNF/CRGO/GC	AA		DPV	1.0-2100	0.057		[148]
	Fe_3O_4/CRGO/GC	$N_2H_4 \cdot H_2O$, ammonia		DPV	160-7200	20	33.5 x 10^{-3}	[117]
	Fe_3O_4/CRGO/GC	NH_4OH		DPV	1000-9000	0.42		[118]
UA	CRGO/GC	$N_2H_4 \cdot H_2O$	11.8	CV				[24]
	PtNP/chitosan/CRGO/GC	$NaBH_4$		DPV	10.0-130.0	0.70		[34]
	PtPdNP/PDDA/CRGO/GC	NaOH		DPV	4-400	0.1		[111]
	AuNP/PAMAM/MWCNT/CRGO/GC	AA		DPV	1-114	0.33		[18]
	PSS/AuNP/PDDA/PAMAM/CRGO/GC	$N_2H_4 \cdot H_2O$		DPV	10-120	0.27		[111]
	Co-TPP/CRGO/GC	$N_2H_4 \cdot H_2O$, ammonia		CV	0.5-40	0.15		[113]
	AuNP/CSHM/CRGO/GC	$N_2H_4 \cdot H_2O$		CV	1.0-300	0.7		[145]
	PdAgNF/CRGO/GC	AA		DPV	1.0-150.0	0.081		[148]
	Fe_3O_4/CRGO/GC	$N_2H_4 \cdot H_2O$, ammonia		DPV	4-20	0.5	4.50	[117]

Table A2: Chemically reduced graphene oxide in electrochemical sensing and biosensing.

Molecule	**Electrode, recognition element**	**Reductant**	**C/O**	**Method**	**Linear range (μM)**	**LOD (μM)**	**Sensitivity ($\mathbf{A}M^{-1}cm^{-2}$)**	**Ref.**
Glucose	CRGO/GC, GluOx	$N_2H_4 \cdot H_2O$	11.8	AM	10-10000	2.0	20.21 x 10^{-3}	[24]
	Fe_3O_4/CRGO/GC, GluOx	$N_2H_4 \cdot H_2O$		CV	500-12000	50		[120]
	CND/CRGO/GC, GluOx	$N_2H_4 \cdot H_2O$, ammonia	7.87	CV	40-20000	40		[119]
	N-doped/CRGO/GC, GluOx	$N_2H_4 \cdot H_2O$	2.6	CV	100-1100	10		[121]
	PHIL/CRGO, GluOx	$N_2H_4 \cdot H_2O$		CV	2000-14000			[123]
	IL/S-CRGO/Nafion/GC, GluOx	$N_2H_4 \cdot H_2O$			10-500	3.33	71.8 x 10^{-6} AM^{-1}	[122]
	Pt/CuO/CRGO/SPE	$NaBH_4$		LSV	$<$ 12000	0.01	3.577	[124]
	Au/CuO/CRGO/SPE	$NaBH_4$		LSV	1000-12000	0.1	2.356	[126]
	Pd/CuO/CRGO/SPE	$NaBH_4$		LSV	6-22000	0.03	3.355	[127]
	Pt/NiO/CRGO/GC	urea		CV	8-14500	2.67	832.95 x 10^{-6}	[125]
NADH	CRGO/GC	$N_2H_4 \cdot H_2O$	11.8	CV	40-800	10	2.68 x 10^{-6}	[24]
	CRGO/GC	malt		CV	10-600	0.33		[128]
	CRGO/GC	NADH		CV	0-400	0.6		[129]
	Fe_3O_4/CRGO/GC	$N_2H_4 \cdot H_2O$		CV	2-150	0.4	0.133	[117]
	AuNP/CRGO/GC	DA, $NaBH_4$		CV	0.050-42			[130]
	MB/DNA/CRGO/GC	$N_2H_4 \cdot H_2O$		CV	10-1500	1.0	12.75 AM^{-1}	[132]
	SWCNT/CRGO/GC	N_2H_4		CV	20-400	0.078	0.204	[131]
H_2O_2	CRGO/GC	$N_2H_4 \cdot H_2O$	11.8	DPV	0.05-1500	0.05		[24]
	AuNP/CRGO/SPE	$NaBH_4$		LSV	20-10000	0.1	1.238	[133]
	CRGO/GC	Tyrosine	6.07	CV	100-2100	80	0.0691	[134]
	SWCNT/CRGO/GC	N_2H_4		CV	0.5 x 10^6-5 x 10^6	1.3	2.7324	[131]
	Fe_3O_4/CRGO/GC	$N_2H_4 \cdot H_2O$		CV	0.02-19	0.006	29.18	[117]
	IL/S-CRGO/GC	$N_2H_4 \cdot H_2O$		CV	100-3400	0.21	0.1364 AM^{-1}	[122]
DNA base G	Fe_3O_4/CRGO/GC	$N_2H_4 \cdot H_2O$		DPV		0.3		[120]
DNA base A	Fe_3O_4/CRGO/GC	$N_2H_4 \cdot H_2O$		DPV		0.8		[120]
Tumor marker CEA	PPy/AuNP/CRGO/GC	$NaBH_4$		DPV	1.0 pg/ml-50 ng/ml	0.40 pg/ml		[136]
Tumor marker CEA	PEI/CRGO/Au	$NaBH_4$		DPV	0.1-120 ng/ml	60 pg/ml		[137]
Tumor marker AFP	PPy/AuNP/CRGO/GC	$NaBH_4$		DPV	1.0 pg/ml-50 ng/ml	0.33 pg/ml		[136]
Lysozyme	PPy/TiO_2/CRGO/Au, aptamer	$N_2H_4 \cdot H_2O$		DPV	7 x 10^{-6}-3.5 x 10^{-3}	5.5 x 10^{-6}		[138]
Protein marker TNF-α	Ag/Pt/CRGO/SPE, aptamer	$NaBH_4$		DPV	0.0-60 pg/ml	2.07 pg/ml		[139]
Estradiol hormone	DHP/CRGO/GC	$NaBH_4$		CV	0.4-10	0.077		[141]